

# Sudden large-volume detachments of low-angle mountain glaciers – more frequent than thought?

Andreas Kääb<sup>1</sup>, Mylène Jacquemart<sup>2</sup>, Adrien Gilbert<sup>3</sup>, Silvan Leinss<sup>4</sup>, Luc Girod<sup>1</sup>, Christian Huggel<sup>5</sup>, Daniel Falaschi<sup>6,7</sup>, Felipe Ugalde<sup>8,9</sup>, Dmitry Petrakov<sup>10</sup>, Sergey Chernomorets<sup>10</sup>, Mikhail Dokukin<sup>11</sup>, Frank Paul<sup>5</sup>, Simon Gascoïn<sup>12</sup>, Etienne Berthier<sup>13</sup>, Jeff S. Kargel<sup>14</sup>

<sup>1</sup> Department of Geosciences, University of Oslo, Norway

<sup>2</sup> Cooperative Institute for Research in Environmental Sciences, University of Colorado at Boulder, United States

<sup>3</sup> Université Grenoble Alpes, CNRS, IGE, Grenoble, France

<sup>4</sup> Institute of Environmental Engineering, ETH Zurich, Switzerland

<sup>5</sup> Department of Geography, University of Zurich, Switzerland

<sup>6</sup> Instituto Argentino de Nivología, Glaciología y Ciencias Ambientales, Mendoza, Argentina

<sup>7</sup> Departamento de Geografía, Facultad de Filosofía y Letras, Universidad Nacional de Cuyo, Mendoza, Argentina

<sup>8</sup> Geostudios, San José de Maipo, Chile

<sup>9</sup> Departamento de Geología, Facultad de Ciencias Físicas y Matemáticas, Universidad de Chile, Santiago, Chile

<sup>10</sup> Faculty of Geography, M.V.Lomonosov Moscow State University, Moscow, Russia

<sup>11</sup> High-Mountain Geophysical Institute, Nalchik, Russia

<sup>12</sup> CESBIO, Université de Toulouse, CNES/CNRS/INRA/IRD/UPS, Toulouse, France

<sup>13</sup> LEGOS, CNES, CNRS, IRD, UPS, Université de Toulouse, Toulouse, France

<sup>14</sup> Planetary Science Institute, University of Arizona, Tucson, AZ, USA

*Correspondence to:* Andreas Kääb (kaeab@geo.uio.no)

## Abstract.

The detachment of large parts of low-angle mountain glaciers, resulting in massive ice-rock avalanches, have so far been believed to be a unique type of event, made known to the global scientific community first for the 2002 Kolka Glacier detachment, Caucasus Mountains, and then for the 2016 collapses of two glaciers in the Aru range, Tibet. Since 2016, several so-far unrecognized low-angle glacier detachments have been recognized and described, and new ones have occurred. In the current contribution, we compile, compare and discuss 20 actual or suspected large-volume detachments of low-angle mountain glaciers at ten different sites in the Caucasus, the Pamirs, Tibet, Altai, Alaska's St. Elias mountain and the Southern Andes. Many of the detachments reached volumes in the order of 10–100 million m<sup>3</sup>. The similarities and differences between the presented cases suggest that glacier detachments often involve a coincidental combination of factors related to lowering of basal friction, high or increasing driving stresses, concentration of shear stress, or low resistance to exceed stability thresholds.

Particularly, soft glacier beds seem to be a common condition among the observed events, as they offer smooth contact areas between the glacier and the underlying substrate, and are prone to till-strength weakening and eventually basal failure under high pore-water pressure. Surface slopes of the detached glaciers range between around  $10^\circ$  and  $20^\circ$ . This may be low enough to enable the development of thick and thus large-volume glaciers, while also being steep enough to allow critical driving stresses to build up. We construct a simple slab model to estimate ranges of glacier slope and width above which a glacier may be able to detach when extensively losing basal resistance. From this model we estimate that all the detachments presented occurred due to a basal shear stress reduction of more than 50%. Most of the ice-rock avalanches resulting from the detachments in this study have a particularly low angle of reach, down to around 0.1 (apparent friction angle), likely due to their high ice content and connected liquefaction potential, the availability of soft basal slurries and large amounts of basal water, as well as the smooth topographic setting typical for glacial valleys. Low-angle glacier detachments combine elements, and likely also physical processes, of glacier surges and ice break-offs from steep glaciers. The surge-like temporal evolution ahead of several detachments and their geographic proximity to other surge-type glaciers suggests the glacier detachments investigated can be interpreted as endmembers of the continuum of surge-like glacier instabilities. Though rare, glacier detachments appear to be more frequent than commonly thought and disclose, despite local differences in conditions and precursory evolutions, the fundamental and critical potential of low-angle soft glacier beds to fail catastrophically.

## 1 Introduction

**Eighteen** years after the detachment of Kolka Glacier in the Russian Caucasus, the 17 July and 21 September 2016 detachments of two neighbouring glaciers in the Tibet's Aru range directed attention to a new type of glacier instability that had been rarely observed and little described before (Gilbert et al., 2018; Käab et al., 2018; Tian et al., 2017). The detachment of Kolka Glacier on 20 September 2002 released  $130 \cdot 10^6 \text{ m}^3$  of ice and rock that claimed  $\sim 135$  lives. Situated near a dormant volcano, Mt. Kazbek, it was long assumed that the Kolka Glacier catastrophe was unique and specific to the glacier's location (Haeblerli et al., 2004; Huggel et al., 2005; Drobyshev, 2006; Evans et al., 2009b). The Aru twin glacier detachments – which released 68 and  $83 \cdot 10^6 \text{ m}^3$  of glacier ice without known conditions of high geothermal flux – have recently raised the questions of whether and where such events may have happened before or need to be expected in the future, what conditions allow low-angle glaciers to detach catastrophically from their beds, and what this means for mountain hazard management. The urgency of these questions is highlighted by the fact that several detachments similar to the Aru events, though smaller, have been detected subsequently (Falaschi et al., 2019; Paul, 2019; Jacquemart et al., 2020).

In contrast to glacier detachments, glacier surges are an extensively studied, though still not fully understood type of glacier instability. Characterized by unusually high ice-flow speeds of up to tens of metres per day over large parts of a glacier, glacier surges last weeks to several years (Harrison and Post, 2003; Jiskoot, 2011; Harrison et al., 2015; Truffer et al., 2021). Clusters of surge-type glaciers are found in many mountain regions around the world (Sevestre and Benn, 2015). The lowering of basal

66 glacier friction that is associated with surging involves abnormally high water pressure, change in the thermal regime, and/or  
responses of subglacial till to increasing shear stress and water input (Clarke et al., 1984; Kamb, 1987; Truffer et al., 2000;  
68 Fowler et al., 2001; Murray et al., 2003; Frappe and Clarke, 2007; Sevestre et al., 2015; Benn et al., 2019).

A second, well-known type of glacier instability happens over a wide range of magnitudes, from icefalls at steep glacier fronts  
70 to large ice avalanches, when partial or entire ice volumes suddenly break off from hanging glaciers that are typically steeper  
than around 30° (Alean, 1985; Huggel, 2009; Faillettaz et al., 2015). The latter empirical value from literature offers a slope  
72 threshold to separate the definitions of ice avalanches from glacier detachments. Impacts associated with ice avalanches, which  
typically have volumes much smaller than  $1 \cdot 10^6 \text{ m}^3$ , are usually limited to a few kilometres, unless the solid ice transforms  
74 into a highly mobile mass flow through liquefaction and incorporation of wet sediments or liquid water in the path (Petrakov  
et al., 2008; Evans and Delaney, 2015). Failure conditions and triggering factors of such steep ice avalanches typically include  
76 glacier geometry (steep ramp-type glaciers, bedrock edges), bedrock topography (e.g. convex bed), atmospheric events (e.g.  
temperature increase), increasing accumulation rates, ice-thermal conditions (e.g. frozen base or changes therein), instabilities  
78 of the underlying bedrock that take with them ice resting on it, or seismic events (Alean, 1985; van der Woerd et al., 2004;  
Huggel, 2009; Fischer et al., 2013; Faillettaz et al., 2015).

80 Compared to the above two types of glacier instability, sudden large-scale detachments of mountain glaciers, primarily  
occurring at low bed slopes, are much less frequent. However, due to a mobility at least as high as that of ice avalanches,  
82 combined with large volumes, glacier detachments can constitute a severe threat to communities and settlements located in  
remote areas.


84 In general, mass movements that result from sudden slope failures in ice- or snow-rich mountain environments are particularly  
mobile, leading to strongly increased run-out distances compared to ice/snow-free conditions (Petrakov et al., 2008; Huggel,  
86 2009; Schneider et al., 2011; Evans and Delaney, 2015). Frictional heating melts ice and snow components, which are either  
part of the initial slope failure or incorporated along the avalanche path. Liquid water, embedded in the glacier and sediments  
88 before failure, can amplify the avalanche mobility. Also ice and snow surfaces, in case the avalanche travels over those, are  
able to reduce basal friction. Here, we define sudden large-volume glacier detachments through their initiation, while the  
90 eventually resulting ice-rock avalanches might be similar to those resulting from other high-mountain slope instabilities. By  
terming these events *low-angle glacier detachments*, we follow the suggestion by Evans and Delaney (2015) who describe the  
92 Kolka case as large-scale detachment of a valley glacier. Other authors, for instance, called these failure events glacier slides,  
in reference to landslides (Petrakov et al., 2008), or glacier collapses (Kääb et al., 2018).

94 The following selection focusses on detachments  $\gg 1 \cdot 10^6 \text{ m}^3$  and from glaciers with surface slopes of less than around 20°, i.e.  
focussing on glaciers from which large-volume detachments are not expected. We are well aware that it can be reasonable to  
96 include events beyond the limits of these criteria in analyses, depending on the goal of the investigation, and that similar events  
beyond the limits of these criteria could involve the same mechanisms that are discussed here. The main scientific purpose of

98 this paper is to provide an overview of all known glacier detachments, either by summarizing existing detailed studies, or by  
providing such details for the first time (see Suppl. Tab. S1 for existing studies and new contributions by the present work).  
100 We aim to show and discuss the relation of low-angle glacier detachments to glacier surges and the continuum of high-  
mountain ice and rock instabilities, such as normal avalanches. The main applied purpose of our study is to make experts  
102 involved in high-mountain hazard management aware of the so far little recognized possibility for glacier detachments, and to  
discuss related potential key indicators and how climate change could factor into the mechanisms.

## 104 **2 Ice-rock avalanches and glacier surges**

In this section we draw some comparisons of low-angle glacier detachments to (1) more typical types of glacier ice and ice-  
106 rock avalanches and (2) glacier surges. The detachment process sequence combines elements of both of these but in a  
combination and under conditions that are distinct.

108 Glacier detachments lead to ice-rock avalanches, but ice-rock avalanches usually are ~~be~~ the result of different other initial  
types of slope failures and event cascades. A wide range of magnitudes, avalanche compositions and impacts have been  
110 observed (Schneider et al., 2011). In this section, we exemplify the diverse characteristics of ice-rock avalanches and the  
resultant mass flows in order to contrast them to sudden large-volume detachments of mountain glaciers. We use the extensive  
112 data collection from Schneider et al. (2011) as background data set for our study, extended by events from Petrakov et al.  
(2008). In Fig. 1, each event of this combined data set is plotted as a **gray** circle according to its horizontal reach (L), elevation  
114 difference (H) and detachment volume (V). The size of the circles in Fig. 1a indicates the ~~event~~ volumes. The ratio H/L is the  
apparent friction coefficient or the angle of reach, also called “Fahrböschung  calculated from the uppermost scarp of the  
116 slope failure to the lowermost part of the mass movement deposits. Dark **grey** circles mark the following examples, standing  
out mainly by type, volume and angle of reach:

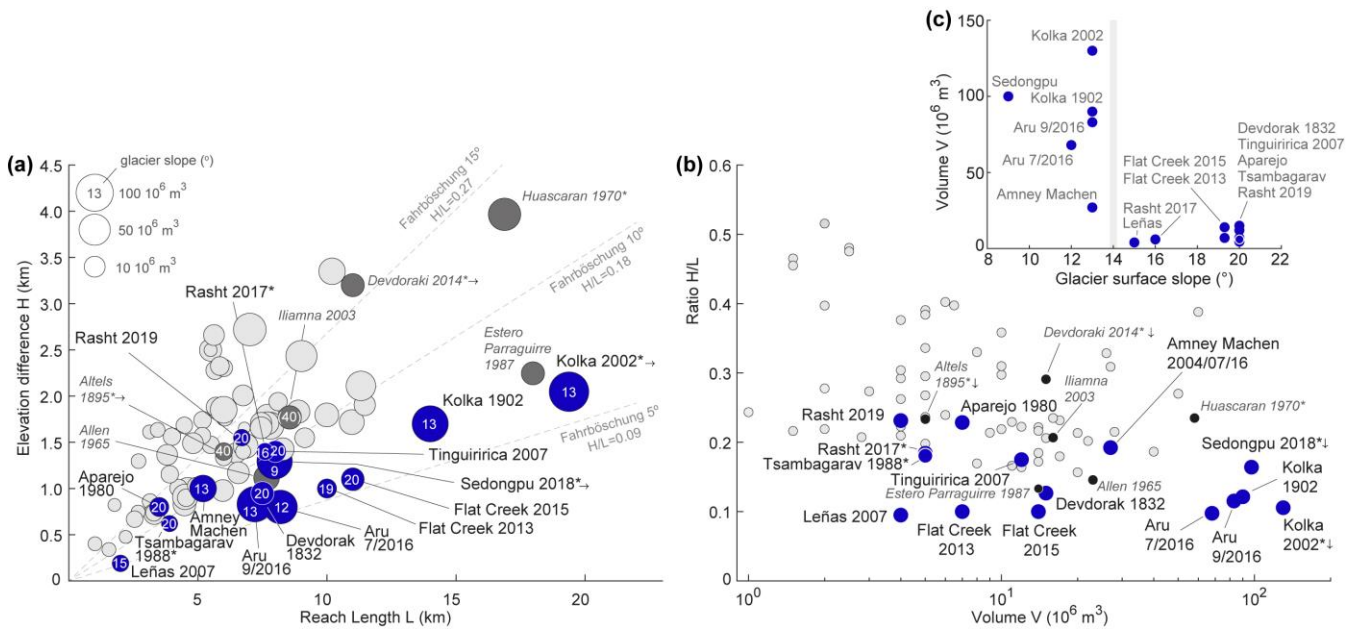
- 118 - In the 1970 Huascarán (Peru) event (and a similar event in 1962), a rock-wall failure triggered by a M7.9 earthquake,  
incorporated large amounts of ice from above and below it, leading to a highly mobile and far reaching rock-ice avalanche  
120 of  $80 \cdot 10^6 \text{ m}^3$  that claimed up to 20'000 lives (e.g., Evans et al., 2009a). In Fig. 1, we use the solid deposits of the avalanche  
to define its reach and elevation difference, neglecting that a subsequent water/mud flood travelled much farther (indicated  
122 by \* symbols in Fig. 1). The 1970 Huascarán avalanche is one of the largest, farthest reaching, and the by far deadliest  
known ice-rock avalanche.
- 124 - A rock failure in the Chilean Andes in 1987 incorporated ice, snow and water which transformed the avalanche into a  
debris flow of  $15 \cdot 10^6 \text{ m}^3$  that sped down the Estero Parraguirre valley and killed more than 37 people (Hauser, 2002). In  
126 our collection, this is the farthest-reaching event (lowest angle of reach;  $H/L \sim 0.12$ ) that did not originate as a glacier  
detachment.

128 - The 1964/65 Allen Glacier event, Alaska, is an example for a very large rock avalanche, likely triggered by an earthquake,  
that was able to run out for an unusually long distance because it landed on a glacier (Post, 1968). Neighbouring glaciers  
130 show similar rock deposits from the same time, and also later earthquakes caused comparable rock avalanches that travelled  
far over low-angle glaciers (e.g., Shugar et al., 2012).

132 - In 1895,  $5 \cdot 10^6 \text{ m}^3$  of at least partially cold-based ice sheared off  $40^\circ$ -steep bedrock from Altels Glacier in the Swiss Alps  
(glacier surface slopes indicated as numbers within the circles in Fig. 1a). The resulting ice avalanche rushed up the opposite  
134 side of the valley and thus did not reach its maximum runout distance (indicated by  $\rightarrow$  symbols in Fig. 1; Faillettaz et al.,  
2011). The Altels event is an example of a very large, pure ice avalanche, stemming from the detachment of a very steep  
136 glacier. Until it sheared off, the glacier was probably held in place by transverse bedrock riegels and cold patches/zones  
where it was frozen to its bed (Wagner, 1996).

138 - A number of ice-rock avalanches have occurred from different locations on Iliamna volcano, Alaska, the last of which is  
documented for June 2019 (Toney et al., 2020). Failure surfaces were typically on the order of  $40^\circ$ , and volumes reached  
140 up to around  $20 \cdot 10^6 \text{ m}^3$  (Caplan-Auerbach and Huggel, 2007; Huggel et al., 2007). These events show that enhanced  
geothermal heat fluxes can be involved in causing ice-rock avalanches.

142 Above, we exemplify ice-rock avalanches other than glacier detachments in order to put the avalanches resulting from glacier  
detachments into the context of high-mountain mass movements. In the following, we also put glacier detachments briefly in  
144 the context of glacier surges. An obvious difference between surges and glacier detachments is that the bed of surging glaciers  
does not fail catastrophically. A substantial body of research is available about glacier surging, covering among others surge  
146 cycles and phases, and thermally and/or hydrologically driven surge mechanisms (see references in the Introduction). Some  
observations of surging mountain glaciers or their surge-like movements fall outside the norm of the majority of surges, but  
148 will become of interest for some glacier detachments contained in this contribution: While the regional pattern of known  
glacier surges exhibits geographical clusters (Sevestre and Benn, 2015), surge-like events are sometimes found far outside the  
150 known surge clusters, as was for example the case for the speed-up of Belvedere Glacier, Italian Alps, in the early 2000s  
(Haeberli et al., 2002; Kääb et al., 2004; Harrison et al., 2015; Truffer et al., 2021) (cf. Tsambagarav detachment, Section 3.4).  
152 Ice flow speeds associated with surges are typically one to two orders of magnitude higher than pre-surge speeds, up to several  
tens of metres per day, or about 5-6 orders of magnitudes slower than ice-rock avalanches. But there are known surges that  
154 reached speeds of up to 1 km/h, i.e. only about 2 orders of magnitude slower than the avalanches (Section 3.6.3; Zhang, 1992).  
Furthermore, disintegration of surging (and non-surging) glaciers, which did not lead to ice-rock avalanches, have also been  
156 reported (e.g., Milana, 2007; Wang et al., 2020). Finally, another non-frequent behaviour of surge-type glaciers is extreme  
surface bulging that has been observed as a consequence of polythermal ice structure (Clarke and Blake, 1991) (cf. e.g. Flat  
158 Creek detachments, Section 3.7).



160 **Figure 1: (a) Known avalanches of rock-ice mixtures plotted by elevation drop H versus reach L. The event volumes**  
 162 **are indicated by circle size (see legend to the upper left of panel a). Blue circles are sudden large-volume detachments**  
 164 **of low-angle mountain glaciers, with the surface slope of the detached glacier parts given inside the circles. The grey**  
 166 **circles are other ice-rock avalanche events, with dark grey events mentioned specifically in the text to illustrate different**  
 168 **event types collected in this figure. The diagonal dashed lines indicate the angle of reach, Fahrböschung, at 5°, 10° and**  
 170 **15°. (b) Events from (a) plotted by reach angle (H / L) versus avalanche volume V. Note the logarithmic scale of the x-**  
 172 **axis (volume). Most events stem from Schneider et al. (2011), extended by data from Petrakov et al. (2008) and the**  
**present study. \* after the event name indicates that a mud or debris flow continued from the rock-ice avalanche**  
**deposits, which is not considered in the calculation of the reach. Arrows behind the event name indicate that the**  
**avalanche was stopped by some obstacle and would otherwise have travelled farther. The direction of the arrow**  
**indicates the direction in which the event symbol would have shifted in the plot without the obstacle. (c) Glacier**  
**detachment volume against glacier surface slope. The grey vertical bar indicates a very rough boundary between the**  
**glacier slope of very large and smaller detachment volumes.**

### 3 Glacier detachment events

174 In the following, we summarize events that we categorize as glacier detachments, i.e. large-volume ice-rock avalanches from  
 176 the sudden failure of low-angle parts of mountain glaciers (blue circles in Fig.1). Based on previously published findings from  
 178 several of the events, we focus our descriptions specifically on disposition factors that could contribute to or hint at the presence  
 180 of particularly low basal friction and high driving stresses. These factors include soft sediments, polythermal ice conditions,  
 abnormal geothermal heat flux, high water input and basal water pressure, glacier surging, additional ice or rock loading, or  
 significant steepening in surface slope. As it has been shown that thermal conditions can also play a role in the detachments of  
 glaciers (Gilbert et al., 2018; Jacquemart et al., 2020), we also try to evaluate permafrost conditions for each event.

We sort the following events by regions, and proceed within the regions from short summaries of well-documented events to more detailed descriptions of not or little studied cases. Discussions of individual events, e.g. regarding pre-satellite era events or a possible recurrence by glacier recovery, are included in the respective subsections, whereas the main discussion Section 4 focuses on the overall comparison between events.

### 3.1 Mount Kazbek, Caucasus mountains

#### 3.1.1 Devdorak, 18<sup>th</sup> century, 19<sup>th</sup> century, 2014

A number of suspected glacier detachments and rock-ice avalanches happened around Mt. Kazbek at the border between Russia and Georgia. During the 18-19<sup>th</sup> centuries, surges of the Devdorak (Georgian name Devdoraki also used in literature) Glacier on the north-eastern flank of Mount Kazbek (Fig. 2; Tab.1) were moving down the Amilishka River (Kabakhi River in its lower part), which drains the glacier. Surge-like advances were recorded in 1776, 1778, 1785, 1808, 1817, and 1832 (Zaporozhchenko and Chernomorets, 2004). On August 13, 1832, parts of the surging Devdorak Glacier tongue detached and the subsequent ice-rock avalanche blocked the main Terek valley, an important transportation route between Russia and Georgia (Petraikov et al., 2008). Eyewitness of the 1832 event, engineer-captain Grauert estimated a volume of  $15.5 \cdot 10^6 \text{ m}^3$  of ice and rock mass blocked the Dariali Gorge of the Terek valley (Zaporozhchenko and Chernomorets, 2004). The causes and mechanisms of this (and other) detachments are not well known, and vary throughout the literature. Ice-rock avalanching onto the glacier, overloading and associated increase in subglacial water pressure could well have played a role.

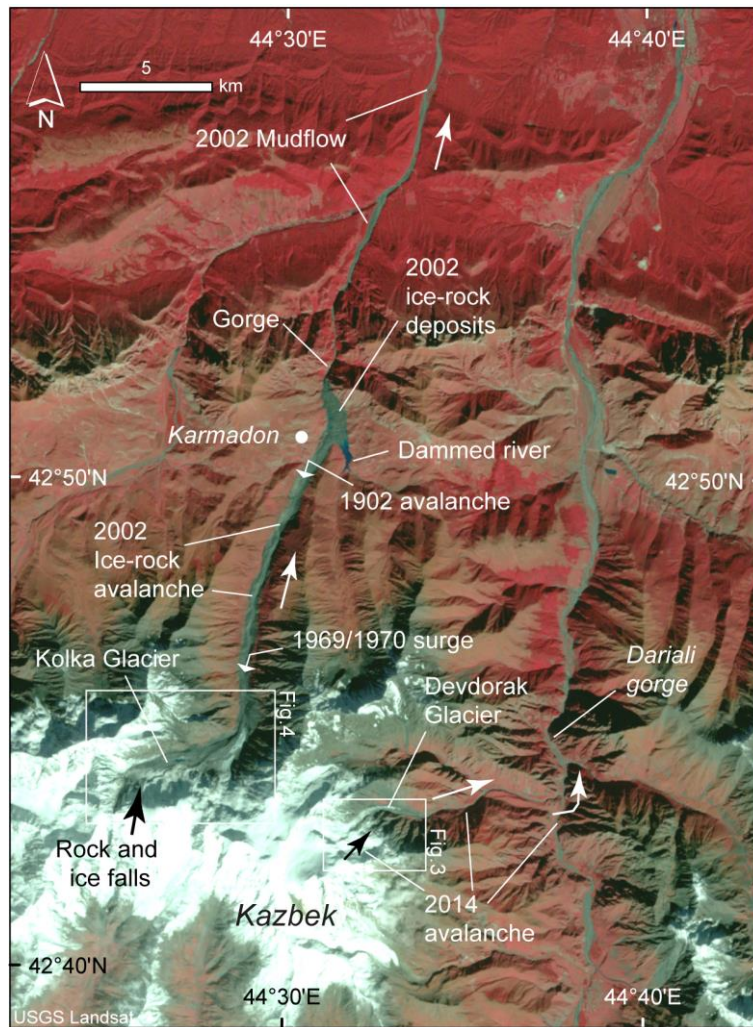
Except for their source area, these at their time well known “Kazbek blockages” followed the same avalanche path as the 2014 Devdorak event described in the following. In 2014, parts of a rock wall and overlying hanging glaciers failed from Mount Kazbek (Figs. 2-3). The resulting highly mobile rock-ice avalanche of  $2\text{-}5 \cdot 10^6 \text{ m}^3$  rushed down the Amilishka / Kabakhi Valley and blocked the main road between Russia and Georgia, killing 9 people (Chernomorets et al., 2016; Tielidze et al., 2019). This event might also have had a longer runout (Fig. 1) but was stopped by a sharp 90°-turn at the confluence of the Devdoraki gorge and the Dariali (or Terek) gorge. The 1832 Kazbek blockage is described as a glacier detachment in the sense of the present contribution in older literature, but more recent interpretations, not least based on the 2014 event, suggest that the 1832 and other such events at the site might have started as rock failures rather than surges (Chernomorets, 2014, Chernomorets et al., 2016). We list the Kazbek blockages as potential glacier detachments here, but stress that it remains uncertain what kind of event they actually were.

Currently, the entire narrow lower part of Devdorak Glacier has a surface slope of around 23°, its tongue closer to 17°. The volcanic nature of Mount Kazbek, the documentation of a number of violent mass flows from the mountain in the past (Chernomorets et al., 2007), field visits, and visual analysis of very high resolution satellite images and terrestrial photos all suggest highly erodible rock and an abundance of fine sediments at many places on Mount Kazbek. On all high-resolution satellite images available since around 2002 (GoogleEarth, Bing Maps, Maxar, Pleiades), Devdorak Glacier appears heavily



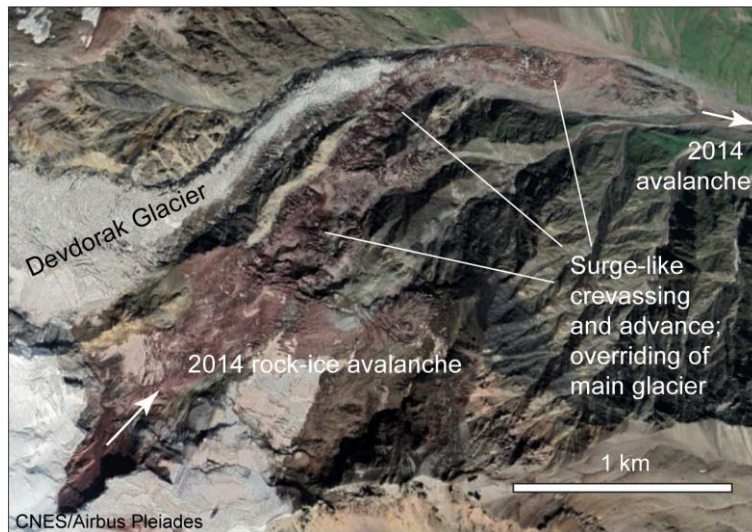
212 crevassed, and is partly covered by fine sediments, likely deposited by mass movements from the surrounding mountain flanks.  
Since 2015, a glacier directly south of Devdorak Glacier has been overriding the main tongue of Devdorak glacier in a surge-  
214 like destabilisation, perhaps triggered by the 2014 Kazbek/Devdorak rock-ice avalanche that overran it (Fig. 3). Possibly as a  
consequence of the tributary surge, Devdorak Glacier itself is currently also advancing (Dokukin et al., 2020). A 1-km global  
216 permafrost model (Obu et al., 2019), not particularly tuned for mountain permafrost, though, suggests the elevation of the  
Devdorak Glacier tongue is roughly at or below today's lower boundary of the discontinuous permafrost zone in the region.

218



220 **Figure 2: Overview over Mount Kazbek, Russia/Georgia, Caucasus Mountains, with elements of the 2002**  
**Kolka/Karmadon and 2014 Devdoraki rock-ice avalanches indicated. Satellite image: Landsat, 6 Oct 2002 (credit:**  
222 **USGS).**





224 **Figure 3: Lower part of Devdorak Glacier and northeastern flank of Mount Kazbek. The position of the image section**  
**is indicated in Fig. 2. Satellite image: Pleiades, © Airbus, 19 Aug 2019.**

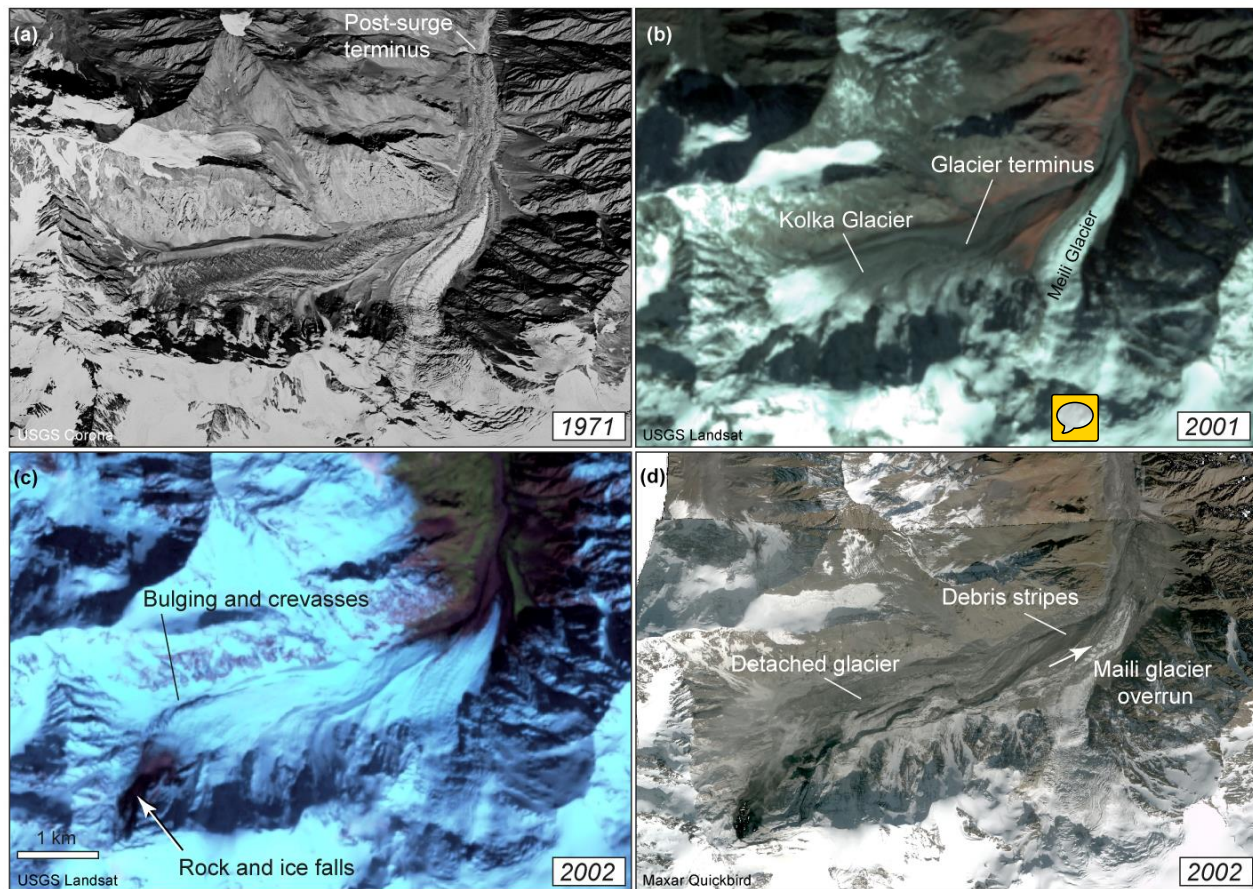
226

### 3.1.2 Kolka, 1902 and 2002

228 The  $130 \cdot 10^6 \text{ m}^3$  Kolka Glacier detachment (Figs. 2 and 4, Tab. 1) of 20 September 2002 has been described and discussed in  
 several studies (Kääb et al., 2003; Haeberli et al., 2004; Kotlyakov et al., 2004; Huggel et al., 2005; Drobyshev, 2006; Evans  
 230 et al., 2009b). During these investigations, it became clear that a similar event must have already happened at least once, at the  
 beginning of July 1902 (and probably also around 1700), whereby the glacier tongue detached after a roughly two-week long  
 232 surge-like advance. Heavy rain and snow melt may have played a role in triggering the 1902 advance. Damming or erosion by  
 water could then have caused the actual detachment and subsequent rock/mud/ice flow (Drobyshev, 2006; Petrakov et al.,  
 234 2008; Kotlyakov et al., 2010b). The descriptions given in these references and their sources clearly describe an event that  
 qualifies as a detachment in the sense of the present contribution. The glacier started surging again in autumn 1968 and  
 236 advanced by 4 km with speeds of up to 220 m/day (Fig. 4), but without catastrophic consequences (Hoinkes, 1972; Rototayev  
 et al., 1983). We do not know which differences in conditions, compared to 1902 and 2002, caused the glacier to not detach in  
 238 1970. Several other glaciers in the Caucasus are known to have surged in the past (Kotlyakov et al., 2010b). We found that  
 Kolka Glacier had a low surface slope of around  $13^\circ$  prior to the 2002 detachment. Evans et al. (2009b) estimated a bed slope  
 240 of  $9^\circ$  after the detachment. Over the course of several weeks before the 2002 detachment, perhaps triggered by earthquakes  
 (Kotlyakov et al., 2004), heavy rock and ice falls from the northern flank of the Kazbek massif deposited several  $10^6 \text{ m}^3$  of  
 242 material on the glacier. During this period of mass-wasting activity, the glacier changed in unusual ways: it bulged and became  
 heavily crevassed (Fig. 4), it developed a scarp at the location of the later detachment, and supraglacial ponds formed

244 (Kotlyakov et al., 2004; Evans et al., 2009b; ~~Kotlyakov et al., 2010b~~). Unusually high geothermal heat fluxes underneath the  
glacier (fumaroles and sulphur smell were reported from the glacier bed shortly after detachment), the impact energy of a large  
246 rock/ice fall, and successive loss of shear stress due to excess water pressure have been proposed as possible factors and  
ultimate triggers of the 2002 detachment (Kotlyakov et al., 2004; Evans et al., 2009b; ~~Kotlyakov et al., 2010b~~). Similarly, the  
248 additional loading of Kolka Glacier from the rock and ice falls has more recently been proposed to have increased the basal  
shear stress until it exceeded a frictional threshold given by the glacier bed material, topography, and hydraulic conditions  
250 (Kääb et al., 2018). After the detachment, lakes were visible on the Kolka Glacier bed, pointing to the involvement of large  
amounts of subglacial water in the detachment. The high mean avalanche velocities of 50-80 m/s (Huggel et al., 2005) suggest  
252 availability of large amounts of water and/or saturated fine-grained till.

The Kolka Glacier tongue is, like Devdorak Glacier, roughly at the lower elevation of the regional discontinuous permafrost  
254 zone, and the glacier must have been temperate throughout, except for the likely polythermal, or even cold steep hanging  
glaciers avalanching from the northern flank of the Kazbek massif onto its surface. The ice-rock avalanche resulting from the  
256 2002 detachment is described in detail in the above literature about the event, but we want to draw attention to the streamlined  
debris stripes, in the following called debris stripes, that were visible in the detachment zone after the event (Fig. 4d; Petrakov  
258 et al., 2004; Huggel et al., 2005), because similar patterns have also been found in several of the other cases of this study.  
Currently, the detached glacier depression is refilling and the glacier is gaining mass again. The fast recovery of the glacier  
260 volume lost by the 1970 surge, and again after the 2002 detachment, is associated with Kolka Glacier's positive mass balance,  
which stands in stark contrast to the predominant strong glacier shrinkage in the Caucasus Mountains (Kutuzov et al., 2019;  
262 Zemp et al., 2019). Kolka Glacier had already reached almost 50% of its pre-detachment volume by 2017 and is projected to  
accumulate 60–70% of its pre-detachment volume by 2025 (Petrakov et al., 2018; Aristov et al., 2019).



264

266

268

270

**Figure 4: Kolka Glacier, Mount Kazbek. (a) Kolka Glacier surged in 1969/70. Satellite image: Corona, 20 Sep 1971 (credit: USGS). (b) Landsat image, 3 Oct 2001 (credit: USGS). (c) Days and weeks before the 2002 detachment, rock and ice falls/avalanches were observed onto the glacier, and the left lateral margin of the glacier was bulged and heavily crevassed. Satellite image: Landsat, 20 Sep 2002, a few hours before detachment (credit: USGS). (d) Quickbird satellite image (© Maxar), 25 Sep 2002, 5 days after detachment. The position of the image sections is indicated in Fig. 2. The location of debris stripes in avalanche direction is indicated.**

272

### 3.2 Rasht, Pamir/Tajikistan

274

In 2017 and 2019, two glacier detachment events happened on the north side of the Peter the First Range (or Petra Pervogo Range, or Peter the Great Range), in the Pamir Mountains of Tajikistan. The resulting masses of both events travelled north into the Rasht Valley through which the Surkhob River flows that later forms the Vakhsh River (Fig. 5).

### 276 3.2.1 Event of 2017

The 2017 event, first mentioned in Dokukin et al. (2019), happened between 10 and 11 July 2017 (Planet images). A glacier  
278 of roughly 1000 m length and 240 m width detached (upper scarp ca. at 3600 m a.s.l.) and the resulting ice-rock avalanche  
flowed down a narrow valley towards the village Tojikobod in the Rasht Valley (Figs. 5 and 6, Tab. 1). In satellite imagery  
280 taken shortly after the event (Planet, Maxar), ice remains can be recognized over a horizontal distance of about 8 km, down to  
an elevation of about 2160 m a.s.l. Beyond this point, a considerable debris/mud flow must have continued for another 2 km  
282 or so. The detached glacier had a surface slope of around  $16^\circ$  (High Mountain Asia DEM; Shean, 2017). We measured  
increased surface speeds of up to 5.8 m/day in early July 2017 (compared to a few dm/day in 2016; velocities from repeat  
284 Planet data) and detected unusual lateral crevasses delineating the later detachment area in images from as early as May 2017  
(Fig. 6). The glacier is likely not surrounded by permafrost (Obu et al., 2019).

286 To roughly estimate the event volume we derive the ice thickness along the center flow line of the glacier based on an estimated  
basal shear assuming a driving stress of  $1.2 \cdot 10^5$  Pa as suggested for mountain glaciers, a slope of  $16^\circ$ , and a form factor of 0.8,  
288 which then results in a thickness of around 60 m (Cuffey and Patterson, 2010). Multiplying half of this depth (i.e. assuming a  
triangular cross-section) with the detached area (ca. 200,000  $\text{m}^2$ ) gives a first volume estimate of roughly  $6 \cdot 10^6$   $\text{m}^3$ . Whereas  
290 satellite images after detachment suggest that much of the glacier bed might actually have a triangular cross-section, it may  
have been more shallow in the lowermost and uppermost parts. As an order of magnitude, we suggest a detachment volume of  
292  $5 \cdot 10^6$   $\text{m}^3$  and assign a conservative error of  $\pm 1 \cdot 10^6$   $\text{m}^3$  to this estimate.

The cirque from which the 2017 event originated was also the source of other slope instabilities over recent years. Another  
294 (much smaller) ice-rock avalanche from a neighbouring glacier occurred between 15 and 24 July 2016 (dates from Planet  
images), with a horizontal reach of roughly 5.5 km. A large debris flow descended the same valley in late August 2016, starting  
296 from the same cirque, likely entraining deposits of the July 2016 avalanche, and reaching the Surkhob River 19.4 km  
downstream where it destroyed several buildings, bridges and agricultural fields.

### 298 3.2.2 Event of 2019

Between 2 and 3 August 2019 a second glacier, ca. 14 km to the west of the one that collapsed in 2017, detached (Figs. 5, 7).  
300 This glacier was slightly smaller than the 2017 one, and had a surface slope of around  $20^\circ$ . The resulting ice-rock avalanche  
travelled north down a narrow valley towards the Rasht Valley, over a horizontal reach of 6.5 km and a vertical drop from  
302 3350 (upper scarp) to 1850 m a.s.l. Superelevations of the ice-rock avalanche path of up to almost 200 m above valley bottom  
suggest high avalanche speeds (McClung, 2001). We estimated the detached volume in the same way as described for the 2017  
304 event (section 3.2.1) and computed a volume of  $4.5 \pm 1 \cdot 10^6$   $\text{m}^3$  (glacier area ca. 230,000  $\text{m}^2$ ; centreline depth 50 m). Based on  
pre- and post-event WorldView stereo DEMs Leinss et al. (2020) estimate a maximum erosion depth of 90 m and a detachment  
306 volume of  $8\text{-}9 \cdot 10^6$   $\text{m}^3$ , i.e. significantly more than our rough general model.

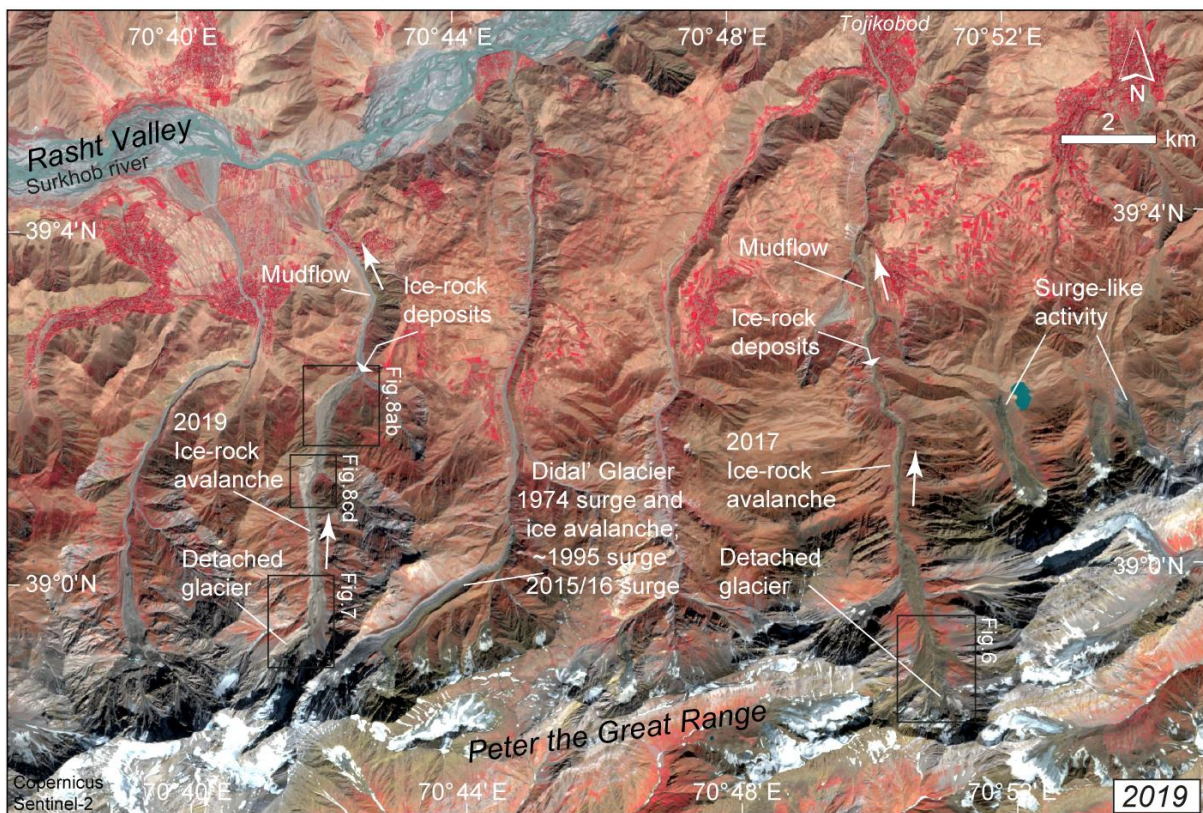


308 This glacier also showed increased sliding speeds and crevassing around the later detachment area for at least 2-3 weeks before  
the failure. For the end of July 2019 we found surface speeds of roughly 2.5 m/day, a marked increase compared to roughly <  
0.1 m/day during 2017–2018 (repeat Planet data). The glacier did not show any visual signs of destabilisation between 2015  
310 and 2018 (Planet images). In 2007 (Maxar; see Supplement) the glacier looked heavily crevassed, possibly an indication of a  
surge-like advance. This condition is still visible in Landsat data 5-6 years later, though less certain due to the lower resolution  
312 of Landsat data (no other data is available to us between 2007 and 2015). Landsat data also suggest that the glacier experienced  
a similar advance in the early 1990s. Under the limitation of the reduced spatial resolution of the Landsat data, however, we  
314 do not find signs of a large detachment event or large ice-rock avalanche. Nevertheless, we draw attention to a surprisingly  
vegetation-free landform visible downstream of the 2019 detachment in pre-event imagery (Fig. 8). The lack of vegetation,  
316 the streamlined microtopography, and zones of rough and chaotic microtopography that resemble avalanche or debris flow  
deposits (Fig. 8; Supplement), led us already before the 2019 event to interpret this landform as a possible geomorphological  
318 imprint of an earlier ice-rock avalanche (Kääb, 2019). Meanwhile, this landform has been overrun by the August 2019 ice-  
rock avalanche, leaving similar new forms, and suggesting that the landform now buried could have originated from a similar  
320 detachment event, probably before 1961 (year of earliest Corona satellite image). Between the 1961 Corona images and very  
high-resolution images from just before the 2019 avalanche no significant changes are visible on the landform.

322 Very-high resolution satellite images over the Peter the First Range suggest abundance of weak bedrock and fine sediments.  
All over the range, signs of large debris flows, rock avalanches or ice-rock avalanches are visible in high resolution satellite  
324 images (Maxar, CNES/Airbus, Planet; Leinss et al, 2020). The Pamirs are known to be very geomorphologically active, with  
a number of associated hazards (Mergili et al., 2012; Gruber and Mergili, 2013; Strom and Abdrakhmatov, 2018) and a cluster  
326 of surge-type glaciers (Kotlyakov et al., 2008; ~~Kotlyakov et al., 2010a~~; Gardelle et al., 2013; Sevestre and Benn, 2015; Lv et  
al., 2019; Goerlich et al., 2020). A number of glaciers in the Peter the Great Range were surging at the time of writing or have  
328 done so in the recent past (Fig. 5). Didal Glacier (ca. 12° steep) surged around 1995, and again during the winter 2015/16  
where it advanced by 2.5 km over a few months. In the valley below Didal Glacier we note lack of vegetation in the valley  
330 and landforms that could well stem from a former ice-rock avalanche. Kotlyakov et al. (2010a) mention a 2.2 km long ice  
avalanche from Didal Glacier in 1974. In comparison, the bottom of the valley through which the 2017 ice-rock avalanche  
332 descended (section 3.2.1) was partly tree covered before, suggesting that no event like the 2017 one has happened there in the  
recent past.

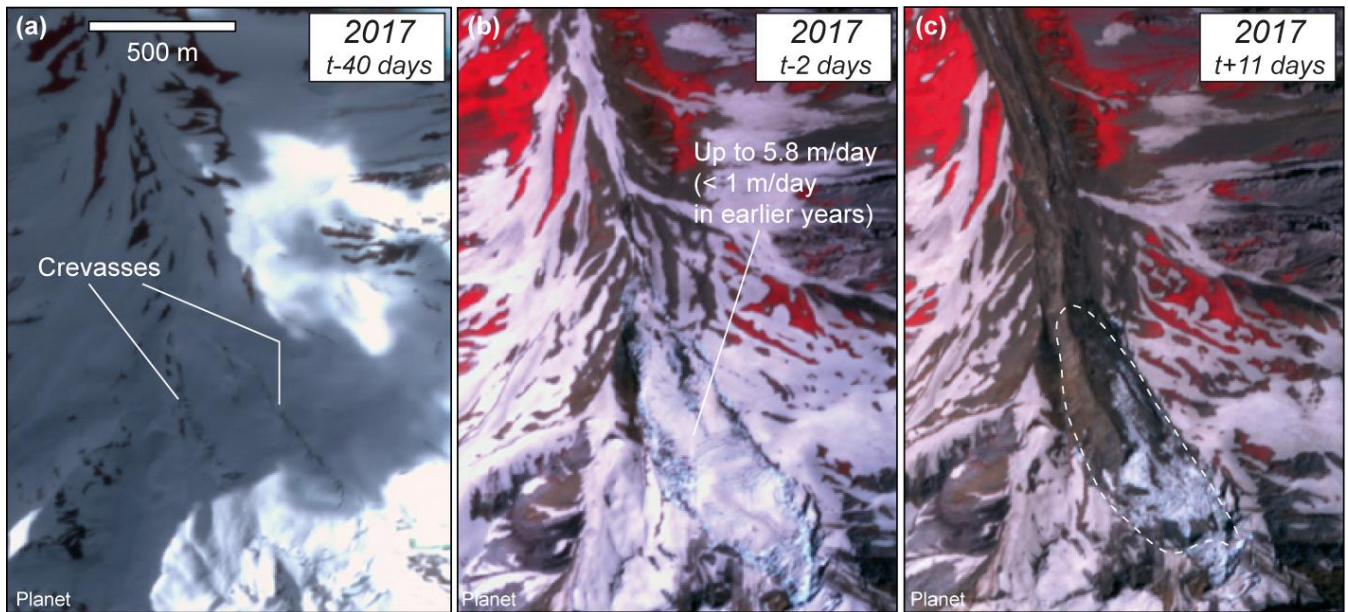
334 Even if not documented in detail in an internationally accessible format so far, to our best knowledge, both the 2017 and 2019  
detachments and their downstream effects were very likely noted by the local communities as the lowermost ice/rock deposits  
336 stopped not far from settlements, agricultural fields, and pastures, and very-high resolution images (Maxar) show that flooding  
happened close to houses and two irrigation channel bridges were partially destroyed.

338

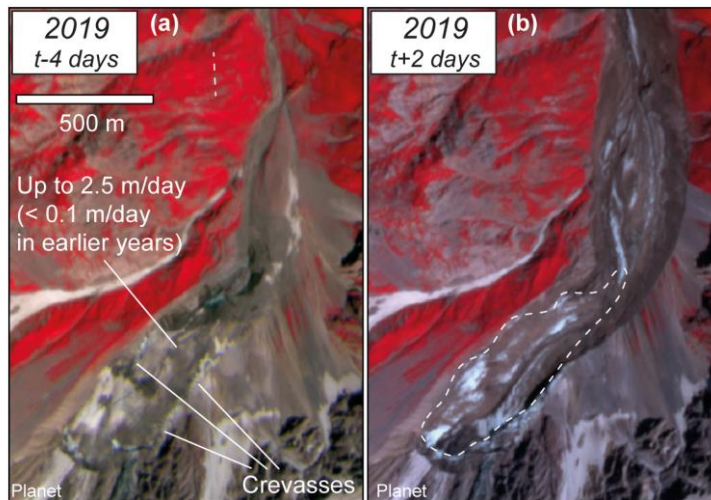


340 **Figure 5: Rasht Valley and Peter the Great Range, Tajikistan. Locations of the 2017 and 2019 ice-rock avalanches are**  
 342 **indicated. Satellite image: Sentinel-2, 19 Sep 2019 (credit: Copernicus Sentinel data).**





344 **Figure 6: Planet images over the Rasht Valley glacier detachment of around 10 July 2017 ( $\approx t$ ). (a) 31 May 2017, (b) 8**  
 346 **July 2017, (c) 21 July 2017. Abnormal marginal crevassing and enhanced speeds were visible several weeks before the**  
**detachment. See Fig. 5 for location. (Satellite images © Planet).**



348 **Figure 7: Planet images over the Rasht Valley glacier detachment of around 2 Aug 2019 ( $\approx t$ ). (a) 29 Jul 2019, (b) 4 Aug**  
 350 **2019. See Fig. 5 for location. (Satellite images © Planet).**



354 **Figure 8: Location of the ~2 Aug 2019 Rasht Valley ice-rock avalanche. See Fig. 5 for image location. (a) and (c): 30 Jul**  
 356 **2007 (© Google Earth and Maxar). (b) and (d): 20 Aug 2019 (© Google Earth and CNES/Airbus). Before the 2019**  
 event, traces of a potential former large mass flow were visible (lack of trees in the valley, sparse vegetation, debris  
 stripes).

358

### 3.3 Aru, 2016, western Tibet

360 On 17 July 2016, a massive volume of glacier ice detached from the lower part of an unnamed glacier in the Aru Range (Rutok  
 County, China) in the western Tibetan Plateau (termed Aru-1). The fragmented ice mass ran out 6 km beyond the glacier  
 362 terminus, killing nine herders and hundreds of their animals, and reached the Aru Co lake (Tian et al., 2017; Kääh et al., 2018).  
 The ice debris covered 8–9 km<sup>2</sup> and a volume of  $68 \cdot 10^6$  m<sup>3</sup> was calculated for the detached glacier part. On 21 September  
 364 2016, a second glacier (Aru-2) detached just a few km south of Aru-1 (Fig. 9). Similar to the July event, the glacier ice  
 fragmented and transformed into a mass flow. The glacier debris in the second detachment covered 6–7 km<sup>2</sup> with a detached  
 366 glacier volume of  $83 \cdot 10^6$  m<sup>3</sup>. The maximum glacier thicknesses that detached were around 115 m (Aru-1) and 145 m (Aru-2),

and maximum deposit thicknesses were around 25 m (Aru-1) and 80 m (Aru-2) (Kääb et al., 2018). The mean speeds of the  
368 Aru ice-rock avalanches were estimated to 30–50 m s<sup>-1</sup>, with maximum speeds of 70–90 m s<sup>-1</sup> (Kääb et al., 2018). (For a  
satellite image of the current situation of the Aru glaciers and the deposits, see the Supplement)

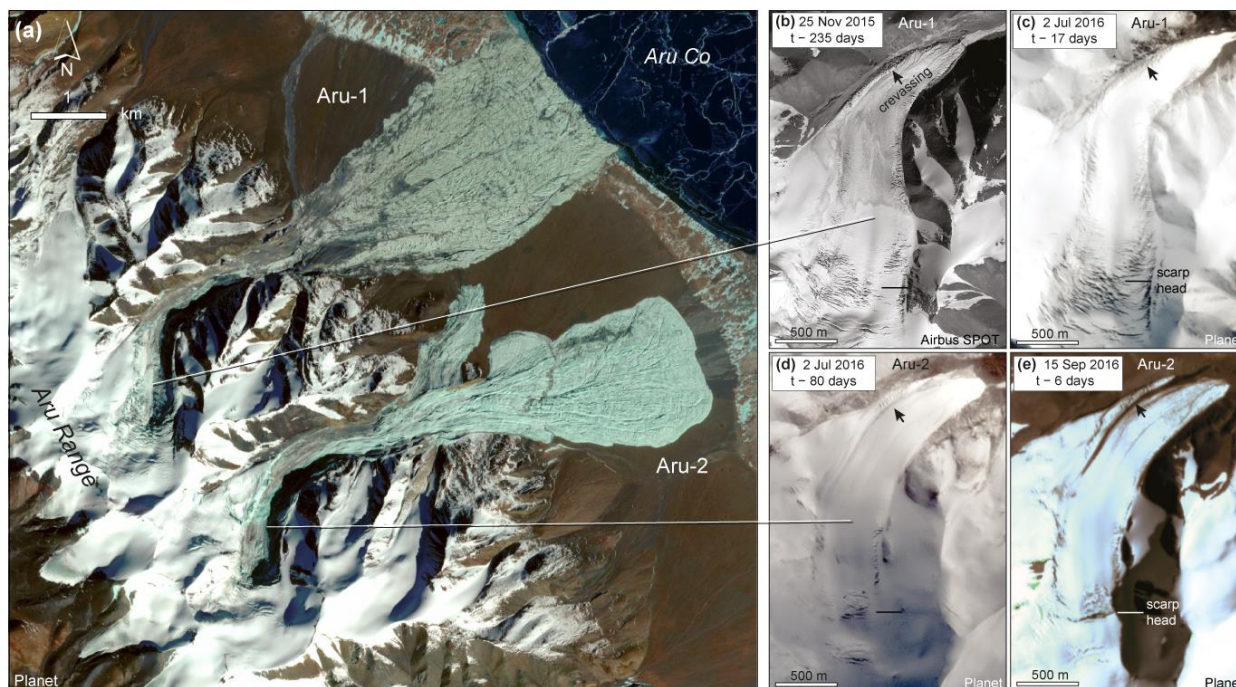
370 Glaciers in the wider region around the Aru range are part of the Karakoram – West Kunlun – Eastern Pamir anomaly  
(Treichler et al., 2019) and experienced a slight increase in thickness of around 0.20–0.30 m/a water equivalent since the early  
372 2000s (Brun et al., 2017; Kääb et al., 2018). Positive mass-balances of the Aru glaciers (modeled based on ERA-interim  
reanalysis data; Kääb et al., 2018) and the widespread growth of endorheic lakes confirmed a precipitation increase in the  
374 region from the late 1990's on (Treichler et al., 2019). Driven by these positive mass balances, the two Aru glaciers underwent  
surge-like accelerations and mass transfers over several years before the detachments (Gilbert et al., 2018; Kääb et al., 2018).  
376 In apparent contrast to the positive mass balances and the surge-like mass transfers, the Aru-1 and Aru-2 glaciers both retreated  
by around 500 m between 1970 and 2015.

378 Since at least 2011 and until 2014, the sections above the eventual detachment zones of both Aru glaciers subsided.  
Simultaneously, glacier sections below bulged upwards. The rates of elevation change derived for 2011–2014 indicate that a  
380 down-glacier mass transfer had already begun during the second half of the 2000s (Gilbert et al., 2018). A modelling study  
based on the observed elevation changes reconstructed changes in basal friction and horizontal velocity prior to the  
382 detachments (Gilbert et al., 2018). It showed that the two glaciers were close to their steady state geometry with no/little sliding  
until 2010. Thereafter, decreasing friction under the whole detachment area of Aru-1 and in more localized zones of Aru-2  
384 started to trigger the surge-like mass transfer. Modelling the glaciers' thermal regimes revealed that the frictional changes  
likely occurred in temperate areas of the two glaciers and that stress concentration occurred at the cold-ice margins (Gilbert et  
386 al., 2018). The surge-like changes of basal friction under the Aru glaciers were thus likely not associated with a change of the  
glaciers' thermal regimes but rather with a change in friction due to increasing water pressure in the already temperate areas.  
388 During the instability development, basal shear stresses in the detachment area dropped by an order of magnitude, leading to  
significant stress concentrations at the detachment margins and in a few spots under the glaciers. These stress concentrations  
390 led to strongly enhanced crevassing at the glacier margins and the zone of the later scarp head several months prior to the Aru-  
1 detachments. Fast-developing crevasses appeared only three weeks before the Aru-2 detachment and were discovered in  
392 satellite images in time to alert Chinese authorities.

The Aru glaciers are surrounded by continuous permafrost of -3 to -4 °C mean annual ground temperature (Obu et al., 2019).  
394 Field observations in the detachment and runout zones showed no presence of a hard-bed lithology beneath the glaciers, and  
very few large boulders were observed in the runout paths (own field visit and Lei et al. 2021). Rather, extensive deposits of  
396 soft, unconsolidated and fine-grained lithologies were identified. The Aru glaciers, situated in a region of positive or zero mass  
balances (Brun et al., 2017; Treichler et al., 2019) could well build up again to a size similar to the one before their 2016



398 collapses. Especially in the path of the Aru-1 avalanche, streamlined debris stripes, not present before the event, are well visible  
at several locations in high-resolution satellite data (Supplementary Fig. S5). We find no other evidence for a similar event in  
400 the recent past at the site, so finding two similar events at neighbouring glaciers is rather remarkable.



402 **Figure 9: Satellite images of the Aru glaciers, western Tibet, and their detachments. (a) Planet infra-red false-colour**  
404 **satellite image of 29 November 2016, after both glaciers collapsed (© Planet). (b) Enhanced crevassing on Aru-1 glacier**  
406 **(SPOT7, © Airbus). Time  $t$  refers to detachment date (17 July 2016 for Aru-1, 21 September 2016 for Aru-2). Note the**  
**particular crevassing at the northern curve of the glacier. (c), Aru-1 (Planet). (d), Aru-2 (SPOT7, © Airbus). (e), Aru-**  
**2 (© Planet), six days before collapse. The horizontal line in panels (b-e) indicates the scarp head positions of the later**  
**detachments.**

408

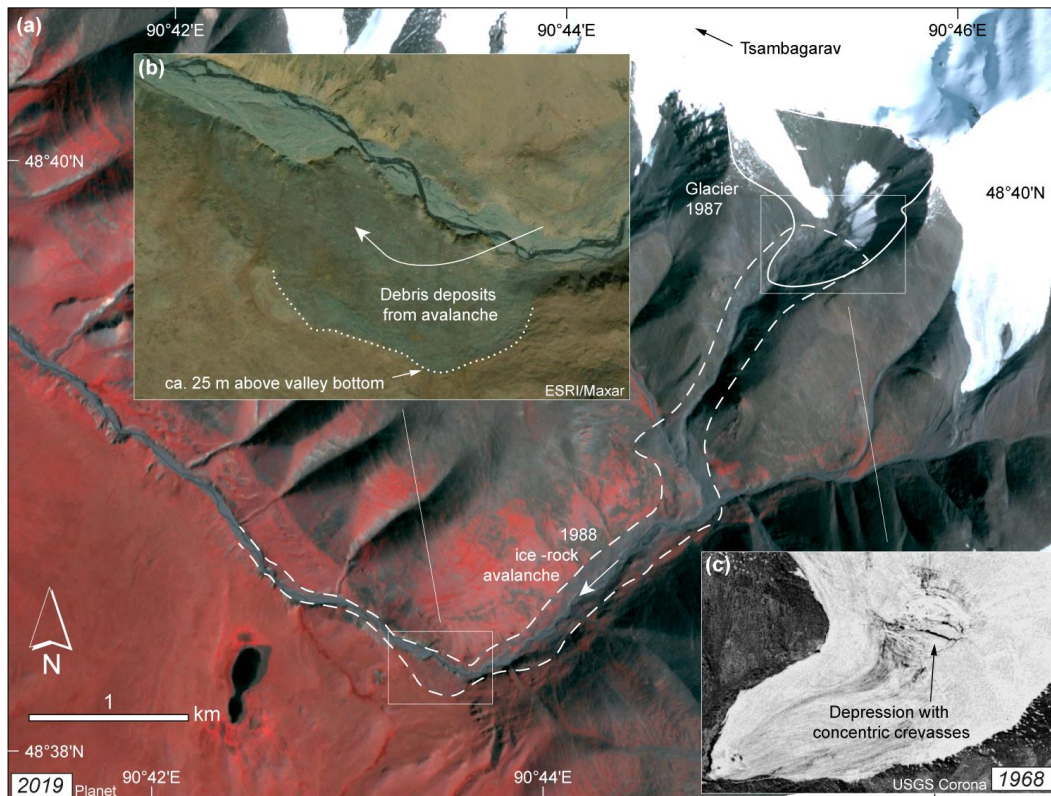
### 3.4 Tsambagarav, 1988, Altai, western Mongolia

410 Information about the 1988 Tsambagarav event is mainly relying on observations and interpretations by Avdeev et al. (1989).  
On the evening of 9 Aug 1988 (local time) the lower part of an unnamed glacier on the southern flank of Tsambagarav mountain  
412 (4193 m a.s.l.), Altai mountains, western Mongolia, detached and formed an ice-rock avalanche. The avalanche travelled about  
5.5 km (Avdeev et al., 1989), and from Landsat data we suggest the last 1-2 km might have been a mud flow (Fig. 10). As a  
414 peculiarity of this event, it seems to have been preconditioned by the 23 July 1988 Tsambagarav M6.4 earthquake. As a  
consequence of this earthquake, a large block (ca.  $6 \cdot 10^6$  m<sup>3</sup>) of the lower part of the glacier was separated from its upper parts

416 and displaced a few meters to south eastern direction. Melt water could then reach the glacier bed beneath the ice block through  
the developing crack. On 9 Aug 1988, the ice block detached from the glacier bed. Avdeev et al. (1989) describe the path of  
418 the resulting ice-rock avalanche in detail, but here we want to highlight two aspects of it. First, after about 1.8 km, the avalanche  
jumped (obviously at high speeds) over a 70-m tall ridge, leaving the ground on leeward side of the ridge intact. Second,  
420 Avdeev et al. (1989) estimate the deposited avalanche volume to about  $12 \cdot 10^6 \text{ m}^3$  (vs.  $6 \cdot 10^6 \text{ m}^3$  detached ice volume) indicating  
that the detachment must have eroded and ingested substantial amount of material along the way. The large debris content of  
422 the deposits likely also played a role in that it took almost 30 yr for the ice content to melt out completely (Agatova et al.,  
2020).

424 On a Corona satellite image from 11 Aug 1968, two obvious transverse crevasses, surrounded by a number of smaller  
concentric crevasses can be seen at the location of the upper scarp of the 1988 earthquake-triggered rupture and later glacier  
426 detachment (Fig. 10c). The entire feature has a diameter in the order of 150 m. Close visual inspection leads us to interpret the  
feature as a depression in the glacier surface. From many contemporary Planet satellite images with snow cover, and from  
428 Landsat 8 thermal data, we do not find indications of enhanced geothermal activity at the depression location. Today, the  
location appears to be the place for a spring that concentrates the subsurface runoff of the entire cirque. This spring could  
430 already have existed in 1988 and led to reduced basal friction and enhanced basal melt at its position, and thus to a depression  
on the glacier surface. Also today's glacier remains show a few obvious crevasses in the same area. Overall, the 1988  
432 detachment seems to have happened at a pre-existing weakness and strongly crevassed location of the glacier.

Avdeev et al. (1989) note a slope angle of the detachment area of  $20^\circ$ - $25^\circ$ . From the SRTM1 DEM we find a slope of the  
434 valley bottom of around  $15^\circ$  at the location of the detached glacier part and assign an arbitrary  $20^\circ$  slope to the pre-detachment  
glacier. Since the detachment in 1988, the entire glacier has shrank substantially and as of 2020 only a small part of it is left.  
436 The detachment site lies in continuous permafrost with mean annual ground temperatures in the order of  $-10^\circ \text{C}$  (Obu et al.,  
2019). Avdeev et al. mention the existence of shattered bedrock in and around the glacier bed, and this is in line with visible  
438 interpretation of contemporary high-resolution satellite images. Ultimately, we cannot draw conclusions about the existence  
of particularly fine-grained sediments at the detachment site. From the weak avalanche traces that are still visible in high-  
440 resolution satellite images, it would be difficult to recognize the site as a place of a former glacier detachment and ice-rock  
avalanche. However, with the information from Avdeev et al. available, one can still detect signs of the past avalanche such  
442 as debris stripes oriented in avalanche direction and debris deposits inundating the mountain grassland (Fig. 10b). We do not  
find similar signs in other glacier valleys surrounding Tsambagarav, and the Corona spy satellite image from 11 Aug 1968  
444 suggests that nothing like this has happened here before. Lastly, we are not aware of recent surge-type activity of glaciers in  
the Altai.



446

448

450

452

**Figure 10: (a) Location of the 9 Aug. 1988 Tsambagarav glacier detachment. Glacier outline of 1987 from Landsat TM indicated as bold line, rough outline of ice-rock avalanche path from 1989 Landsat data as dashed line. The **small** white rectangle indicates the position of panel (b) (Satellite image, 2019, © Planet). (b) Detail of 2015 Worldview data (© ESRI/Maxar). The upper elevation of debris deposits from the avalanche in this right turn is about 25 m above valley bottom. (c) A 11 Aug 1968 photo from a Corona satellite shows crevasses around a depression on the glacier surface, at the location of the upper scarp of the 1988 detachment (credit: USGS).**

454

### **3.5 Amney Machen, 2004, 2007, 2016, and 2019, eastern Tibet**

456

458

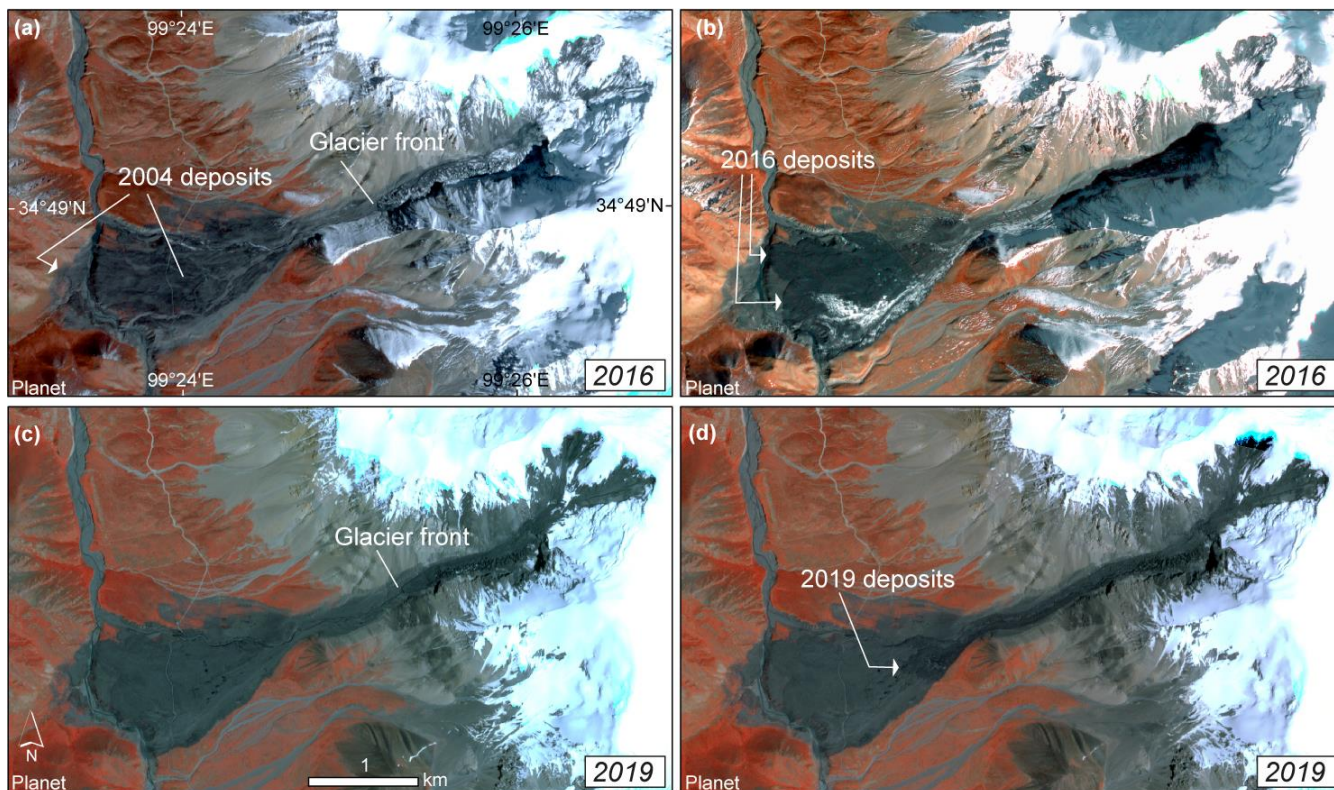
460

462

A sequence of surge-like advances, some of them ending in detachments of the glacier tongue, have been observed for a glacier in the Amney Machen mountain range, Eastern Tibet (Fig. 11, Tab. 1; Paul, 2019). The isolated mountain range is home to several surging glaciers (Wenying, 1983). The first ice-rock avalanche happened between 26 January and 3 February 2004, and the involved volume was estimated to be  $20\text{-}25 \cdot 10^6 \text{ m}^3$ , perhaps up to  $36 \cdot 10^6 \text{ m}^3$  according to a local information sign-board (Paul, 2019). Three years later, between 23 September and 2 November 2007, a second detachment followed a surge-like recovery of the glacier tongue that had detached in 2004. The 2007 detachment was considerably smaller in volume than the one in 2004. A third detachment, also smaller than that in 2004, occurred between 4 and 7 October 2016 (date from Planet images). Following this event, the glacier tongue started to recover again, and another small avalanche occurred from it



between 9 and 20 July 2019. Paul (2019) notes the weak rocks and fine sediments visible in the rock ribs in the glacier's steep source area. The glacier recovered rapidly after each detachment, suggesting that it is largely nourished by ice and rock fall from the headwall, and that a rock/ice melange likely makes up the glacier tongue. The surface slope of the detaching lower part of the glacier is around  $15^\circ$ . The glacier lies in an area of continuous permafrost with ground temperatures in the order of  $-3$  to  $-6^\circ\text{C}$  (Obu et al., 2019). Debris stripes oriented in avalanche direction are visible in high-resolution satellite images (not shown).



470 **Figure 11: Unnamed glacier in the Amney Machen range, Tibet. Satellite images of (a) 2 Oct 2016, (b) 23 Oct 2016, (c)**  
472 **9 Jul 2019, and (d) 25 Jul 2019. Detachments of the glacier tongue happened before (a), between (a) and (b), and between**  
**(c) and (d). (Satellite images © Planet).**

### 474 **3.6 Sedongpu/Gyala, 2018, south-eastern Tibet**

During 2017 and 2018 the Sendongpu basin below the western flank of the Gyala Peri peak (7294 m a.s.l.; Fig. 12) in south-  
476 eastern Tibet was the source of a series of large mass flows. Some of them dammed the Yarlung Tsangpo river, which posed a serious flood hazard to the upstream Gyalha village and large downstream areas, and triggered hazard management and

478 investigations of the causes (Tong et al., 2018; Liu et al., 2019; Chen et al., 2020). The largest of the mass flows stemmed  
from the detachment of a large, low-angle glacier in 2018.

### 480 **3.6.1 Events before 2018**

In order to elucidate significant elements of the recent mass-flow history from the basin that might have conditioned the 2018  
482 detachment and that are not documented in detail elsewhere, we start our description with the oldest satellite data available to  
us. In Corona satellite reconnaissance data of 8 Dec 1969, a narrowing in the Yarlung Tsangpo river where the Sedongpu  
484 valley joins the river, points to deposits from previous mass flows. However, trees on these deposits suggest no recent large  
mass flow activity. The main glacier in the basin, here called Sedongpu Glacier (Fig. 12), shows some signs of enhanced flow  
486 such as large crevasses. On Corona satellite data of 6 Nov 1974 the glacier has advanced some 800 m into steeper terrain.  
Fresh traces of a large mass flow are visible between the glacier front and the main Yarlung Tsangpo river, and fresh deposits  
488 seem to have covered or destroyed the forest on the older deposits in the river, but the main glacier is still in place. The glacier  
showed one single tongue in 1969, but had split into two tongues during its advance by 1974, a feature that it still exhibited in  
490 2016. Chen et al. (2020) describe an ice avalanche from the Sedongpu basin that dammed the Yarlung Tsangpo river in 1968,  
but do not mention any other events before 2014. From our interpretation of the Corona satellite data there was either one more  
492 event between 1969 and 1974, or the event dated ‘1968’ actually happened a few years later. The next large mass flow (listed  
as ice avalanche in Chen et al. (2020) and debris flow in Tong et al. (2018); we interpret at least a large debris content)  
494 happened in 2014. The source of the mass flow must have been in the upper part of the main Sedongpu Glacier or its headwall,  
as both lateral moraines of the glacier were heavily eroded from the glacier side (RapidEye satellite data of 2013–2015). The  
496 glacier surface was not visibly changed along the glacier centre line, suggesting that the mass flow must have flowed along  
both glacier margins. Although difficult to determine in the satellite data available to us, the flow may have eroded the  
498 lowermost part of the glacier tongue.

Between 20 and 27 Oct 2017 (Planet and Sentinel-2 images) a huge rock avalanche started high up from the north ridge of  
500 Gyala Peri and ran over large parts of the Sedongpu basin and down to Yarlung Tsangpo, damming the river (Figs. 12 and 13).  
The event seems to have had a severe impact on Sedongpu Glacier. We generated two elevation models from 13 Nov 2015  
502 Spot6 and 30 Dec 2018 Pleiades tri-stereo data that produced robust results despite the extreme topographic conditions.  
Differencing the two DEMs indicates that the October 2017 rock avalanche removed around 17 and 33·10<sup>6</sup> m<sup>3</sup> of material  
504 from two close-by but separated areas, respectively (Fig. 12c). If both failures happened as part of the same event, the total  
volume of 50·10<sup>6</sup> m<sup>3</sup> makes this one of the larger rock avalanches detected in recent decades. Based on visual inspection of  
506 satellite data, we consider it very likely that the avalanche also involved small glaciers from the west wall of Gyala Peri and  
incorporated ice from the surface of the glaciers lower down, as it ran over them. The Chinese seismic database registered two  
508 large ‘landslide’ events on 22 Oct 2017: A M3.2 event at 6:20 about 16 km west of Sedongpu and a M4.0 event at 6:22 directly  
at Sedongpu. Chen et al. (2020) and Tong et al. (2018) confirm that at least the latter signal stems from the Gyala Peri rock-

510 ice avalanche. Subsequent satellite images suggest that the avalanche must have changed the surface of Sedongpu Glacier  
drastically. It covered the glacier and much of the basin with debris and dust. A small, surge-like lobe with ponds on it appeared  
512 at the transition between the headwall and the tongue of Sedongpu Glacier (Fig. 13, and GoogleEarth, BingMaps). The eastern  
tributary glacier to Sedongpu Glacier also showed a surge-like lobe (Sentinel-2, Planet, GoogleEarth). Driven by the  
514 geomorphological changes in the basin, a series of debris flows, some involving ice and likely nourished from the large  
amounts of unconsolidated debris left behind by the rock-ice avalanche, occurred after 22 Oct 2017 and into 2018 (Tong et al.,  
516 2018; Chen et al., 2020). The two 18 Nov 2017 M5.2 and M6.9 Linzhi/Milin/Nyingchi earthquakes, with epicentres only a  
few km from Sedongpu, may have contributed to triggering of the debris flows (Hu et al., 2019). Lastly, we report hundreds  
518 of small earthquakes recorded under the Gyala Peri massif in 2017 and 2018, most up to M2, some up to M3, which we have  
not analysed further in the present study (Chinese Earthquake Data Center, 2020).

### 520 **3.6.2 Detachment in 2018**

Following the 2017 rock-ice avalanche the main Sedongpu Glacier underwent drastic changes (Fig. 13). Ponds developed on  
522 its surface and along the margins. Surface velocities increased from a background velocity of  $\sim 0.3$  m/d (ca. 100 m/a) in 2017  
to 1–3 m/d end of January 2018, 10 m/d in mid-September 2018, and 25 m/d in mid-October 2018 (velocities derived from  
524 offset tracking in repeat Planet, Sentinel-1, and Sentinel-2 data). The glacier surface showed several crevassed bulges (Fig.  
13b) in January 2018, and progressively more crevasses appeared as the glacier tongue expanded (Fig. 13c). The lower, flat  
526 glacier part separated from the steep head-wall. Between 19 Sep 2018 (last optical image due to later cloud cover) and 13 Oct  
2018 (Sentinel-1) the glacier advanced by almost 1 km. On 17 or 18 October (Tong et al., 2018; Chen et al., 2020), the entire  
528 tongue of Sedongpu Glacier detached over a length of about 3.5 km (glacier width between 250 and 550 m) (Figs. 12 and 13).  
Planet images of 27 Oct 2018 and Chinese media images confirm that large amounts of ice blocked the Yarlung Tsangpo river  
530 (Fig. 12d). Parts of the emptied glacier bed filled up with enough ice debris that another mass flow originated from there on  
29 Oct 2018. The dam in the Yarlung Tsangpo river was estimated to be roughly  $40\text{--}60 \cdot 10^6$  m<sup>3</sup> in volume (Chen et al., 2020).  
532 Differencing our 2015 SPOT6 and 30 Dec 2018 Pleiades tri-stereo DEMs (Fig. 13d) shows two areas of distinct volume loss:  
around  $80 \cdot 10^6$  m<sup>3</sup> are missing from the main branch of the glacier, and around  $50 \cdot 10^6$  m<sup>3</sup> from its terminus and frontal moraine.  
534 An ASTER satellite stereo DEM of 11 Nov 2017 suggests that the volume loss over the glacier tongue and frontal moraine  
cannot have occurred before November 2017. From our data we cannot tell how much of the total  $130 \cdot 10^6$  m<sup>3</sup> stems from the  
536 main first glacier detachment event of 17/18 Oct 2018, and how much from the 29 Oct 2018 event. However, satellite images  
indicate that the first event involved by far the largest volume. The detached glacier part had an overall slope of only 8–9°.  
538 According to Obu et al. (2019) it should have been several hundred meters below the regional permafrost limit, but cold or  
polythermal ice is certainly found in the west wall of Gyala Peri, and could theoretically be advected into the basal parts of the  
540 glacier near its tongue.

Between 19 Sep and 26 Oct 2018 (Planet) a  $\sim 9 \cdot 10^6$  m<sup>3</sup> rock(-ice) avalanche (volume from 2015 SPOT6 and 2018 Pleiades tri-  
542 stereo DEM difference) originated from the south-western flank of Gyala Peri and likely reached Sedongpu Glacier (Fig. 12).  
The avalanche covered a small glacier below its starting zone which started a surge-like advance early 2018. Due to insufficient  
544 satellite data (cloud cover in optical data; low resolution and radar shadow in SAR data), though, we cannot tell if this avalanche  
happened before, during or after the 17/18 Oct 2018 glacier detachment, and could thus have triggered the glacier detachment.  
546 Seismic records are also inconclusive regarding the rock avalanche and the glacier detachment, with two dozens of M1–2  
earthquakes recorded under the Gyala Peri massif between mid September and end of October 2018.

548 From all the evidence collected above, it seems very likely that the 22 Oct 2017 Gyala Peri rock avalanche, which travelled  
over the Sedongpu Glacier, primed the glacier for its detachment a year later, perhaps with additional influence of the 18 Nov  
550 2017 earthquakes, though the exact controlling mechanisms remain unclear. The effects that the ongoing mass-wasting  
activities from Gyala Peri had on Sedongpu Glacier can have been manifold: additional loading on the glacier can have  
552 increased normal and shear stresses, and the 2017 rock avalanche and earthquakes could have mechanically weakened the  
glacier and its bed, potentially disrupting the subglacial drainage system. The large amounts of fine dust deposited on the  
554 glacier will likely have changed (enhanced?) its surface melt rates. Lastly, independent factors such as high temperatures and  
precipitation amounts (Tong et al., 2018; Liu et al., 2019), associated with large water input into the glacier, could have  
556 complicated the changes caused by rock-avalanche impact. The supraglacial and glacier-marginal ponds, unusual on temperate  
glaciers (see Haeberli et al. 2002, Käab et al. 2004), suggest that the glacier was under high internal water pressure. The bulging  
558 ice and the strong downstream gradient in surface velocities suggest that a surge-like instability first developed in the upper  
section of the low-angle part of the glacier. Just how this instability propagated down-glacier, whether by exerting pressure on  
560 the lower glacier from above, or by a propagation of exceptionally low basal friction values (Thogersen et al., 2019) remains  
unclear. High-resolution imagery and media photos of the glacier bed and detachment deposits, as well as the various debris  
562 flows that originated from the basin, suggest that the detached glacier rested on a soft bed with substantial amounts of fine  
material. The geology of the area is described as marble (Liu et al., 2019), which at least opens up the possibility of fine-  
564 grained sediments.

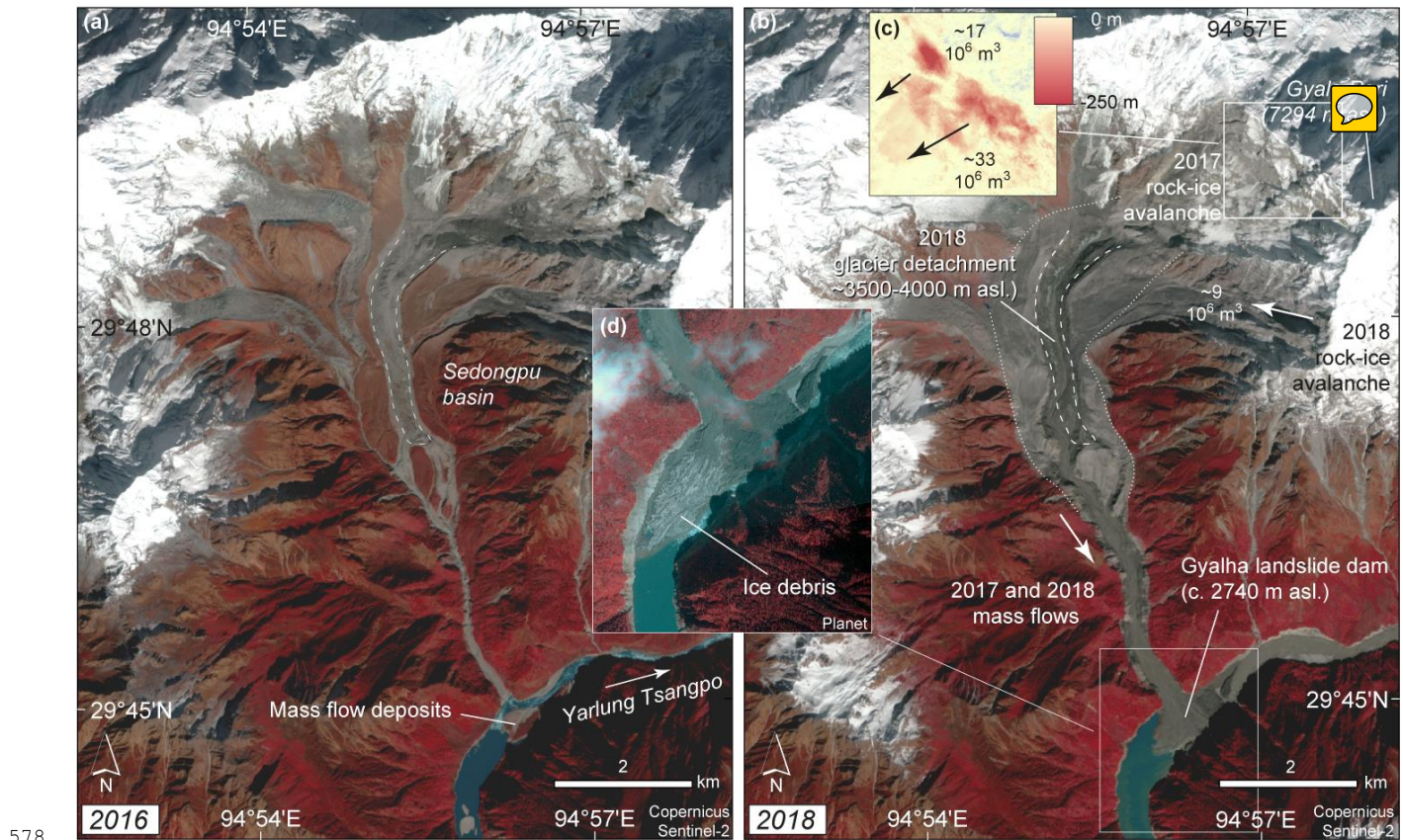
It remains to be seen to which extent the Sedongpu Glacier is able to rebuild, given the strongly negative mass balances in the  
566 region (Käab et al., 2015; Brun et al., 2017; Treichler et al., 2019, Shean et al., 2020).

### 3.6.3 Zelunglung Glacier surge-like instabilities

568 The region around Sedongpu does not seem to host any obvious surge-type glaciers. However, the events at Zelunglung Glacier  
(29.62° N, 95.00° E; GLIMS G095018E29637N, RGI60-13.01428), 20 km south of Sedongpu, are worth mentioning. In 1950,  
570 1968, and 1984 extraordinary instabilities propelled the glacier forward and blocked the Yarlung Tsangpo river (Zhang, 1992).  
The 1984 event seems to have involved only a smaller section of the glacier. Corona reconnaissance satellite images of 1969  
572 show a massive advance (by about 4.5 km compared to 2018), but no detached glacier. However, the glacier had obviously



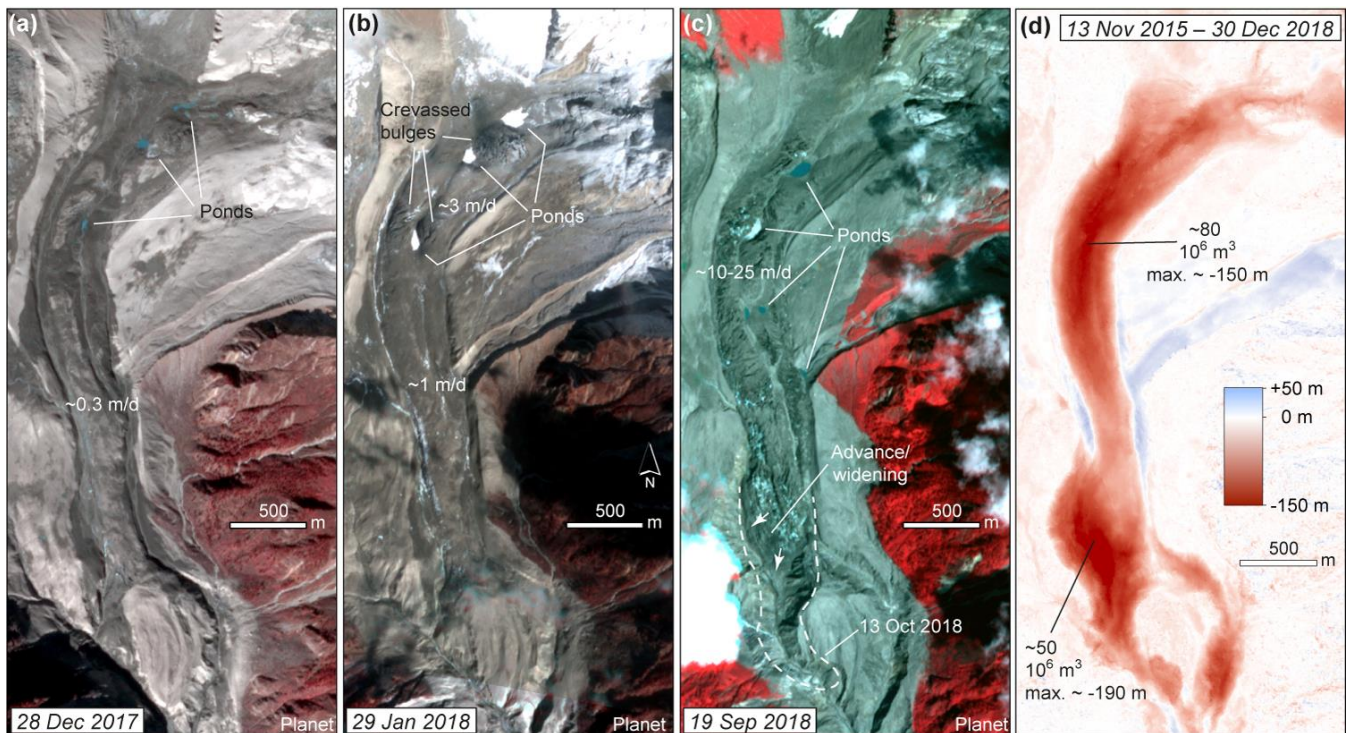
574 overridden its frontal moraine, reaching almost down to Yarlung Tsangpo. Deposits, visually similar to those of ice-rock  
 576 avalanches in general cover much of the main Yarlung Tsangpo river bed on a length of about 2.5 km downstream measured  
 from the confluence with the Zelunglung valley. Glacier advance rates of up to 1 km/h are reported for the 1950 event (Zhang,  
 1992). Such rates are far above what is typical for surges and the glacier might have, at least in 1950, undergone an event close  
 to a sudden detachment in the sense of the present contribution.



580 **Figure 12: Location of the 17/18 Oct 2018 Sedongpu glacier detachment, south-eastern Tibet. (a) Sentinel-2 image of**  
 582 **20 Nov 2016 (credit: Copernicus Sentinel data), before a series of mass flows happened that culminated in glacier**  
 584 **detachment. Already earlier, mass flows from the basin have blocked the Yarlung Tsangpo river. (b) Sentinel-2 image**  
 of 31 Oct 2018 showing the area impacted by the 22 Oct 2017 rock avalanche from the Gyal Peri peak, and the 17/18  
 Oct 2018 glacier detachment. (c) Detail of elevation model differences between SPOT6 13 Nov 2015 and Pleiades 30  
 Dec 2018 tri-stereo data. Elevation losses amount up to 330 m, but the colour scale is saturated at -250 m. (d) Detail of  
 the glacier detachment deposits in the main river (© Planet; image of 27 Oct 2018, 10 days after detachment).

586

588



590 **Figure 13: (a)-(c) Evolution of Sedongpu Glacier towards instability and detachment. Average surface velocities around**  
 592 **the image dates are indicated. (Satellite images © Planet). Velocities and glacier position after 19 Sep 2018 (25 m/d)**  
 594 **are derived from Sentinel-1 radar images. (d) Detail of elevation model differences between SPOT6 13 Nov 2015 and**  
**Pleiades 30 Dec 2018 tri-stereo data. Elevation losses amount up to 190 m, but the colour scale is saturated at -150 m.**

### 3.7 Flat Creek, 2013, 2015 and 2016, Alaska

596 Flat Creek Glacier, a small glacier in the north-eastern corner of Alaska's St. Elias mountains (Fig. 14), produced two large  
 598 glacier detachments in 2013 and 2015. This region in Alaska is home to many surging glaciers (e.g., Harrison et al., 2015;  
 600 Sevestre and Benn, 2015; Kochtitzky et al., 2019), and a glacier in a valley adjacent to Flat Creek surged between 2012 and  
 602 2016. Located in the rain shadow of the St. Elias range, the area receives on average about 350 mm of precipitation annually  
 (2008 – 2018). A mean annual air temperature of  $-14^{\circ}\text{C}$  at the former terminus of Flat Creek Glacier, ground temperature  
 measurements, and electrical resistivity tomography surveys strongly suggest that the headwall is underlain by continuous  
 permafrost (Jacquemart et al., 2020).



604 On 5 August 2013, the lower 500 m of the glacier detached, releasing  $6.8\text{-}11.2 \cdot 10^6 \text{ m}^3$  of ice and lithic material. On 31 July  
 2015, most of the remaining glacier ice (up to the drainage divide) detached, evacuating an additional  $17.6\text{-}20.1 \cdot 10^6 \text{ m}^3$   
 (Jacquemart et al., 2020). Both events produced runouts of over 11 km (angle of reach  $6\text{-}7^{\circ}$ ), deposited vast amounts of lithic



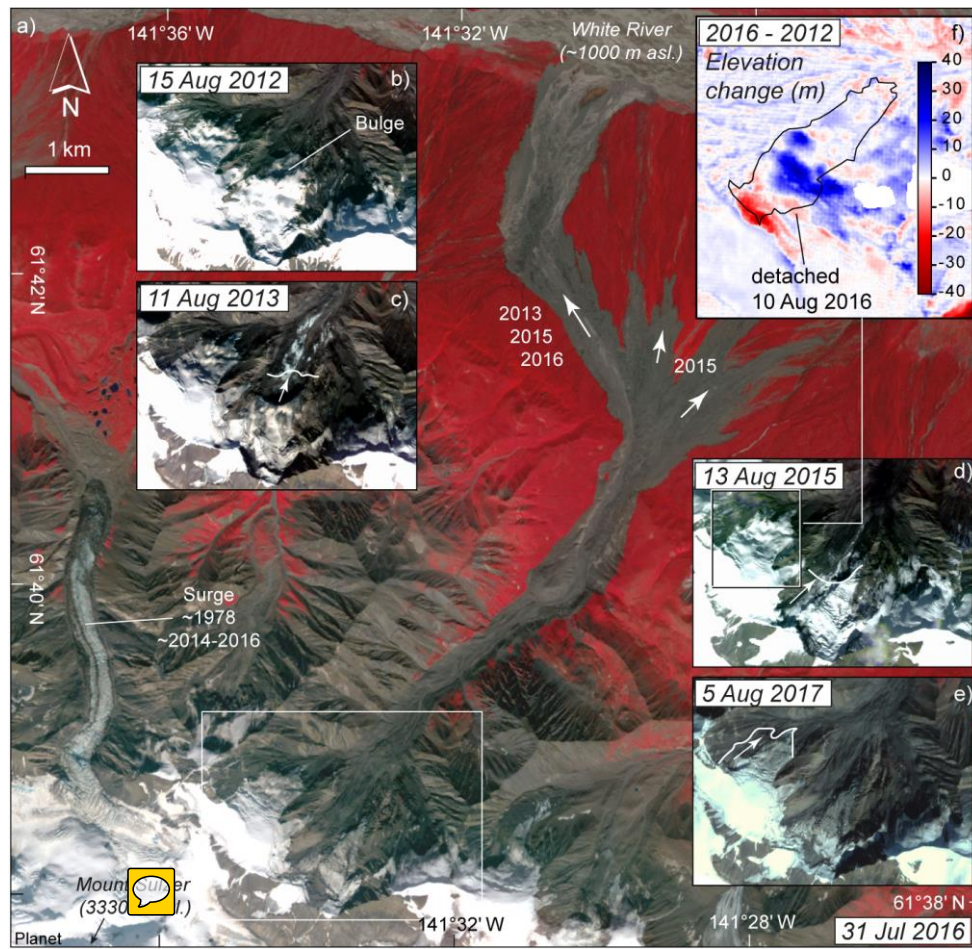
606 material, and buried several km<sup>2</sup> of old growth forest (400+ years old). The large amount of fine-grained sediment found in  
the deposits suggests that the failures occurred within the glacier bed rather than at the ice-bed interface. The detachment slope  
608 was determined to be ~20°.

A remarkable feature of Flat Creek glacier was a ~70 m tall bulge upstream of a stagnant, crevasse-free tongue. A similar  
610 bulge on Trapridge glacier, a polythermal surge-type glacier 80 km south-east of Flat Creek, was shown to have formed because  
a cold-ice tongue buttressed temperate ice upstream (Clarke and Blake, 1991). Based on the low annual air temperature and  
612 the presence of continuous permafrost, Jacquemart et al. (2020) concluded that the bulge on Flat Creek glacier was also the  
consequence of a polythermal regime. Measurements of the bulge position in satellite images suggest that the bulge advanced  
614 between 2011 and 2013, likely increasing driving stresses locally.

The 2013 and 2015 detachments both occurred at the peak of their respective melt seasons. Using a degree-day model,  
616 Jacquemart et al. (2020) found that the water availability during the exceptionally warm summer of 2013 was primarily melt  
driven and up to 4.8 standard deviations ( $\sigma$ ) above the long term mean (1979–2015). No detachments were detected in 2014,  
618 when water availability was below average ( $-0.5 \sigma$ ). Water availability was again higher in 2015 ( $+1 \sigma$ ), when the second  
detachment occurred.

620 In 2016, a third glacier detachment released from a much steeper glacier (~30°) in the same cirque (not described in Jacquemart  
et al. (2020) but mentioned in Jacquemart and Loso (2019)). We differenced a 13 March 2016 Arctic DEM  a structure-  
622 from-motion DEM from a 2019 aerial survey and estimate the volume of this detachment to be  $4.7 \pm 0.18 \cdot 10^6$  m<sup>3</sup>. DEM  
differences over 2012–2016 show bulging  of up to 30 m in the lower part of the later detachment and surface lowering in its  
624 upper part (Fig. 14 f, and Supplement). The detachment causes have not yet been investigated, but the moving mass of ice was  
caught on video by rangers on a coincidental overflight. The speed of the observed mass flow was about three times slower  
626 than that of the 2013 and 2015 events. Nevertheless, the churning mass of ice blocks (termed a “slush-avalanche” by  
Jacquemart and Loso (2019)) provides a sense of what the much larger flows may have looked like.

628



630 **Figure 14: a) Overview of the three detachments and ice-rock avalanches from Flat Creek Glacier, Alaska, since 2012.**  
 632 **b) On the 15 Aug 2012 inset, a bulge is visible on the lower part of the glacier. c) On the 11 Aug 2013 inset, the glacier**  
 634 **part that detached on 5 Aug 2013 is indicated together with the front position before the event (white line). d) On the**  
 636 **13 Aug 2015 inset, the detachment of 31 Jul 2015 and the front position before it are indicated. e) On the 5 Aug 2017**  
**inset, the area of the 10 Aug 2016 detachment is shown. All images © Planet (Dove and RapidEye satellites). (For more**  
**images and front positions see Jacquemart et al. (2020)). f) DEM difference between 13 Mar 2016 (Arctic DEM) and**  
**summer 2012 (Alaska IFSAR) showing surge-like mass redistribution (see also Supplement).**

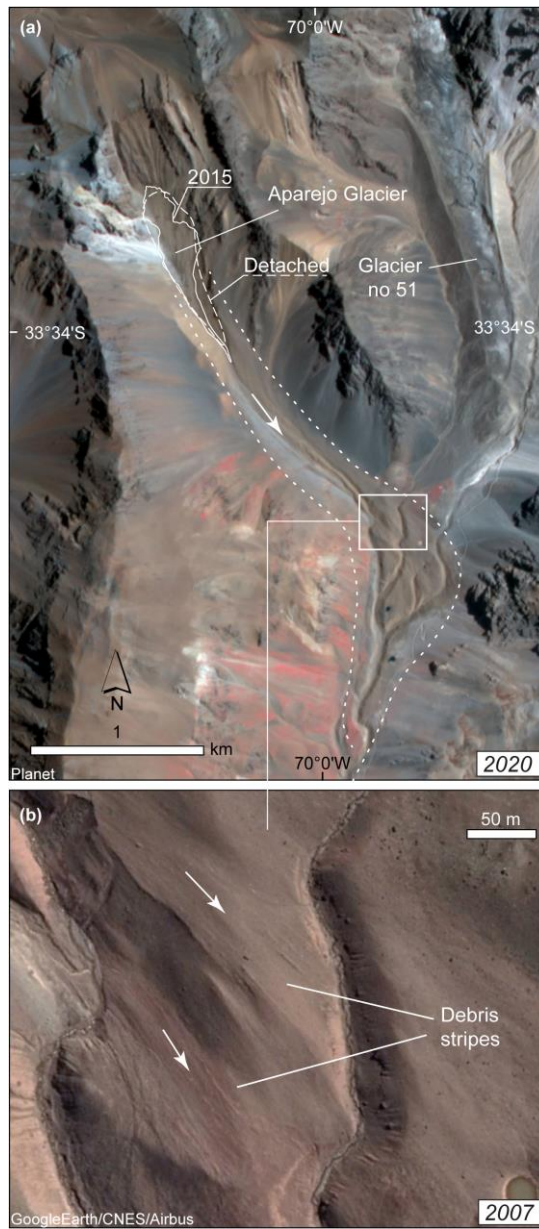
### 638 3.8 Aparejo, 1980, Chilean Andes

On 1 March 1980,  $7 \cdot 10^6 \text{ m}^3$  (85% of its total volume) sheared off the debris-covered Aparejo Glacier in the Chilean Andes,  
 640 mobilizing the detached mass 3.7 km down-valley with an estimated speed of 110 km/h (Ugalde et al., 2015; Ugalde, 2016;  
 Ugalde et al., 2017) (Fig. 15). The slide deposit covered an area of  $0.55 \text{ km}^2$  with ice and rock debris piled up to 17 m thick.  
 642 The volume of the deposit was estimated at  $8.1 \cdot 10^6 \text{ m}^3$  (Marangunic, 1980). Five mountaineers witnessed the event and noted

several supraglacial ponds and 2-3 cm of wet snow on the surface of the glacier (Marangunic, 1980). These observations  
644 suggest that the triggering mechanism of the glacier detachment likely involved an extreme reduction of the basal drag due to  
high water saturation of the glacier bed. Aparejo Glacier appears to sit on a glacier bed composed primarily of weak subglacial  
646 till, and the slope on the lower two thirds of the glacier averages 7°. Snowmelt infiltration and warm precipitation due to a  
sudden increase of the zero-degree isotherm elevation could have provided the main source of infiltrated water, leading to  
648 enhanced water pressure at the glacier bed. During a field inspection on 12 March 1980, Marangunic (1980) found that the  
nearby debris-covered glacier to the east, glacier no 51 according to the Chilean glacier inventory at the time (Fig. 15), also  
650 showed significant signs of surge-like instability, such as a heavily crevassed front and patches of freshly exposed ice along  
its entire length. The prominent terminal moraine of this glacier may have contained its detachment, though.

652 The Aparejo glacier is situated in a region of complex geology with a number of weak rock formations, including sandstones  
and fine-grained conglomerate in the immediate vicinity of the glacier (Ugalde, 2016). Ugalde (2016) sampled the grain size  
654 distribution of the remains of the lower ice-rock avalanche deposits and did not find them to contain more fines than a typical  
moraine, but notes that spatial variability was high and that the 35 years since the detachment may have depleted the deposits  
656 of fine particles. In the former avalanche path, modern satellite images show streamlined debris stripes similar to those reported  
from several other detachments in this contribution. Remarkably, similar debris stripes are also visible in Hycon airphotos  
658 from 1956. Interestingly, the geomorphology of the deposit area is similar between the 1956 airphotos and the post 1980-event  
high-resolution satellite images. One possible interpretation of this is that large mass flows had already originated from the  
660 Aparejo cirque at earlier times. A detailed field investigation would be required to determine whether the debris stripes consist  
of glacial flutes formed under a previous glacier extent or stem from a catastrophic detachment.

662 In 2015, the glacier had around 15% of its pre-detachment volume, covering much of the original area, and with a surface  
slope of around 20° (Ugalde, 2016). The current glacier terminus lies at around 3400 m a.s.l., slightly below the lower regional  
664 limit of discontinuous permafrost, estimated by Brenning (2005) to be at around 3500 m a.s.l. Consistent with regional glacier  
mass balance trends (Falaschi et al., 2018b; Braun et al., 2019; Dussaillant et al., 2019), decreasing ice thicknesses have been  
666 identified on the lower and middle section of the Aparejo glacier (Ugalde et al., 2017), pointing to the glacier shrinking under  
current climate conditions.



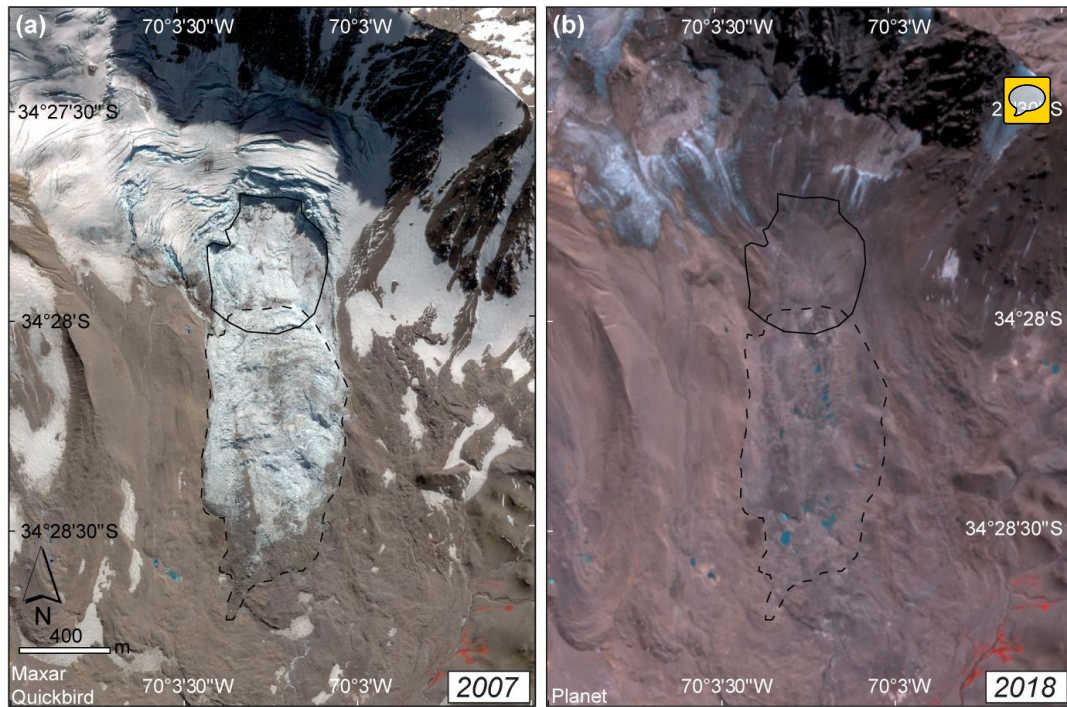
668

670 **Figure 15: Aparejo Glacier, Chilean Andes. (a) Satellite image (© Planet) of 27 Jan 2020 with the outlines of the**  
 672 **detached glacier as solid line, and the outlines of the 1980 detachment and runout roughly indicated as dashed lines**  
**(outlines after Marangunic, 1980; Ugalde, 2016; Ugalde et al., 2017). (b) Detail of avalanche path (rectangle in (a)) with**  
**streamlined debris stripes. Satellite image: © Google Earth and CNES/Airbus, 29 Feb 2016.**



674 **3.9 Leñas, 2007, Argentinean Andes**

676 The  $4 \cdot 10^6 \text{ m}^3$  detachment of Leñas Glacier between 5 and 14 March 2007 was discovered only recently, since it happened in  
678 a very remote region and had no down-stream impacts (Fig. 16). Meanwhile, the case is described in detail by Falaschi et al.  
(2019). The detached lower glacier section had a surface slope of around  $15\text{-}16^\circ$ . The glacier tongue at around 3450 m a.s.l. is  
680 suggested to lie within the zone of discontinuous permafrost in the region. The bed characteristics of the glacier are not known,  
but large amounts of fine sediments were found over the run-out area of the event. A number of glacier surges are documented  
682 in the wider region but not for Leñas Glacier itself (Falaschi et al., 2018a, 2019). At the location of the later head scarp of the  
detachment, pronounced transverse crevasses are visible in airphotos from 1970 and in a satellite image from a few weeks  
684 before the event (SPOT5). It is hard to determine, however, if these crevasses could have been signs of abnormal glacier  
behaviour, or rather a pre-existing feature that then naturally formed the upper failure scarp. Transverse undulations of the  
glacier surface as indicated in the 2000 SRTM DEM, and a slight increase of surface gradients at the location of the crevasse  
zone favour the latter scenario.



686

688 **Figure 16: (a) Quickbird satellite image of 19 Apr 2007 over Leñas Glacier, Argentinian Andes, a few days after detachment (© Maxar). (b) Planet image of 28 Mar 2018. Bold lines in both panels indicate the detached glacier part, dashed lines the outlines of the avalanche deposits. (© Planet).**

690

## 3.10 Tinguiririca, 1994 and 2007, Chilean Andes

### 692 3.10.1 The 1994, 2007 and a possible 1962 event

A detachment from a glacier on the southern flank of the Tinguiririca Volcano (Fig. 17) happened between 27 June (Landsat  
694 5 TM) and 6 July 1994 (Landsat 5 TM). For the event, we estimate a detached glacier area of  $0.2 \text{ km}^2$ . Using glacier thickness  
estimates derived for the 2007 case (described below), we estimate a detachment volume of roughly  $4\text{--}5 \cdot 10^6 \text{ m}^3$ . The climatic  
696 conditions between 1994 and 2007 were obviously favourable enough (i.e. little negative or even balanced regional glacier  
mass balances; Masiokas et al., 2016; Dussailant et al., 2019) for the glacier to recover to its pre-detachment geometry.

698 At the same location, a glacier area of  $0.46 \text{ km}^2$  detached between 7 January (Landsat ETM+ image without collapse) and 14  
January 2007 (Landsat ETM+ with collapse), producing an ice/debris avalanche of  $10\text{--}14 \cdot 10^6 \text{ m}^3$  volume (Schneider et al.,  
700 2011; Iribarren Anacona et al., 2015; Figs. 17, 18). We estimate that the detached glacier had a surface slope of around  $20^\circ$ .  
Before the 2007 detachment, the glacier's lowest elevation was at about 3500 m a.s.l., roughly at the lower regional limit of  
702 discontinuous permafrost (Brenning, 2005). The volcanic nature of Tinguiririca should be associated with weak rocks and  
sediments. There are fumarolic fields and hot springs within a few km of the detached glacier (Pavez et al., 2016), and an  
704 inactive volcanic crater lies just a few hundred metres to the west of the detached glacier. In very high-resolution satellite  
images of 2007 and later (GoogleEarth, BingMaps), clear signs of hydrologic activity are visible in the upper part of the  
706 detachment area: freshly eroded channels, wet looking areas, and deposits from small debris flows – all perhaps signs of  
geothermally-enhanced melt of snow and ice (Fig. 18). In the path of the ice-rock avalanche we find streamlined debris stripes  
708 similar to those found in the Kolka, Rasht 2019, and Aparejo avalanche paths (Fig. 18). As of late 2019, the glacier has not  
recovered from its 2007 detachment and there are only a few small snow (or ice?) fields visible at its location. Elevation  
710 differences between 2000 (SRTM DEM, before detachment), 2007–2010 (ALOS PRISM, after detachment), and 2010–2015  
(TanDEM-X; both the ALOS PRISM and TanDEM-X DEMs are multi-year composites and therefore their date range is given)  
712 suggest that the detached glacier had average and maximum thickness of 21–28 m and 50 m, respectively. Combined with the  
detached glacier area of about  $0.5 \text{ km}^2$  we estimate a detachment volume of roughly  $10.5\text{--}14 \cdot 10^6 \text{ m}^3$ , which is in good  
714 agreement with Iribarren Anacona et al. (2015). The Tinguiririca case illustrates how glacier removal by the 1994 detachment  
was largely reversible as the glacier built up again to failure conditions under the climate at that time, whereas the 2007 glacier  
716 removal seems irreversible under current climate and associated negative glacier mass balances in the region (Falaschi et al.,  
2018b; Braun et al., 2019; Dussailant et al., 2019).

718 In airphotos from 1962 and Corona-series reconnaissance-satellite images from 1967 we notice debris stripes in the valley  
similar to the ones visible after the 1994 and 2007 events, and other cases described in this contribution. Over the glacier, the  
720 1962 airphotos clearly show that a glacier detachment similar to the 1994 event must have occurred not long (weeks, months  
or a few years?) before the image was taken. Stripes of debris or ice remains after the avalanche are still well preserved in the  
722 1962 images over the glacier (Fig. 18d). (The associated terrain sections are under snow cover in the 1967 Corona images).





### 3.9.2 A potential large pre-1970s detachment of the neighbouring glacier

724 In the neighbouring valley to the east (Fig. 19) we note geomorphological traces that could be investigated further with regard  
to their origin from volcanic mass movements, earlier glacier stages, glacier surging, or more glacier-detachment like events.

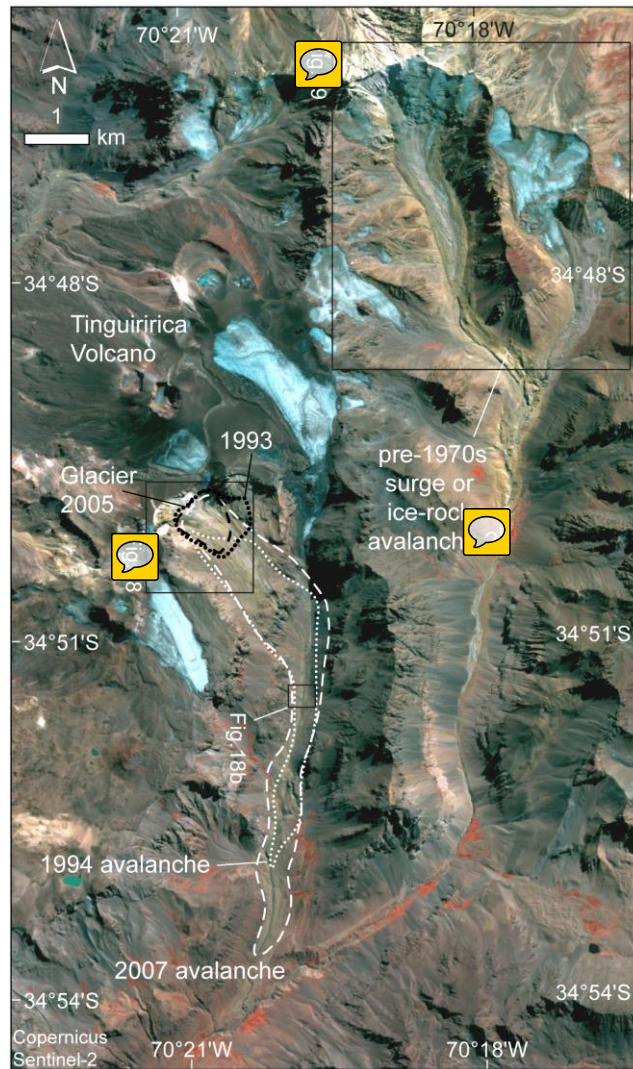
726 In the lower part of this potential event path we find debris stripes, similar to the ones from the Tinguiririca, Aparejo and other  
avalanches of this study, largely unchanged since the first available Corona-series reconnaissance-satellite images in 1967  
728 (Fig. 19c), and airphotos from 1962. Only detailed field work would be able to rule out the possibility that ~~this~~ debris stripes  
consist of glacial flutes or small lateral moraines formed during a previous glacier extent, or were produced by a glacier surge.

730 It should also be investigated whether such debris stripes can remain largely intact after having been overrun by an ice-rock  
avalanche or if it is an indicator of the most recent event (see also Aparejo, where similar questions turned up).

732 In the upper part of this valley, or in the potential event source area, we observe two noticeable changes over time. First, the  
tongue of this unnamed glacier (RGI60-17.01112, GLIMS ID: G289692E34781S) was much smaller in 1962 airphotos than it  
734 is in 2020. Its advance of roughly 1.5 km since 1962, most of which occurred between 1975 and 1986 (Landsat), is in stark  
contrast to the pronounced shrinkage of the other glaciers in the area (Fig. 17 ~~and~~ 19). Indeed, differencing a DEM, which we  
736 produced from 1962 stereo-airphotos, from the SRTM or TanDEM-X DEMs confirms elevation gains on the glacier tongue  
of up to 120 m between 1962–2000 (SRTM), or up to 150 m between 1962 and 2010-2015 (TanDEM-X; Fig. 19c). This  
738 development could point to the recovery of the glacier tongue after a removal some time before 1962. The volume gain of the  
glacier tongue between 1962 and 2000 is around  $70 \cdot 10^6 \text{ m}^3$ , or  $100 \cdot 10^6 \text{ m}^3$  between 1962 and 2015.

740 Second, we detected an elevation decrease of the glacier forefield of around 10–15 m between 1962 and 2000, which could  
point to the deflation of debris-covered ground ice, deposited by a possible surge or glacier detachment (Fig. 19c). Third, a  
742 comparison of the 1962 airphotos to contemporary images revealed a heavily bulged glacier surface between 3900 m a.s.l. and  
4650 m a.s.l. (Fig. 19a,b). Visually, this bulging is similar to the bulge found on Flat Creek Glacier prior to its 2013 detachment  
744 (section 3.7). The slope of the glacier tongue is around  $8\text{--}10^\circ$ , and around  $35^\circ$  for the steep upper part. The bulging upper part  
of the glacier is far above the regional permafrost limit so that polythermal ice conditions might well be found in parts of it.

746 We also examined a 1955 Hycon aerial photo (no stereo data to produce a DEM available to us), but visual interpretations  
from it remain inconclusive. Under illumination conditions that are very different from those of the 1962 images, the headwall  
748 glacierisation and the tongue seem larger in 1955 than in 1962, resembling rather its shape and extent of the 1980s. Below the  
position of the current (2020) glacier terminus, there seem to be dead-ice remains visible in the 1955 images. These are also  
750 visible in the 1962 images, though shrunk. It remains thus to be clarified at this point to which extent the features observed  
can be explained by a surge, or series of surges of the glacier before 1955, or between 1955 and 1962, or by a detachment-like  
752 event.

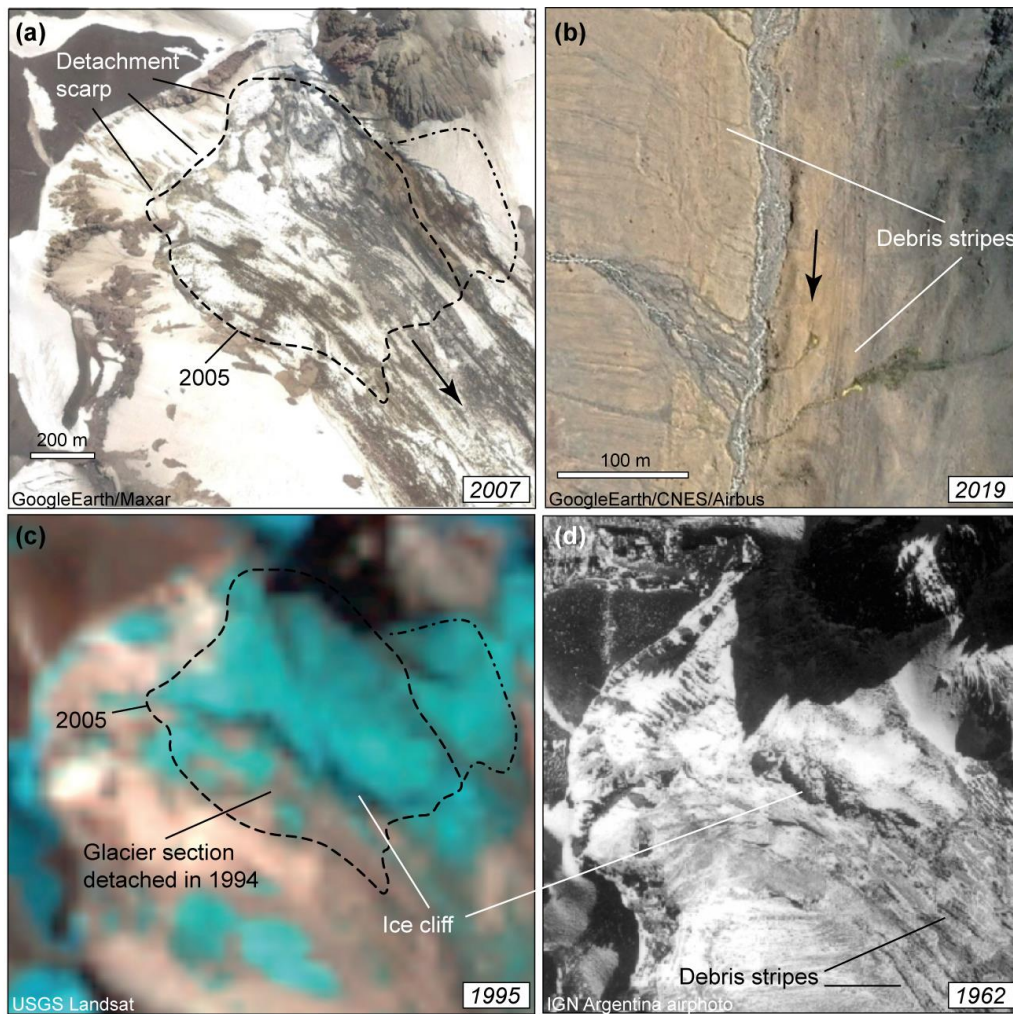


754

756

758

**Figure 17: Tinguiririca Volcano, Chilean Andes. Outlines of the 1994 and 2007 ice-rock avalanches, and the 1993 and 2005 area of the detached glacier as dotted or dashed lines, respectively. These outlines have been digitised for this study but were found to agree well with the ones in Iribarren Anacona et al. (2015). Satellite image: Sentinel-2, 14 Mar 2020 (credit: Copernicus Sentinel data).**

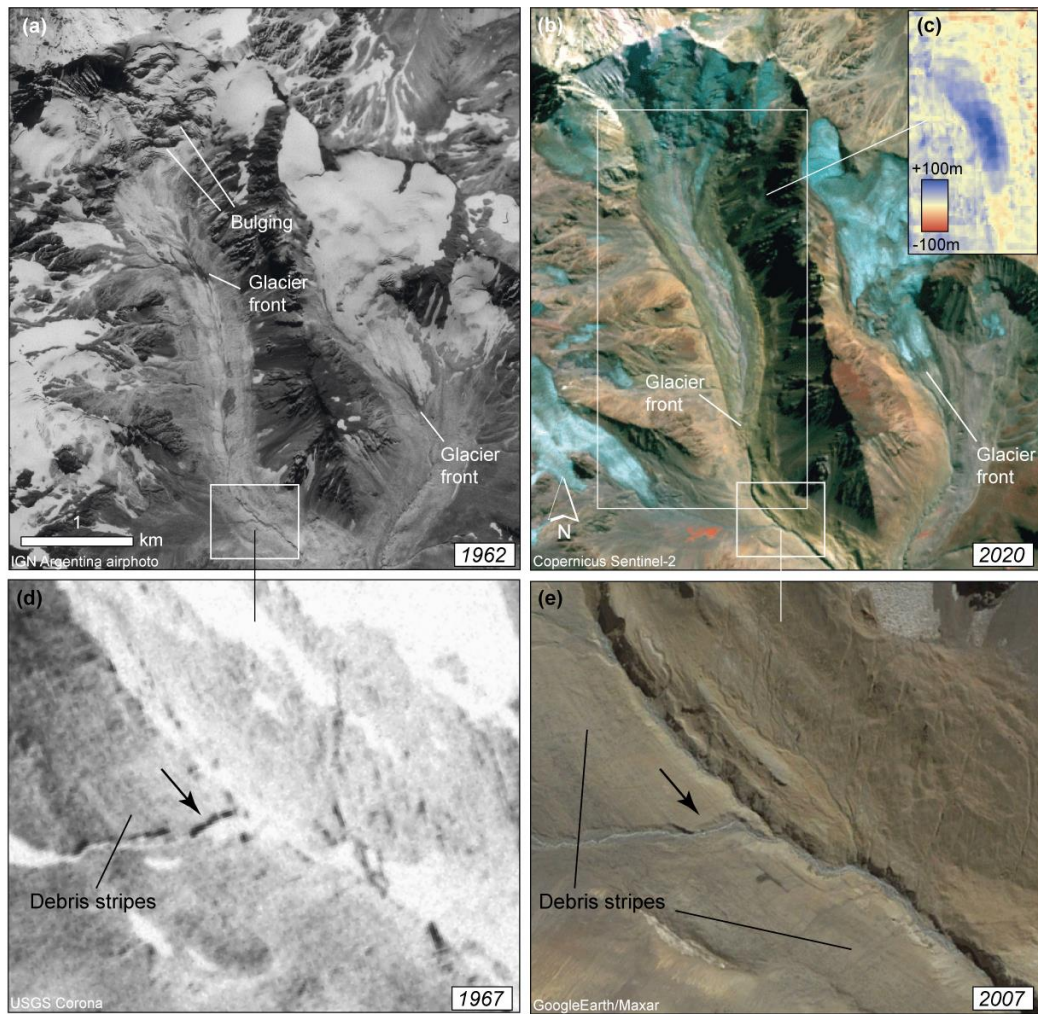



760

762 **Figure 18:** (a) Glacier detachment area at Tinguiririca Volcano on 24 Jan 2007 (satellite image: © Google Earth and  
 764 Maxar). See Fig. 17 for location. Glacier outlines from 26 Feb 2005 Landsat data (latest snow-free image before 2007  
 766 detachment) indicated by dashed line. From the 30-m resolution Landsat data it is unclear whether the dash-dotted ice  
 768 section was connected to the main glacier. (b) Debris stripes left by the 2007 ice-rock avalanche (30 Jan 2019; © Google  
 Earth and CNES/Airbus). (c) A Landsat image of 19 Mar 1995 (first snow-free image after 1994 detachment; credit:  
 USGS) shows that the southern part of the glacier detached in the 1994 event. Glacier outlines of 2005 dashed as in (a).  
 (d) The glacier on an aerial image of 8 Apr 1962 (© National Geographical Institute of Argentina). Clearly, a glacier  
 section similar to the 1994 event has detached not long before the image date, leaving also a similar ice cliff. Streamlined  
 debris stripes from the resulting avalanche are still well visible.

770





772 **Figure 19: Glacier valley with potential former surge or glacier detachment, east of Tinguiririca Volcano. See  . 17**  
 774 **for location. (a) Orthoprojected airphoto of 8 Apr 1962 (© National Geographical Institute of Argentina). (b) Sentinel-**  
 776 **2 image of 14 Mar 2020, showing an advance of 1.5 km relative to 1962, **in contrast the other retreating glaciers** in the**  
 778 **area (credit: Copernicus Sentinel data). (c) Elevation differences between DEMs from 1962 stereo airphotos and the**  
**2000 SRTM show gains over the glacier tongue of up to 120 m, and losses of around 10-15 m in the forefield. (d) Corona**  
**satellite image of 23 Feb 1967 with debris stripes (credit: USGS). (e) Satellite image of 19 Mar 2007 (© Google Earth**  
**and Maxar). (a) and (b), and (d) and (e) show the same terrain section each. Locations of (c), (d) and (e) indicated as**  
**white rectangles in (a) and (b).**

780



## 4 Discussion

### 782 4.1 Simplified force and energy balance

#### 4.1.1 Idealized slab model

784 The condition under which a detachment might occur can be qualitatively understood from a simple force balance analysis. To simplify the problem, we represent the potential detachment as a rectangular slab (Fig. 20a). The force balance between  
786 gravitational (left part of Eq. 1) and resistance forces (right part of Eq. 1) gives the following relationship:

$$W L h \rho g \sin(\alpha) = W L \tau_b + 2 h L \tau_d \quad (1)$$

788 and by solving for  $\tau_d$  :

$$\tau_d = \frac{W}{2h}(\rho g h \sin(\alpha) - \tau_b) \quad (2)$$

790 where  $\tau_d$  is the lateral shear stress (Pa),  $W$  is the slab width (m),  $L$  is the slab length (m; cancelling out),  $h$  is the slab thickness (m),  $\rho$  the density of ice ( $\text{kg m}^{-3}$ ),  $g$  is the gravitational acceleration ( $\text{m s}^{-2}$ ),  $\alpha$  is the slab slope, and  $\tau_b$  is the basal shear stress (Pa). Assuming that the glacier driving stress is originally in balance with the basal shear stress under normal conditions ( $\tau_b = \tau_0$ ) we have:

$$794 \quad \tau_0 = \rho g h \sin(\alpha) \quad (3)$$

which gives the following equation by combining (2) and (3) in a way that a ratio  $\frac{\tau_b}{\tau_0}$  appears, which allows us to compare  
796 potential failure conditions to normal conditions:

$$\tau_d = \frac{W \rho g \sin(\alpha)}{2} \left(1 - \frac{\tau_b}{\tau_0}\right) \quad (4)$$

798 A collapse can only happen if  $\tau_d$  exceeds the mechanical resistance of the slab margins (critical shear strength  $\tau_c$ ). Using the work of Gilbert et al. (2018) where the evolution of the force balance toward the collapse of Aru glaciers has been quantified,  
800 we estimate  $\tau_c \cong 0.28$  MPa for the Aru glaciers and apply this value to the simplified glacier slab. This allows, using Eq. (4), to define a stability diagram as a function of detachment width and slope, and the ratio  $\frac{\tau_b}{\tau_0}$  (Fig. 20b).

802 This stability criterion seems to be respected by most of the detachments of our study (Fig. 20b) showing that the rough slab approximation may be a way to initially and qualitatively analyse which glaciers might be susceptible to detaching. In  
804 particular, the analysis shows which combinations of slope and width are unlikely to produce detachment when  $\tau_d$  remains below  $\tau_c$  even for  $\tau_b = 0$  (i.e. complete loss of basal friction; green area in Fig 20b). Under the provisional assumption that  $\tau_c$   
806 is similar for all the glaciers investigated, this analysis also shows that the detachments presented here happened for an average loss of friction between around 50 and 100% (i.e.  $0 < \tau_b/\tau_0 < 0.5$ ). In reality, it is reasonable to assume that the basal friction

808 rarely goes all the way to zero. Additionally, the critical lateral shear stress will vary between glaciers, depending for instance  
810 on whether the critical lateral resistance is provided by ice or by morainic margins, their properties, and on topographic forms  
812 of resistance like glacier curves or bedrock bumps. For the Amney Machen detachment, which did not follow our provisional  
814 criteria (it failed at a critical shear stress of 0.2 MPa, which is smaller than the 0.28 MPa estimated for Aru), the detachment  
816 flanks consisted of sediments and might thus be weaker than the ice margins along which the Aru glaciers detached. For some  
glaciers the effective width of the detachment is difficult to estimate as it varies along the glacier length and we cannot be sure  
at which width the failure started to develop. For Tinguiririca, the effective detachment width is particularly uncertain as the  
glacier rested on a bed ramp rather than between valley or moraine flanks. It remains to be investigated how the deviation of  
the cross-sections of the detached glaciers from the idealized slab influences our stability analysis.

#### 4.1.2 Energy from precursory acceleration

818 As will be discussed in the following sections in more detail, several of the detachments presented here showed precursory  
accelerations, some clearly surge-like. In the present section we discuss to what extent the melt-water production associated  
820 with this precursory motion could feedback on the reduction of basal shear stress. We take the case of the Aru-1 event (based  
on data in Gilbert et al. 2018) as an example. The first major dissipative losses of this event were during the pre-detachment  
822 accelerated sliding, which attained about 0.5 m/day. Whereas some energy drove crevasse development and brittle-ductile  
changes in ice crystals, we suppose that most of this phase of energy dissipation occurred at the bed by grinding of rocks and  
824 ice, and melting of ice. The typical glacier thickness was 100 m, so 1 m<sup>2</sup> of bed area by 100 m column of ice at a density of  
900 kg/m<sup>3</sup> would have a mass of about 90,000 kg. Each day it slid downslope by about 0.5 m, including an elevation drop of  
826 about 0.1 m. The daily loss of potential energy of each such column of ice was thus about 88,300 J (about 1 W/m<sup>2</sup>). If the ice  
was at the melting point, which it was across much of the bed within the frozen perimeter (Gilbert et al., 2018), this energy  
828 could melt up to around 0.26 kg of ice per m<sup>2</sup> of thawed bed per day. If this continued for 200 days at such rapid sliding, about  
53 kg of liquid water would be generated per m<sup>2</sup> of thawed bed area, amounting to a roughly 5 cm layer of water (some energy  
830 may also have been expended in crushing rocks and ice). This water could be expelled, or it could be contained within the  
frozen confines of the polythermal glacier. If confined, this water could be ingested into basal till, perhaps dilating the volume  
832 of till and spreading it over a larger fraction of the bed, thus reducing the total frictional resistance in the thawed parts of the  
glacier. Or the water itself could spread over a larger fraction of the bed, or it could pool against the frozen toe and margins of  
834 the glacier. Additional water – maybe a lot more – likely was provided to the subglacial bed environment from rainfall and  
snowmelt sources. The role of the above 5-cm average thickness of frictional meltwater could become important if (i) it is a  
836 substantial proportion of the thickness of the basal till, (ii) if it is a significant proportion of the meteorological meltwater that  
reaches the bed, and/or (iii) if it can spread laterally over a large part of the thawed bed.

838 Not all detachments presented here were preceded by longer phases of surge-like acceleration, and surge-like acceleration  
typically does not lead to glacier detachment. Still, the above estimates exhibit a feedback process that could through  
840 precursory acceleration facilitate substantial reduction of basal shear stress and ultimately failure of soft beds.

## 4.2 Similarities and differences

842 The most apparent similarities among the detachments compiled in this contribution (Tab. 1) are their geographic proximity  
to surge-type glaciers – in some cases the detached glaciers themselves exhibited surging or surge-like behaviour – as well as  
844 the existence of weak bedrock and/or fine sediments around and likely at the base of the glaciers (Fig. 21). Both commonalities  
suggest that the sudden detachments of low-angle glaciers discussed here could be seen as rare and extreme endmembers of  
846 the range of surge-type and surge-like glacier instabilities (Quincey et al., 2015; Herreid and Truffer, 2016). The detachments  
could be a specific kind of glacier surge where the force balance cannot be achieved by a global control, typically by  
848 longitudinal and lateral stresses, when basal friction is suddenly reduced. In case of a low bed roughness and an absence of  
sufficient topographic support, the reduced amount of stress accommodated by basal resistance can only be transferred to the  
850 margins (Fig. 20a) and leads to an expanding instability (Thogersen et al., 2019). This ultimately leads to a runaway  
acceleration and detachment. The loss of friction involved in such behaviour, more than 50% according to our idealized slab  
852 analysis, may only be reached by sustained low effective pressure. Such conditions are more plausible on soft-bed glaciers in  
contrast to hard-bed glaciers where increasing sliding velocity would lead to cavity opening and increasing drainage efficiency,  
854 making preservation of high water pressure at the glacier bed unlikely.

In this context, we note that the surface slopes of the detached glaciers were between  $9^\circ$  and  $21^\circ$  (average  $15.9^\circ$ , standard  
856 deviation  $3.6^\circ$ ), which is at the upper end for slopes of surge-type glaciers, yet surprisingly low for glaciers causing ice  
avalanches. The slope range of around  $10\text{--}20^\circ$  may be a necessary condition for glacier detachments, as a slope lower than  $9^\circ$   
858 is unlikely to drive a stress concentration that exceeds the critical shear stress even in the case of total loss of basal shear stress  
(Figure 20b) (Section 4.1). At the same time, glaciers within the  $10\text{--}20^\circ$  slope range still have considerable thickness and thus  
860 volume, while higher slopes sustain thinner glaciers and much smaller volumes involved in a potential failure (Fig. 1c). Our  
limited data-base of detachment events suggests a transition between larger and smaller detachment volumes at roughly around  
862  $14^\circ$  (Fig. 1c).

From a more mechanical point of view, low-angle glacier detachments can also be seen as part of the continuum between  
864 surges and ice break-offs from steep glaciers. Not least owing to their slope, glaciers have a range of possibilities to adapt to  
changes in their stress regimes (see Fig. 22). Flat glaciers can respond by adjusting their geometry, for instance through advance  
866 and surging. On very steep terrain, glaciers may not be able to adjust their geometry smoothly and ice breaks off. In contrast  
to the factors involved in typical ice break-offs from steep glaciers (see Section 1), glacier detachments appear to have in  
868 common basal failure on soft beds. Therefore, low-angle glacier detachments combine the elements of both instability  
processes: the inability to rapidly adjust geometry in response to stress changes, similar to steep glaciers, and a surge-like

870 process that propagates an initial instability through large parts of the glacier (Thogersen et al., 2019), allowing entire glacier  
tongues to be mobilized. The latter framework for low-angle glacier detachments and the above one of surge endmembers are  
872 not mutually exclusive but rather linked by the role of glacier slope, fine basal tills, and the surge-like propagation of  
instabilities.

874 The role of basal water pressure in the detachments is difficult to examine in detail, but most detachments should have involved  
severe reduction in friction (Section 4.1), likely due to high basal water pressure. Ways to rapidly increase basal water pressure  
876 include: an increase in water input (e.g., large high-altitude rain events (Kääb et al., 2018) or increased surface snow/ice melt  
(Jacquemart et al., 2020)) into a subglacial drainage system not capable of adjusting fast enough; inefficiencies or blockages  
878 of this drainage system; or increased permeability of the glacier through enhanced crevassing (e.g., Tsambagarav) (Dunse et  
al., 2015). Sudden weakening of the strength of subglacial till under high pore-water pressure and over large parts of the glacier  
880 bed was shown to be a key process leading to the Aru detachments (Gilbert et al., 2018). Ongoing surge-like activity may  
enhance sensitivity to water input (Flowers et al., 2016).

882 In Figure 22 we attempt to summarize the main drivers of the glacier detachments described here. We define a detachment's  
*disposition* as the sum of long-term factors that might promote glacier detachments and refer to *triggers* to describe short-term  
884 factors that might suddenly tip the scale toward a catastrophic failure. Fundamentally, it seems that different combinations of  
dispositions and triggers are able to produce instability. Aside from the similarities mentioned above, the observed detachments  
886 all present some unique conditions, many of which remain shrouded in uncertainty. The observed failure conditions (Fig. 20)  
include ruptures during surge-like glacier instabilities (Kolka 1902, Aru, Amney Machen, Sedongpu; unclear for Devdorak)  
888 or earthquake triggered rupture (Tsambagarav), or increase of driving stress due to thickening caused by snow accumulation  
(Aru) or rock-ice avalanches (Kolka 2002, Amney Machen, uncertain: Sedongpu). Geothermal activity could have played a  
890 role at Tinguiririca and Kolka, but is unlikely for the other events. The thermal setting of the detached glaciers can play a role  
if permafrost around the glaciers potentially causes frozen margins or the glaciers exhibit a polythermal structure (Aru, Flat  
892 Creek, Tsambagarav, uncertain: Tinguiririca, Leñas). However, other detachments happened under conditions very likely free  
of cold ice. Some of the detached glaciers seem to have been composed of a mixture of debris and ice (Amney Machen, Flat  
894 Creek; likely at least for Devdorak, Kolka, Sedongpu). Such mixtures can be profoundly weaker than clean glacier ice,  
particularly at temperatures close to the melting point (Moore, 2014), but it is unclear at this point whether and how these  
896 mixtures and their weakness may have contributed to the detachments. In contrast, the ice of the Aru glaciers and the glacier  
at Tsambagarav clearly consisted of rather clean ice. Failure circumstances are particularly unclear to us for Aparejo and Leñas.

898 The angles of reach of the ice-rock avalanches associated with glacier detachments (Fahrböschung between about 5° and 10°),  
both absolutely and relative to their volume, are lower or at the lower end of those observed for other types of ice-rock  
900 avalanches (Fig. 1a, b). The particularly high ice content of glacier detachments might reduce friction of the mass movements  
through liquefaction (Schneider et al., 2011), promoting the long runouts. Remarkably, many (perhaps all) detached glaciers



902 appear to have sat on particularly fine-grained glacier beds. The large amounts of soft sediments under the glaciers with  
potentially low friction angle, combined with low effective pressure due to the presence of large amounts of basal water at the  
904 time of detachments, may have been able to reach unusually low basal shear stress. In addition, smooth u-shaped glacial valleys  
might favour low angles of reach by channelizing the mass flows, reducing energy dissipation, and presenting few topographic  
906 obstacles along the path (Schneider et al., 2011). The glacier detachments' long runout flows remind also of rocky  
"sturzstroms", some of which reached friction angles (H/L) as low as those found for the ice-rock avalanches from glacier  
908 detachments (Hsü, 1975). "Sturzstroms" and these ice-rock avalanches may share some physics, including reduced basal  
fraction from acoustic fluidization, or movement on air or vapour cushions of flow materials. One mechanism for long runout  
910 of dry granular flows involves acoustic fluidization (Gareth and Melosh, 2003), where the physics analogue in the long runout  
ice-rock avalanches may be acoustic fluidization of ice, especially in cases where the role of liquid water was mainly restricted  
912 in producing the initial mobilization of the glacier detachment.

### 4.3 Influence of climate change

914 Inevitably, these events rise the question of whether climate change could be a driving factor of glacier detachments. Some  
cases investigated here suggest that detachments could be part of a cycle from reservoir refilling to occasional threshold  
916 exceedance, similar to what is found for glacier surges and some avalanching glaciers (Benn et al., 2019; Amney Machen,  
Tinguirica, Devdorak, Kolka, uncertain: Rasht). But several cases of this study also illustrate developments where climate  
918 change can cause transient conditions that lead to failure. A number of dispositions and triggers listed in Fig. 22 may be  
impacted by climatic changes and may bring a glacier closer to failure, or prevent future failures, respectively.

920 Repeated detachments of the same glacier, or detachments connected to surge-like behaviour, require that the climate  
conditions and associated glacier mass balances enable reservoir recovery or built-up of accumulation areas (Devdorak, Aru,  
922 Amney Machen, Kolka 1902). Climate change might shift glaciers out of the envelope of conditions that are favourable for  
surging, or shift them into it (Hock et al., 2019). Whereas glacier rebuilding seems to be underway at Kolka and Aru, it is open  
924 for Sedongpu, unlikely for Tinguirica, and did not happen at all for Tsambagarav. The glacier's potential to regain a substantial  
size is critically linked to the potential for repeated detachment events, and thus important for hazard management.

926 The enhanced rock-ice avalanching onto Kolka Glacier in 2002, possibly responsible for its detachment, or the 2017 Gyala  
Peri rock avalanche over the Sedongpu Glacier, are likely a reflection of a general trend of climate change impact on  
928 polythermal, glacierised rock walls, where the reduction of ice cover and permafrost thaw increases the rock and ice fall  
frequency and enhances the potential for long-reaching cascading events (Fischer et al., 2013; Hock et al., 2019). Indeed,  
930 summers were exceptionally warm and glacier mass balances negative in the Caucasus Mountains, around Kolka Glacier, over  
1998–2001 (Zemp et al., 2019). Glacier shrinkage due to negative mass balance (Larsen et al., 2015; Treichler et al., 2019;  
932 Zemp et al., 2019) has exposed large parts of the – at earlier times mostly ice-covered – headwalls of Flat Creek, Amney  
Machen, Leñas, and likely Petra Pervogo/Rasht. This exposes bedrock to erosion making it available for mass flows and

934 incorporation in and underneath the glaciers, a process that is particularly important for soft rock lithologies. The partial loss  
of glacier cover may also interrupt existing patterns of stress transfer and cause new temporary stress concentrations (see also  
936 Fig. 20) that may exceed stability thresholds in certain locations. Some glacier detachments could thus be connected to the  
transient development of headwall glacier loss.

938 Climate change increases the amount of meltwater and transitions from snowfall to rainfall, and may thus favour development  
of instabilities, at least for the polythermal glaciers (Aru and Flat Creek, uncertain: Tsambagarav) where such amounts of  
940 meltwater are unusual at the scale of the last century. The relative increase of meltwater can be particularly significant for  
cold/dry climate glaciers. The synchronization of the twin Aru detachments within just two months of each other points to a  
942 climatic driven instability, perhaps involving some meteorological synchronization such as exceptional amounts of high-  
elevation rain or snow and ice melt, or extreme weather. Also, and without understanding the triggers of the Aru events in  
944 detail, the frequency and magnitude of certain potential climatic causes and meteorological trigger events, such as heavy rain  
falls or warm spells, can increase with climatic changes.

946 Also our simplified considerations on the force balance of a glacier slab (Section 4.1) provide hints to how climate change  
could influence detachments. For this strongly idealized geometry, fast and extensive reduction of basal shear stress obviously  
948 reduces stability. Increase of glacier slope (e.g., from bulging), or thickness and density of the slab (e.g., additional loading  
from ice or rock avalanche deposition), faster than the glacier's ability to adjust, will increase driving stress. Finally, climate  
950 change could also reduce the lateral shear stress, for instance by thawing of frozen glacier margins.

#### 4.4 Hazard management

952 From a more applied hazard management perspective, sudden massive glacier detachments pose a high magnitude/low-  
frequency problem, and their low probability/high consequence nature makes them hard to incorporate in hazard management  
954 and planning. The particularly low friction coefficients ( $H/L$ ) involved in the detachments enable them to travel over low  
slopes (where other types of ice-rock avalanches would stall) and to cover large distances. The detachment events seem very  
956 rare, but their large volumes, fast evolution, and the exceptionally long runout distances and high speeds hold the potential for  
severe impacts even far away from the source. Our compilation of all (so far) known cases shows that low-angle glacier  
958 detachments might have, though rare, occurred more frequently than commonly thought. The differences between the events  
suggest that there is no straightforward way to predict where they might occur, but the following list of the most common  
960 conditions might support a more systematic assessment. Events happened at places

- (i) with abundant weak bedrocks/fine sediments,
- 962 (ii) where glacier surface slope is between about  $10^\circ$  and  $20^\circ$ ,
- (iii) where surge-like glacier instabilities are observed in the region, sometimes for the detached glacier itself  
964 (exception: Tsambagarav), and

(iv) where similar events or other violent ice-rock mass flows have happened before (based on direct observation or a geomorphological imprint).

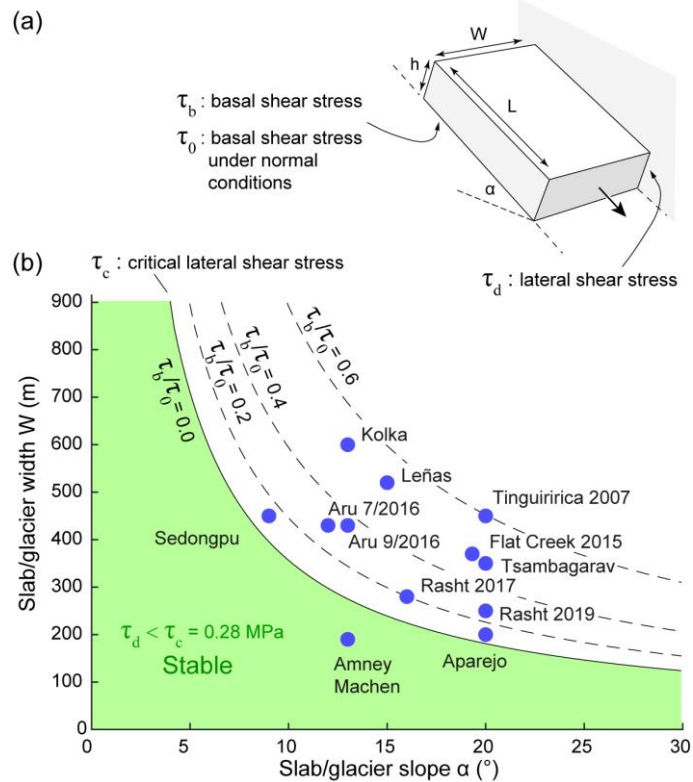
966

This set of very rough qualitative criteria might allow a first-order assessment of whether glacier detachments are possible in any given region. It is crucial to be aware of, however, that these criteria and their interplay are likely transient so that in particular criterion (iv) can be misleading. Particularly important for hazard management is – yet again – the conclusion that climate change is able to shift hazard zones beyond historical precedence, so that also so far unaffected areas might suddenly be susceptible (Hock et al., 2019).

For several of the events we find in aerial and satellite images streamlined debris features in the avalanche paths. Field investigations for Kolka Glacier (Petraikov et al., 2004) and Flat Creek (study in prep.) show ground traces related to the avalanche movement at two very different scales. Debris features of meters in width and tens or hundreds of meters long resemble glacial flutes, but might also consist of pavements. These features can be recognized in high-resolution aerial and satellite images and are in this study in a general way called debris stripes, acknowledging that they are not investigated in detail or understood. At a much smaller scale (mm-cm in width, dm-m in length) and thus not visible in aerial and satellite images, boulders in the avalanche path can show scratches in avalanche direction, similar to glacier striations. Notably, both scales of avalanche traces show that the ice-rock avalanches presented here were not entirely turbulent. More research is necessary to correctly interpret these signatures and differentiate them from glacial flutes, small moraines, and other longitudinal glacial and geomorphodynamic features.

Systematic monitoring turns out to be one of the most feasible responses to changes in hazard conditions, and the increasing temporal and spatial resolution, and improving availability of satellite imagery, is particularly helpful for glacier detachment assessment. For several of the cases in this contribution, abnormal glacier crevassing and accelerating precursory speeds were visible days to weeks before failure (Kolka 2002, Rasht, Aru, Sedongpu, Tsambagarav, uncertain: Flat Creek), but the significance of such a development was realized for the second Aru detachment only due to its spatial and temporal proximity to the first Aru detachment. On the other hand, abnormal crevassing does not necessarily indicate an impending detachment, see Rasht (situation in 2007, Supplementary Fig. S2) or Leinss et al. (2019), where the glacier geometry has likely stabilized a detaching ice mass. Overall, predicting glacier detachments can likely only be achieved by strong efforts in detailed remote-sensing based monitoring and, if feasible, by ground-based measurements, which contribute to an improved understanding of conditions and relevant processes, past events, glacier velocities and slope deformations, glacier bed geology and lithology, surge behaviour and dynamics, and short-term and long-term temperature and precipitation records (Kääb et al. 2018).

992



994

996

998

Figure 20: (a) Slab geometry used for the force balance analysis. (b) Stability diagram showing under which condition the slab would remain stable in the case of a total loss of basal friction ( $\tau_b = 0$ ; green area) and for different ratios friction  $\tau_b/\tau_0$  (i.e. partial loss of basal friction; dashed lines). Blue dots show averaged slope and width of all detachment reported in this study. The critical lateral shear stress  $\tau_c$  has been estimated from the Aru glacier detachments using the force balance constructed in Gilbert et al. (2018).

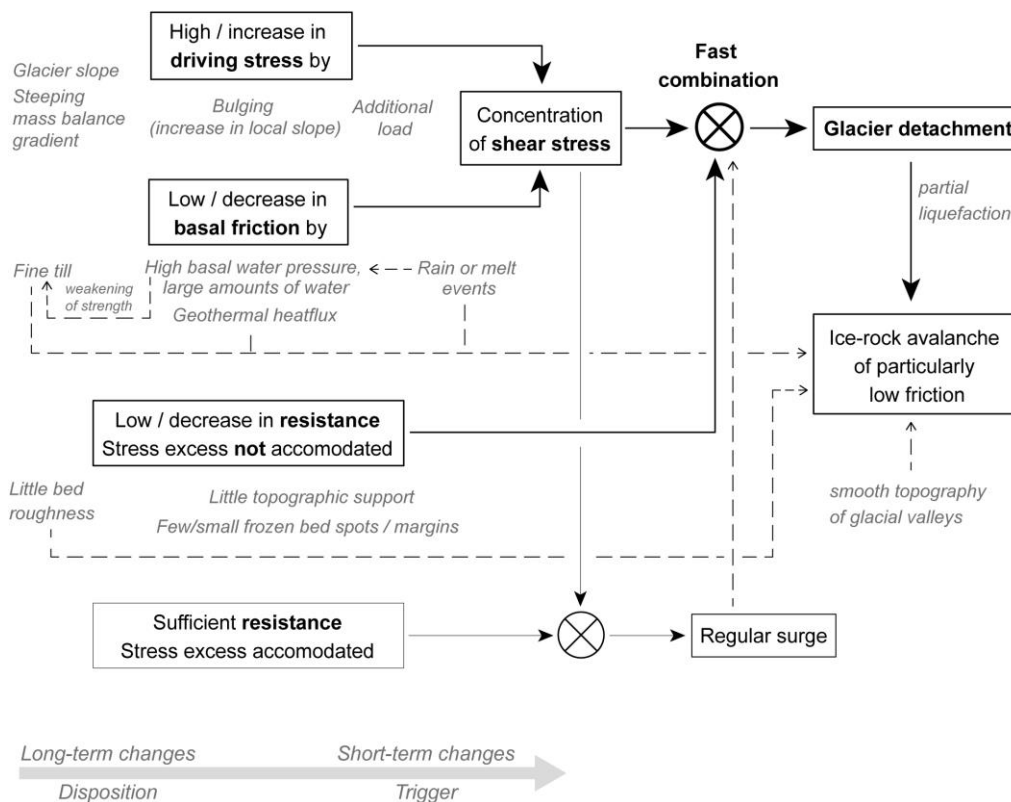
1000

Name of event	Earlier surges in the region?	Weak rocks, fine sediments ?	Glacier tongue within perm	Abnormal crevassing before failure?	Enhanced water input into glacier (melt, rain) ?	Repeat events known?	Signs of high water pressure ?	Signs of earlier mass flows?	Surge-like activity related to event?	Loading prior to event (snow, rock)?	Earlier surges same glacier ?	Bulging before event?
Kolka	green	green	green	green	green	green	green	green	green	green	green	green
Devdorak	green	green	green	green	green	green	green	green	green	green	green	green
Aru	green	green	green	green	green	green	green	green	green	green	green	green
Sedongpu	green	green	red	green	green	green	green	green	green	green	green	green
Rasht	green	green	green	green	green	green	green	green	green	green	green	green
Amney Machen	green	green	green	green	green	green	green	orange	green	green	green	red
Flat Creek	green	green	green	green	green	green	green	red	green	red	red	green
Tinguiririca	green	green	green	green	green	green	green	green	red	red	red	red
Aparejo	green	green	green	green	green	red	green	green	red	red	red	red
Leñas	green	green	green	green	green	red	green	orange	red	red	red	red
Tsambagarav	red	green	green	green	green	red	green	red	x	red	red	orange
	yes	yes, but uncertain		unknown			no, but uncertain		no			x Earthquake-triggered rupture ca. 2 weeks before detachment



1002 **Figure 21: Possible indicators for and factors involved in low-angle glacier detachments.**

1004



1006 **Figure 22: Schematic on which conditions and changes to a low-angle mountain glacier can in combination lead to the**  
 1008 **spatio-temporal interference of particularly high and concentrated shear stresses and low resistance, eventually**  
 1010 **exceeding stability thresholds and causing detachment. The failure conditions can change at a range of time scales, so**  
 1012 **that detachment is the result of a highly transient and rare interplay of factors. It is key that the low basal friction and**  
 1014 **high driving stresses, the resulting concentration of high shear stresses, and the lack of sufficient resistance develop**  
**rapidly, or are combined rapidly, preventing the glacier to adjust to changing forces in a steady way. Several of the**  
**factors potentially involved in the detachment are subsequently also able to strongly reduce basal friction of the**  
**resulting ice-rock avalanche and lead thus to particularly low angles of reach. Boxes in the figure indicate main physical**  
**conditions, grey italic text indicates different actual processes that can fulfil these conditions, sorted from long-term**  
**(left) to short-term (right) variability.**

1016 **5 Conclusions**

In this contribution we describe around 20 ice-rock avalanche events that we characterize as sudden large-volume detachments of low-angle glaciers. Overall, these events seem to be more frequent than previously thought. The detached volumes ranged



from a few up to more than  $100 \cdot 10^6 \text{ m}^3$ . We described one new event in the same size-class as the 2002 Kolka and the 2016 Aru glacier detachments (Sedongpu 2018) and as a side-result quantified one of the larger high-mountain rock avalanches of recent decades (Gyala Peri 2017).

Despite the relatively low number of low-angle glacier detachments and their site-specific variations that leave considerable uncertainties, we were able to identify a set of conditions and evolutions likely involved in these glacier failures. We consider this an important step, given that a few years ago the possibility for low-angle mountain glaciers to detach and produce massive ice-rock avalanches was hardly known. Interestingly, the fact that the spatio-temporal factor combinations leading to exceptionally low basal friction and very high shear stress concentration, and eventually to detachment, are different among the cases, suggests that there exists an exceptional but still fundamental possibility of low-angle glacier beds to fail catastrophically. Awareness of this fundamental potential for catastrophic basal instability expands our understanding of glacier flow.

Many of the glacier detachments show some relation to surge-type glacier movement, and could be seen as a rare and extreme endmember of this much more common glacier instability. Glacier detachments combine elements of surging, where the glacier adjusts its geometry to satisfy the force balance, with those of ice break-offs from steeper glaciers, where the glacier is not able to adjust in a steady way. The surface slopes of  $9\text{--}21^\circ$  of the detached glacier parts, though quite low for glaciers that produce ice avalanches, might rank high in comparison with surge-type glacier tongues. Slopes in this range exert higher shear stresses than is typical for surge-type glaciers and favour thus the possibility of exceeding a critical stress level that then leads to sudden failure. At the same time, in comparison to glaciers in very steep terrain that tend to be thin, glaciers of  $10\text{--}20^\circ$  surface slope can build up thicker ice, which leads to the larger volumes typically involved in detachments. Using a strongly simplifying slab model we estimate ranges for glacier slope and width above which a glacier could detach when widespread and strong loss of its basal resistance cannot be accommodated anymore by lateral resistance. We estimate a critical shear stress of 0.28 MPa that could be supported by the glacier margins of the Aru detachments. We also estimate that (surge-like) precursory acceleration of glacier sliding before detachment could produce substantial amounts of ice melt at the glacier base that would facilitate reduction of the shear stress of soft beds.

Weak bedrock and/or the existence of soft and highly erodible sediments under the detached glaciers was identified for most of the observed glacier detachments, plausible for the ones we determined retroactively, and hints at till-strength weakening under high pore-water pressure as a concrete failure process. There appear to be different trajectories into, or out of, the narrow envelope of potential failure conditions, not least driven by climatic changes. The fact that most collapses happened during local spring/summer suggests that a meltwater or high-altitude rain driven increase of basal pore water pressure can play an important role in triggering the events, whether directly or in some delayed form. Atmospheric warming enhances such hazard conditions. For some detachment sites, negative regional glacier mass balances can prevent detached glaciers from fully rebuilding and thus from detachments to repeat over time, at least at earlier volumes. The special case of Tsambagarav

1052 demonstrates that an earthquake was not able to trigger a glacier detachment (reinforcing earlier findings that low-slope glaciers  
appear quite resistant to ground shaking; Kargel et al., 2016) but to precondition one glacier for failure along a weakness  
existing already before the earthquake.

1054 Detailed investigations of the events described in this study showed that a wide variety of dispositions and triggers can lead to  
a glacier detachment. This makes it challenging for practitioners working in high-mountain hazard management to anticipate  
1056 and predict such events. From this practical standpoint, however, this study attempts to raise awareness about the – albeit low  
– possibility of sudden, large-volume detachments of low-angle glaciers at locations with

- 1058 ● particularly soft and erodible lithologies, and, likely related, the
- existence of surge-type glaciers and surge-like glacier evolution.
- 1060 ● Repeated events or geomorphological imprints of potential earlier collapses or other violent ice-rock mass flows can  
be further investigated, but events can also happen without historical precedence through shifts in the array of failure  
1062 conditions.
- Several of the glaciers investigated here showed abnormal crevassing and enhanced precursory surface speeds in the  
1064 days to weeks before detachment.
- The surface slopes found in this study for the detached glaciers ranged between roughly  $10^\circ$  and  $20^\circ$ , and we propose  
1066 a rough combination of glacier slope and width above which glaciers could detach in case of extensive loss of basal  
friction (section 4.1).

1068 Due to the large amounts of snow and ice involved in glacier detachments, the high chance of lubrication and of liquefaction  
of glacier ice and subglacial sediments, and smooth geometries of glacial valleys, avalanche friction is typically greatly  
1070 reduced. This results in the particularly high mobility of the ice-rock avalanches resulting from low-angle glacier detachments  
and can lead to substantial damage far from the source. Between the large runout distances and the varying factors that can  
1072 impact a glacier's detachment probability, high-mountain hazard management will, after the first general assessment provided  
in this study, benefit from more detailed investigations of glacier detachments, the conditions that lead to them and the  
1074 mechanics that drive them.

1076

**Table 1: Parametres for the low-angle glacier detachments of this contribution. For repeat events the parameters given refer to the underlined year.**

Name of event	Region	Years	Lat, Lon	GLIMS, RGI IDs	Reach L (km)	Drop H (km)	Volume (10 <sup>6</sup> m <sup>3</sup> )	Glacier surface slope (°)	Section
Devdorak	Caucasus	(1776, 1778, 1785, 1808, 1817 ?)1832, 2014	42.72°N, 44.55°E	G044517E4271 5N, RGI60-12.00840	10.5	3.2	15	17(?)	3.1
Kolka	Caucasus	~1835?, 1902, 2002	42.73°N, 44.44°E	G044447E4273 3N, RGI60-12.00131	19	2.0	130	13	3.1
Rasht	Pamirs	2017	38.975°N, 70.850°E	G070852E3897 4N, RGI60-13.18284; USSR 504	7.6	1.4	6	16	3.2
Rasht	Pamirs	2019	38.989° N, 70.693° E	G070689E3898 1N, RGI60-13.20645; USSR 518	6.7	1.5	4.5	20	3.2
Aru 1	Western Tibet	Jul 2016	34.02° N, 82.250° E	G082249E3402 3N, RGI RGI60-13.51473, Chinese: CN5Z412C0011	8.2	0.8	68	12	3.3
Aru 2	Western Tibet	Sep 2016	34.00° N, 82.265° E	G082268E3400 5N, RGI60-13.51476, Chinese inv.: CN5Z412C0007	7.2	0.83	83	13	3.3
Tsambagarav	Western Mongolia, Altai	Aug 1988	48.66° N, 90.75° E,	G090733E4867 6N, RGI60-10.02686	4-5.5	0.7	6	20	3.4
Amney Machen	Eastern Tibet	2004, 2007, 2016, 2017, 2019	34.82°N, 99.44°E	G099443E3482 4N, RGI60-13.23943, Chinese inv: CN5J352E0017,	5.2	1.0	27	13	3.5
Sedongpu	South-eastern Tibet	2018	29.80° N, 94.92° E	G094940E2981 1N, RGI60-13.01391, Chinese inv.: SDP1	8	1.3	100	9	3.6
Flat Creek	Saint Elias Mts.	2013, 2015, 2016	61.50° N, 141.54° W	G218441E6163 8N, RGI60-01.17460	11	1.1	14	20	3.7
Aparejo	Chilean Andes	1980	33.56° S, 70.01° W	only World Glacier Inv. CL1M005D004 9	3.7	0.8	7.2	20	3.8
Leñas	Argentinean Andes	2007	34.46° S, 70.05° W	G289941E3445 9S, RGI60-17.01251	2	0.2	4.2	15	3.9



Tinguiririca	Chilean Andes	~1960,1994, <u>2007</u>	34.83° S 70.35° W	only World Glacier Inv. CL1M00420016	7.9	1.4	12	20	3.10
--------------	---------------	----------------------------	----------------------	--	-----	-----	----	----	------

---

1080

## Code availability

1084 Not relevant

## Data availability

1086 Sentinel-1 and Sentinel-2 data are freely available from the ESA/EC Copernicus Sentinels Scientific Data Hub at  
https://scihub.copernicus.eu (Copernicus, 2020), Landsat satellite data, Corona satellite data, and SRTM-C DEMs from United  
1088 States Geological Survey (USGS, 2020), SRTM-X and TanDEM-X DEMs from the German Aerospace Center (DLR, 2020),  
the ALOS World DEM from the Japan Aerospace Exploration Agency (JAXA, 2020), Chinese earthquake data from the China  
1090 Earthquake Data Center. Planet data (Dove and RapidEye) are not openly available as Planet is a commercial company.  
However, scientific access schemes to these data exist (https://www.planet.com/markets/education-and-research/). Data from  
1092 Maxar satellites (GeoEye, Ikonos, WorldView, Quickbird) and Airbus (Pléiades, Spot) are commercial, but in parts explorable  
from GoogleEarth and BingMaps.

## 1094 Author contribution

A.K. wrote the text, did most new analyses and prepared the figures. M.J. and A.G. wrote parts of the text, edited all text, and  
1096 contributed comments and discussions. L.G. prepared the Sedongpu DEMs. All authors edited text and contributed with data,  
comments and discussions.

## 1098 Competing interests

All authors declare that they have no competing interests.

## 1100 Acknowledgements

This paper is an extended and updated version of the Louis Agassiz medal lecture by A.K. given at the European Geosciences  
1102 Union General Assembly 2019. We would like to thank Martin Truffer and an anonymous referee for their very constructive  
comments. The force balance model, section 4.1, is based on a concept proposed to us by Martin Truffer. We are grateful to  
1104 the providers of free data for this study; European Space Agency (ESA) / European Commission (EC) Copernicus for Sentinel-

2 data, USGS for Landsat, Corona, and SRTM data, DLR for SRTM and TanDEM-X data, and Planet for their cubesat data  
1106 via Planet's Ambassadors Program. E.B. and S.G. acknowledge support from the French Space Agency (CNES) through  
TOSCA and DINAMIS programs. S.C. acknowledges support from Lomonosov Moscow State University on the theme  
1108 "Mapping, modeling and risk assessment of dangerous natural processes". D.P. and S.C. acknowledge the Russian Foundation  
for Basic Research. Paola Banegas from SEGEMAR Mendoza provided the 1962 aerial photos over Tinguririca.

## 1110 **Financial support**

This work was funded by the ESA projects Permafrost\_CCI (4000123681/18/I-NB), Glaciers\_CCI (4000109873/14/I-NB,  
1112 4000127593/19/I-NS), and the ESA EarthExplorer10 Mission Advisory Group (4000127656/19/NL/FF/gp), by the European  
Research Council under the European Union's Seventh Framework Programme (FP/2007-2013) / ERC grant agreement no.  
1114 320816, and the Russian Foundation for Basic Research (grant 18-05-00520). JSK thanks NASA's Interdisciplinary Science  
Program (grant 80NSSC18K0432).

1116



1118

## References


- 1120 Alean, J.: Ice avalanche activity and mass balance of high-altitude hanging glaciers in the Swiss Alps, *Ann Glaciol*, 6, 248-249, 1985.
- 1122 Agatova, A. K., Nepop, R. K., Otgonbayar Demberel, and Ganyushkin, D. A.: The influence of the seismic process on the modern glaciation of the Tsambagarav massif (Western Mongolia), XVII Glaciological Symposium, St. Petersburg, 2020.
- 1124 Aristov, K. A., Petrakov, D. A., Kovalenko, N. V., Timonin, S. A., Kolchin, A. A., and Drobyshev, V. N.: Monitoring of 1126 Kolka Glacier in 2014–2017 by terrestrial stereophotogrammetry. *Led i Sneg. Ice and Snow [In Russian], Led i Sneg (Ice and Snow)*, 59, 49–58, <https://doi.org/10.15356/2076-6734-2019-1-49-58>, 2019.
- 1128 Asoyan, D. S., and Rototaeva, O. V. Devdoraki Glacier, Kazbek: history of studies of natural hazards in XIX and the beginning of XXI centuries. *Led i Sneg. Ice and Snow*, 56(2): 253-264, <https://doi.org/10.15356/2076-6734-2016-2-253-264>, 2016.
- 1130 Avdeev, V. A., Nartov, S. V., Baljinniam, I., Monhoo, D., and Erdenbileg, B.: Tsambagarav earthquake of July 23, 1988, *Geology and Geophysics*, 11, 118–124. (in Russian), 1989.
- 1132 Benn, D. I., Fowler, A. C., Hewitt, I., and Sevestre, H.: A general theory of glacier surges, *J Glaciol*, 65, 701-716, <https://doi.org/10.1017/jog.2019.62>, 2019.
- 1134 Braun, M. H., Malz, P., Sommer, C., Farias-Barahona, D., Sauter, T., Casassa, G., Soruco, A., Skvarca, P., and Seehaus, T. C.: Constraining glacier elevation and mass changes in South America, *Nat Clim Change*, 9, 130, <https://doi.org/10.1038/s41558-018-0375-7>, 2019.
- 1136 Brenning, A.: Geomorphology, hydrological and climatic significance of rock glaciers in the Andes of Central Chile (33–35°S), *16*, 231-240, <https://doi.org/10.1002/ppp.528>, 2005.
- 1138 Brun, F., Berthier, E., Wagnon, P., Kääh, A., and Treichler, D.: A spatially resolved estimate of High Mountain Asia glacier mass balances from 2000 to 2016, *Nature Geosci*, 10, 668-673, <https://doi.org/10.1038/ngeo2999>, 2017.
- 1140 Caplan-Auerbach, J., and Huggel, C.: Precursory seismicity associated with frequent, large ice avalanches on Iliamna volcano, Alaska, USA, *J Glaciol*, 53, 128-140, <https://doi.org/10.3189/172756507781833866>, 2007.
- 1142 Chen, C., Zhang, L. M., Xiao, T., and He, J.: Barrier lake bursting and flood routing in the Yarlung Tsangpo Grand Canyon in October 2018, *J Hydrol*, 583, Artn 124603, <https://doi.org/10.1016/j.jhydrol.2020.124603>, 2020.
- 1144 Chernomorets, S. S. New “Kazbek blockage” on 17 May 2014. *Priroda*, 7: 67-72 <https://istina.msu.ru/download/6618200/1k5k5t:82mOHGauqEFijKJOHSXRSTVDIT8/> (in Russian), 2014.
- 1146 Chernomorets, S., Savernyuk, E., Petrakov, D., Dokukin, M., Gotsiridze, G., Gavardashvili, G., Drobyshev, V., Tutubalina, O., Zaporozhchenko, E., Kamenev, N., Kamenev, V., Kääh, A., Kargel, J., and Huggel, C.: The Devdorak ice-rock avalanche and consequent debris flow from the slope of Mt. Kazbek (Caucasus, Georgia) in 2014, EGU General Assembly Conference Abstracts, April 01, 2016, 2016.
- 1148 Chernomorets, S. S., Tutubalina, O. V., Seinova, I. B., Petrakov, D. A., Nosov, K. N., and Zaporozhchenko, E. V.: Glacier and debris flow disasters around Mt. Kazbek, Russia/Georgia, in: *Debris-Flow Hazards Mitigation: Mechanics, Prediction, and Assessment*, edited by: Chen, C. L., and Major, J. J., Millpress, Netherlands, 2007.
- 1154 Clarke, G. K. C., Collins, S. G., and Thompson, D. E.: Flow, thermal structure, and subglacial conditions of a surge-type glacier, *Can J Earth Sci*, 21, 232-240, <https://doi.org/10.1139/e84-024>, 1984.
- 1156



- 1158 Clarke, G. K. C., and Blake, E. W.: Geometric and thermal evolution of a surge-type glacier in its quiescent state - Trapridge  
Glacier, Yukon-Territory, Canada, 1969-89, *J Glaciol*, 37, 158-169, 1991.
- 1160 Copernicus Open Access Hub, Copernicus programme, European Commission and European Space Agency, available at:  
<https://scihub.copernicus.eu>, last access: 17 October 2019, 2019.
- 1162 Crandell, D. R., and Fahnestock, R. K.: Rockfalls and avalanches from little Tahoma Peak on Mount Rainier, Washington,  
*U.S. Geol. Surv. Bull.*, 1221-A, A1-A30, 1965.
- 1164 Dokukin, M. D., Bekkiev, M. Y., Kalov, R. H., Savernyuk, E. A., and Chernomorets, S. S.: Signs of catastrophic glacier  
detachments (Analysis of multitemporal space information) (In Russian), in: *Dangerous natural and technogenic  
processes in mountain regions: models, systems and technologies*, Moscow, 522-528, 2019.
- 1166 Dokukin, M. D., Savernyuk, E. A., and Chernomorets, S. S. Rock Avalanches in the Alpine Zone of the Caucasus in the 21  
Century. *Priroda*, 7: 52-62, (in Russian), 2015.
- 1168 Dokukin, M. D., Bekkiev, M. Yu., Kalov, R. Kh., Chernomorets, S. S., and Savernyuk, E. A. Activation of rock avalanches  
in the Central Caucasus and their impact on the dynamics of glaciers and debris flows. – *Led i Sneg. Ice and Snow*,  
1170 60(3), 361-378, 2020.
- 1172 Drobushhev V.N., Torchinov H-M.Z., Tutubalina O.V., and Hubaev H.M. Main topographical data and kinematics of the  
Devdorakskiy collapse on May 17, 2014. *Vestnik of the Vladikavkaz Scientific Centre*, 4: 30-41, (in Russian), 2014.
- 1174 Drobyshev, V. N.: Glacial catastrophe of 20 September 2002 in North Osetia, *Russian Jo. Earth Sci*, ES4004,  
<https://doi.org/doi:10.2205/2006ES000207>, 2006.
- 1176 Dunse, T., Schellenberger, T., Hagen, J. O., Kääb, A., Schuler, T. V., and Reijmer, C. H.: Glacier-surge mechanisms  
promoted by a hydro-thermodynamic feedback to summer melt, *Cryosphere*, 9, 197-215, <https://doi.org/10.5194/tc-9-197-2015>, 2015.
- 1178 Dussaillant, I., Berthier, E., Brun, F., Masiokas, M., Hugonnet, R., Favier, V., Rabatel, A., Pitte, P., and Ruiz, L.: Two  
decades of glacier mass loss along the Andes, *Nat Geosci*, 12, 803, <https://doi.org/10.1038/s41561-019-0432-5>, 2019.
- 1180 Evans, S. G., Bishop, N. F., Smoll, L. F., Murillo, P. V., Delaney, K. B., and Oliver-Smith, A.: A re-examination of the  
mechanism and human impact of catastrophic mass flows originating on Nevado Huascarán, Cordillera Blanca, Peru  
1182 in 1962 and 1970, *Eng Geol*, 108, 96-118, <https://doi.org/10.1016/j.enggeo.2009.06.020>, 2009a.
- 1184 Evans, S. G., Tutubalina, O. V., Drobyshev, V. N., Chernomorets, S. S., McDougall, S., Petrakov, D. A., and Hungr, O.:  
Catastrophic detachment and high-velocity long-runout flow of Kolka Glacier, Caucasus Mountains, Russia in 2002,  
*Geomorphology*, 105, 314-321, <https://doi.org/10.1016/j.geomorph.2008.10.008>, 2009b.
- 1186 Evans, S. G., and Delaney, K. B.: Catastrophic mass flows in the mountain glacial environment, in: *Snow and Ice-related  
Hazards, Risks, and Disasters*, edited by: Haerberli, W., and Whitemann, C., *Hazards and Disasters Series*, Elsevier,  
1188 Amsterdam, 563-606, 2015, <https://doi.org/10.1016/B978-0-12-394849-6.00016-0>.
- 1190 Faillettaz, J., Sornette, D., and Funk, M.: Numerical modeling of a gravity-driven instability of a cold hanging glacier:  
reanalysis of the 1895 break-off of Altsgletscher, Switzerland, *J Glaciol*, 57, 817-831, 2011.
- 1192 Faillettaz, J., Funk, M., and Vincent, C.: Avalanching glacier instabilities: Review on processes and early warning  
perspectives, *Rev. Geophys.*, 53, 203-224, <https://doi.org/10.1002/2014rg000466>, 2015.
- 1194 Falaschi, D., Bolch, T., Lenzano, M. G., Tadono, T., Lo Vecchio, A., and Lenzano, L.: New evidence of glacier surges in the  
Central Andes of Argentina and Chile, *Prog Phys Geog*, 42, 792-825, <https://doi.org/10.1177/0309133318803014>,  
2018a.
- 1196 Falaschi, D., Lenzano, M. G., Tadono, T., Vich, A., and Lenzano, L.: Balance de masa geodésico 2000-2011 de los glaciares  
de la cuenca del río Atuel, Andes Centrales de Mendoza, *Geoacta*, 42, 7-22, 2018b.
- 1198 Falaschi, D., Kääb, A., Paul, F., Tadono, T., Rivera, J. A., and Lenzano, L. E.: Brief communication: Collapse of 4 Mm(3) of  
ice from a cirque glacier in the Central Andes of Argentina, *Cryosphere*, 13, 997-1004, <https://doi.org/10.5194/tc-13-997-2019>, 2019.
- 1200


- 1202 Fischer, L., Huggel, C., Kääh, A., and Haeberli, W.: Slope failures and erosion rates on a glacierized high-mountain face  
under climatic changes, *Earth Surf. Proc. Land.*, 38, 836-846, <https://doi.org/10.1002/Esp.3355>, 2013.
- 1204 Flowers, G. E., Jarosch, A. H., Belliveau, P. T. A. P., and Fuhrman, L. A.: Short-term velocity variations and sliding  
sensitivity of a slowly surging glacier, *Ann Glaciol*, 57, 71-83, <https://doi.org/10.1017/aog.2016.7>, 2016.
- 1206 Fowler, A. C., Murray, T., and Ng, F. S. L.: Thermally controlled glacier surging, *J Glaciol*, 47, 527-538,  
<https://doi.org/10.3189/172756501781831792>, 2001.
- 1208 Frappe, T. P., and Clarke, G. K. C.: Slow surge of Trapridge Glacier, Yukon territory, Canada, *J Geophys Res-Earth*, 112,  
Art. F03s32, <https://doi.org/10.1029/2006jf000607>, 2007.
- 1210 Gardelle, J., Berthier, E., Arnaud, Y., and Kääh, A.: Region-wide glacier mass balances over the Pamir-Karakoram-  
Himalaya during 1999-2011, *Cryosphere*, 7, 1263-1286, 2013.
- 1212 Gareth, G.S. and Melosh, H.J.: Acoustic fluidization and the extraordinary mobility of sturzstroms. *J Geophys Res-Earth*,  
108 (B10), 2473, <https://doi.org/10.1029/2003JB002465>, 2003.
- 1214 Gilbert, A., Leinss, S., Kargel, J., Kääh, A., Gascoïn, S., Leonard, G., Berthier, E., Karki, A., and Yao, T. D.: Mechanisms  
leading to the 2016 giant twin glacier collapses, Aru Range, Tibet, *Cryosphere*, 12, 2883-2900,  
<https://doi.org/10.5194/tc-12-2883-2018>, 2018.
- 1216 Goerlich, F., Bolch, T., and Paul, F.: More dynamic than expected: an updated survey of surging glaciers in the Pamir, *Earth  
Syst. Sci. Data*, 12, 3161-3176, <https://doi.org/10.5194/essd-12-3161-2020>, 2020.
- 1218 Gruber, F. E., and Mergili, M.: Regional-scale analysis of high-mountain multi-hazard and risk indicators in the Pamir  
(Tajikistan) with GRASS GIS, *Nat Hazard Earth Sys*, 13, 2779-2796, <https://doi.org/10.5194/nhess-13-2779-2013>,  
1220 2013.
- 1222 Haeberli, W., Kääh, A., Paul, F., Chiarle, M., Mortara, G., Mazza, A., and Richardson, S.: A surge-type movement at  
Ghiacciaio del Belvedere and a developing slope instability in the east face of Monte Rosa, Macugnaga, Italian Alps,  
56, 104-111, 2002.
- 1224 Haeberli, W., Huggel, C., Kaab, A., Zraggen-Oswald, S., Polkvoj, A., Galushkin, I., Zotikov, I., and Osokin, N.: The  
Kolka-Karmadon rock/ice slide of 20 September 2002: an extraordinary event of historical dimensions in North  
1226 Ossetia, Russian Caucasus, *J Glaciol*, 50, 533-546, <https://doi.org/10.3189/172756504781829710>, 2004.
- 1228 Harrison, W. D., and Post, A. S.: How much do we really know about glacier surging?, *Ann Glaciol*, 36, 1-6,  
<https://doi.org/10.3189/172756403781816185>, 2003.
- 1230 Harrison, W. D., Osipova, G. B., Nosenko, G. A., Espizua, L., Kääh, A., Fischer, L., Huggel, C., Craw Burns, P. A., Truffer,  
M., and Lai, A. W.: Glacier Surges, in: *Snow and Ice-related Hazards, Risks, and Disasters*, edited by: Haeberli, W.,  
and Whitemann, C., Elsevier, Amsterdam, 437-485, 2015.
- 1232 Hauser, A.: Rock avalanche and resulting debris flow in Estero Parraguire and Río Colorado, Región Metropolitana, Chile,  
in: *Catastrophic Landslides: Effects, Occurrence, and Mechanisms*, edited by: Evans, S. G., and DeGraff, J. V.,  
1234 Geological Society of America Reviews in Engineering Geology 15, Boulder, CO, 135-148, 2002.
- 1236 Herreid, S., and Truffer, M.: Automated detection of unstable glacier flow and a spectrum of speedup behavior in the Alaska  
Range, *J Geophys Res-Earth*, 121, 64-81, <https://doi.org/10.1002/2015jf003502>, 2016.
- 1238 Heybrock, W. Earthquakes as a Cause of Glacier Avalanches in the Caucasus. *Geographical Review*, 25. (3): 423-429,  
<https://doi.org/10.2307/209310>, 1935.
- 1240 Hock, R., Rasul, G., Adler, C., Cáceres, B., Gruber, S., Hirabayashi, Y., Jackson, M., Kääh, A., Kang, S., Kutuzov, S.,  
Milner, A., Molau, U., Morin, S., Orlove, B., and Steltzer, H.: High Mountain Areas, in: *IPCC Special Report on the  
1242 Ocean and Cryosphere in a Changing Climate (SROCC)*, edited by: Pörtner, H.-O., Roberts, D. C., Masson-Delmotte,  
V., Zhai, P., Tignor, M., Poloczanska, E., Mintenbeck, E., Alegria, A., Nicolai, M., Okem, A., Petzold, J., Rama, B.,  
and Weyer, N. M., IPCC, Geneva, 2019.
- 1244 Hoinkes, H.: Die Ausbrüche (surges) des Kolka-Gletschers in Nord-Ossetien, Zentraler Kaukasus, *Z. Gletscherkd. Glazial-  
geol.*, 253-270, 1972.

- 1246 Hsü, K. J.: Catastrophic debris streams (Sturzstroms) generated by rockfalls, *Geol. Soc. Am. Bull.*, 86, 129-140, 1975.
- 1248 Hu, K. H., Zhang, X. P., You, Y., Hu, X. D., Liu, W. M., and Li, Y.: Landslides and dammed lakes triggered by the 2017 Ms6.9 Milin earthquake in the Tsangpo gorge, *Landslides*, 16, 993-1001, <https://doi.org/10.1007/s10346-019-01168-w>, 2019.
- 1250 Huggel, C., Zraggen-Oswald, S., Haeberli, W., Kääb, A., Polkvoj, A., Galushkin, I., and Evans, S. G.: The 2002 rock/ice avalanche at Kolka/Karmadon, Russian Caucasus: assessment of extraordinary avalanche formation and mobility, and application of QuickBird satellite imagery, *Nat. Hazard. Earth Sys.*, 5, 173-187, <https://doi.org/10.5194/nhess-5-173-2005>, 2005.
- 1252 Huggel, C., Caplan-Auerbach, J., Waythomas, C. F., and Wessels, R. L.: Monitoring and modeling ice-rock avalanches from ice-capped volcanoes: A case study of frequent large avalanches on Iliamna Volcano, Alaska, *J Volcanol Geoth Res*, 168, 114-136, <https://doi.org/10.1016/j.jvolgeores.2007.08.009>, 2007.
- 1254 Huggel, C.: Recent extreme slope failures in glacial environments: effects of thermal perturbation, *Quaternary Sci Rev*, 28, 1119-1130, <https://doi.org/10.1016/j.quascirev.2008.06.007>, 2009.
- 1258 Iribarren Anacona, P., Mackintosh, A., and Norton, K. P.: Hazardous processes and events from glacier and permafrost areas: lessons from the Chilean and Argentinean Andes, *Earth Surf Proc Land*, 40, 2-21, <https://doi.org/10.1002/esp.3524>, 2015.
- 1260 Jacquemart, M., and Loso, M.: Catastrophic glacier collapse and debris flow at Flat Creek, Wrangell-St. Elias National Park and Preserve. *Alaska Park Science*, 18(1), 16-25, 2019.
- 1262 Jacquemart, M., Loso, M., Leopold, M., Welty, E., Berthier, E., Hansen, J. S. S., Sykes, J., and Tiampo, K.: What drives large-scale glacier detachments? Insights from Flat Creek glacier, St. Elias Mountains, Alaska, *Geol*, <https://doi.org/10.1130/g47211.1>, 2020.
- 1264 Jiskoot, H.: Glacier surging, in: *Encyclopedia of Snow, Ice and Glaciers*, edited by: Singh, V. P., and Haritashya, U. K., Springer, 415-428, 2011.
- 1266 Kamb, B.: Glacier surge mechanism based on linked cavity configuration of the basal water conduit system, *J Geophys Res-Sol Ea*, 92, 9083-9100, <https://doi.org/10.1029/Jb092ib09p09083>, 1987.
- 1270 Kargel, J. S., Leonard, G. J., Shugar, D. H., Haritashya, U. K., Bevington, A., Fielding, E. J., Fujita, K., Geertsema, M., Miles, E. S., Steiner, J., Anderson, E., Bajracharya, S., Bawden, G. W., Breashears, D. F., Byers, A., Collins, B., Dhital, M. R., Donnellan, A., Evans, T. L., Geai, M. L., Glasscoe, M. T., Green, D., Gurung, D. R., Heijnen, R., Hilborn, A., Hudnut, K., Huyck, C., Immerzeel, W. W., Jiang, L. M., Jibson, R., Kaab, A., Khanal, N. R., Kirschbaum, D., Kraaijenbrink, P. D. A., Lamsal, D., Liu, S. Y., Lv, M. Y., McKinney, D., Nahirnick, N. K., Nan, Z. T., Ojha, S., Olsenholler, J., Painter, T. H., Pleasants, M., Pratima, K. C., Yuan, Q. I., Raup, B. H., Regmi, D., Rounce, D. R., Sakai, A., Donghui, S., Shea, J. M., Shrestha, A. B., Shukla, A., Stumm, D., van der Kooij, M., Voss, K., Xin, W., Weihs, B., Wolfe, D., Wu, L. Z., Yao, X. J., Yoder, M. R., and Young, N.: Geomorphic and geologic controls of geohazards induced by Nepal's 2015 Gorkha earthquake, *Science*, 351, 140, <https://doi.org/10.1126/science.aac8353>, 2016. Khatisyan, G. S. The Kazbek glaciers in the period from 1862 to 1887. *Izvestiya Imperatorskago Russkago Geograficheskago Obschestva* 24(5): 326-347 (in Russian), 1889.
- 1272 Kochtitzky, W., Jiskoot, H., Copland, L., Enderlin, E., McNabb, R., Kreutz, K., and Main, B.: Terminus advance, kinematics and mass redistribution during eight surges of Donjek Glacier, St. Elias Range, Canada, 1935 to 2016, *J Glaciol*, 65, 565-579, <https://doi.org/10.1017/jog.2019.34>, 2019.
- 1274 Kotlyakov, V. M., Rototaeva, O. V., and Nosenko, G. A.: The September 2002 Kolka glacier catastrophe in North Ossetia, Russian Federation. Evidence and analysis, *Mt Res Dev*, 24, 78-83, 2004.
- 1276 Kotlyakov, V. M., Osipova, G. B., and Tsvetkov, D. G.: Monitoring surging glaciers of the Pamirs, central Asia, from space, *Ann Glac*, 48, 125-134, <https://doi.org/10.3189/172756408784700608>, 2008.
- 1278 Kotlyakov, V. M., Osipova, G. B., and Tsvetkov, D. G.: Investigations of the fluctuations of surge-type glaciers in the Pamir based on observations from space, in: *Glaciers of Asia*, U.S. Geological Survey Professional Paper 1386, edited by: Williams, R. S. J., and Ferrigno, J. G., USGS, 77-93, 2010a.
- 1280
- 1282
- 1284
- 1286
- 1288
- 1290

- 1292 Kotlyakov, V. M., Rototaeva, O. V., and Nosenko, G. A.: Fluctuations of glaciers of the Central Caucasus and Gora El'brus,  
with a section on the glaciological disaster in North Osetiya, in: *Glaciers of Asia*, U.S. Geological Survey  
1294 Professional Paper 1386, edited by: Williams, R. S. J., and Ferrigno, J. G., USGS, 59-76, 2010b.
- Kutuzov, S., Lavrentiev, I., Smimov, A., Nosenko, G., and Petrakov, D.: Volume changes of Elbrus glaciers from 1997 to  
1296 2017, *Front Earth Sc-Switz*, 7, 153, <https://doi.org/10.3389/feart.2019.00153>, 2019.
- Kääb, A., Wessels, R., Haerberli, W., Huggel, C., Kargel, J., and Khalsa, S. J. S.: Rapid ASTER imaging facilitates timely  
1298 assessment of glacier hazards and disasters, *EOS Trans AGU*, 84, 117,121, 2003.
- Kääb, A., Huggel, C., Barbero, S., Chiarle, M., Cordola, M., Epifani, F., Haerberli, W., Mortara, G., Semino, P., Tamburini,  
1300 A., and Viazzo, G.: Glacier hazards at Belvedere Glacier and the Monte Rosa east face, Italian Alps: processes and  
mitigation, *Interpraevent*, 2004, 67-78,
- 1302 Kääb, A., Treichler, D., Nuth, C., and Berthier, E.: Brief Communication: Contending estimates of 2003–2008 glacier mass  
balance over the Pamir–Karakoram–Himalaya, *Cryosphere*, 9, 557-564, <https://doi.org/10.5194/tc-9-557-2015>, 2015.
- 1304 Kääb, A., Leinss, S., Gilbert, A., Buhler, Y., Gascoin, S., Evans, S. G., Bartelt, P., Berthier, E., Brun, F., Chao, W. A.,  
Farinotti, D., Gimbert, F., Guo, W. Q., Huggel, C., Kargel, J. S., Leonard, G. J., Tian, L. D., Treichler, D., and Yao,  
1306 T. D.: Massive collapse of two glaciers in western Tibet in 2016 after surge-like instability, *Nat Geosci*, 11, 114-120,  
<https://doi.org/10.1038/s41561-017-0039-7>, 2018.
- 1308 Kääb, A.: Collapsing Glaciers, *Geophysical Research Abstracts*, European Geosciences Union General Assembly 2019, Vol.  
21, 8799, 2019.
- 1310 Larsen, C. F., Burgess, E., Arendt, A. A., O'Neel, S., Johnson, A. J., and Kienholz, C.: Surface melt dominates Alaska  
glacier mass balance, *Geophys Res Lett*, 42, 5902-5908, <https://doi.org/10.1002/2015gl064349>, 2015.
- 1312 Lei, Y., Yao, T., Tian, L., Sheng, Y., Lazhu, Liao, J., Zhao, H., Yang, W., Yang, K., Berthier, E., Brun, F., Gao,  Zhu, M.,  
and Wu, G.: Response of downstream lakes to Aru glacier collapses on the western **Tibetan Plateau, 15**, 199-214,  
1314 <https://doi.org/10.5194/tc-15-199-2021>, 2021.
- Leinss, S., Willmann, C., and Hajnsek, I.: Glacier Detachment Hazard Analysis in the West Kunlun Shan Mountains, *Int*  
1316 *Geosci Remote Se*, 4565-4568, 2019.
- Leinss, S., Bernardini, E., Jacquemart, M., and Dokukin, M.: Glacier detachments and rock-ice avalanches in the Petra  
1318 Pervogo range, Tajikistan (1973–2019), *Nat. Hazards Earth Syst. Sci. Discuss.*, <https://doi.org/10.5194/nhess-2020-285>, under review, 2020.
- 1320 Liu, C. Z., Lu, J. T., Tong, L. Q., Chen, H. Q., Liu, Q. Q., Xiao, R. H., and Tu, J. N.: Research on glacial/rock fall-landslide-  
debris flows in Sedongpu basin along Yarlung Zangbo River in Tibet, *Geol. China*, 46, 219-234, 2019.
- 1322 Lv, M. Y., Guo, H. D., Lu, X. C., Liu, G., Yan, S. Y., Ruan, Z. X., Ding, Y. X., and Quincey, D. J.: Characterizing the  
behaviour of surge-and non-surge-type glaciers in the Kingata Mountains, eastern Pamir, from 1999 to 2016,  
1324 *Cryosphere*, 13, 219-236, <https://doi.org/10.5194/tc-13-219-2019>, 2019.
- Marangunic, C.: Informe sobre deslizamientos de glaciares en el Estero del Aparejo, Valle del Río Maipo, Área  
1326 Metropolitana, Oficina Nacional de Emergencias, Santiago, Chile, 8p, 1980.
- Masiokas, M. H., Christie, D. A., Le Quesne, C., Pitte, P., Ruiz, L., Villalba, R., Luckman, B. H., Berthier, E., Nussbaumer,  
1328 S. U., Gonzalez-Reyes, A., McPhee, J., and Barcaza, G.: Reconstructing the annual mass balance of the Echaurren  
Norte glacier (Central Andes, 33.5 degrees S) using local and regional hydroclimatic data, *Cryosphere*, 10, 927-940,  
1330 <https://doi.org/10.5194/tc-10-927-2016>, 2016.
- McClung, D. M.: Superelevation of flowing avalanches around curved channel bends, *J Geophys Res-Sol Ea*, 106, 16489-  
1332 16498, <https://doi.org/10.1029/2001jb000266>, 2001.
- Mergili, M., Kopf, C., Mullebner, B., and Schneider, J. F.: Changes of the cryosphere and related geohazards in the high-  
1334 mountain areas of Tajikistan and Austria: a comparison, *Geogr Ann A*, 94A, 79-96, <https://doi.org/10.1111/j.1468-0459.2011.00450.x>, 2012.
- 1336 Milana, J. P.: A model of the Glaciar Horcones Inferior surge, Aconcagua region, Argentina, *J Glaciol*, 53, 565-572,  
<https://doi.org/10.3189/002214307784409324>, 2007.



- 1338 Moore, P. L.: Deformation of debris-ice mixtures, *Rev Geophys*, 52, 435-467, <https://doi.org/10.1002/2014rg000453>, 2014.
- 1340 Murray, T., Strozzi, T., Luckman, A., Jiskoot, H., and Christakos, P.: Is there a single surge mechanism? Contrasts in dynamics between glacier surges in Svalbard and other regions, *J Geophys Res-Sol Ea*, 108, 2237, <https://doi.org/10.1029/2002JB001906>, 2003.
- 1342 Obu, J., Westermann, S., Bartsch, A., Berdnikov, N., Christiansen, H. H., Dashtseren, A., Delaloye, R., Elberling, B., Etzelmuller, B., Kholodov, A., Khomutov, A., Kaab, A., Leibman, M. O., Lewkowicz, A. G., Panda, S. K., Romanovsky, V., Way, R. G., Westergaard-Nielsen, A., Wu, T. H., Yamkhin, J., and Zou, D. F.: Northern Hemisphere permafrost map based on TTOP modelling for 2000-2016 at 1 km(2) scale, *Earth-Sci Rev*, 193, 299-316, <https://doi.org/10.1016/j.earscirev.2019.04.023>, 2019.
- 1348 Paul, F.: Repeat Glacier Collapses and Surges in the Amney Machen Mountain Range, Tibet, Possibly Triggered by a Developing Rock-Slope Instability, *Remote Sens-Basel*, 11, Artn 708, <https://doi.org/10.3390/rs11060708>, 2019.
- 1350 Pavez, C., Tapia, F., Comte, D., Gutierrez, F., Lira, E., Charrier, R., and Benavente, O.: Characterization of the hydrothermal system of the Tinguiririca Volcanic Complex, Central Chile, using structural geology and passive seismic tomography, *J Volcanol Geoth Res*, 310, 107-117, <https://doi.org/10.1016/j.jvolgeores.2015.11.018>, 2016.
- 1352 Petrakov, D. A., Tutubalina, O. V., and Chernomorets, S. S.: The 2002 Genaldon glacial catastrophe: one year later, *Kryosfera Semlu*, VIII, 29-39, 2004.
- 1354 Petrakov, D. A., Chernomorets, S. S., Evans, S. G., and Tutubalina, O. V.: Catastrophic glacial multi-phase mass movements: a special type of glacial hazard, *Advances in Geosciences*, 14, 211-218, 2008.
- 1356 Petrakov, D. A., Aristov, K. A., A.A., A., Boyko, E. S., Drobyshev, V. N., Kovalenko, V., Tutubalina, O. V., and Chernomorets, S. S.: Rapid regeneration of the Kolka Glacier (Caucasus) after 2002 glacial disaster, *Earth's Cryosphere (Kriosfera Zemli)*, 22, 51-62, [https://doi.org/10.21782/EC2541-9994-2018-1\(51-62\)](https://doi.org/10.21782/EC2541-9994-2018-1(51-62)) 2018.
- 1358 Post, A.: Effects on Glaciers, in: *The great Alaska earthquake of 1964. Part A: hydrology*, National Academy of Sciences, Washington DC, 266-308, 1968.
- 1360 Quincey, D. J., Glasser, N. F., Cook, S. J., and Luckman, A.: Heterogeneity in Karakoram glacier surges, *J Geophys Res-Earth*, 120, 1288-1300, <https://doi.org/10.1002/2015jf003515>, 2015.
- 1362 Reineggs, J. *Allgemeine historisch- topographische Beschreibung des Kaukasus. - Gotha; St. Petersburg, Bd. 1, 296 S., http://elib.shpl.ru/ru/nodes/24706-bd-1-1796*, 1796.
- 1364 Rototayev, K. P., Khodakov, V. G., and Krenke, A. N.: *Study of the Surging Kolka Glacier*, Nauka, Moscow, 168 pp. (in Russian), 1983.
- 1366 Schneider, D., Huggel, C., Haeblerli, W., and Kaitna, R.: Unraveling driving factors for large rock-ice avalanche mobility, *Earth Surf. Proc. Land.*, 36, 1948-1966, <https://doi.org/10.1002/esp.2218>, 2011.
- 1368 Sevestre, H., and Benn, D. I.: Climatic and geometric controls on the global distribution of surge-type glaciers: Implications for a unifying model of surging, *J. Glaciol.*, 61, 646-662, <https://doi.org/10.3189/2015JoG14J136>, 2015.
- 1370 Sevestre, H., Benn, D. I., Hulton, N. R. J., and Baelum, K.: Thermal structure of Svalbard glaciers and implications for thermal switch models of glacier surging, *J Geophys Res-Earth*, 120, 2220-2236, <https://doi.org/10.1002/2015jf003517>, 2015.
- 1372 Shean, D. E., Bhushan, S., Montesano, P., Rounce, D. R., Arendt, A., and Osmanoglu, B.: A Systematic, Regional Assessment of High Mountain Asia Glacier Mass Balance, *Front Earth Sc-Switz*, 7, Artn 363 <https://doi.org/10.3389/feart.2019.00363>, 2020.
- 1374 Sheridan, M. F., Stinton, A. J., Patra, A., Pitman, E. B., Bauer, A., and Nichita, C. C.: Evaluating Titan2D mass-flow model using the 1963 Little Tahoma Peak avalanches, Mount Rainier, Washington, *J Volcanol Geoth Res*, 139, 89-102, <https://doi.org/10.1016/j.jvolgeores.2004.06.011>, 2005.
- 1378 Shugar, D. H., Rabus, B. T., Clague, J. J., and Capps, D. M.: The response of Black Rapids Glacier, Alaska, to the Denali earthquake rock avalanches, *J Geophys Res-Earth*, 117, Artn F01006, <https://doi.org/10.1029/2011jf002011>, 2012.
- 1380 Statkowski, B. I. *Origin of repeating Kazbek blockage and measures for its prevention. Tiflis (in Russian)*, 1877.
- 1382

- 1384 Statkowski, B. Problèmes de la Climatologie du Caucase. Paris, Gauthier-Villars, Imprimeur-Librairie. Successeur de Mallet-  
Bachelier. 279 p. <https://gallica.bnf.fr/ark:/12148/bpt6k9643218p.texteImage> , 1879.
- 1386 Stebnitsky, I. I. On the distribution of glaciers in the Caucasus. – *Izvestiya Kavkazskogo otdela Imperatorskago Russkago  
Geograficheskago Obschestva*, V(1): 1-21 (in Russian), 1877.
- 1388 Strom, A., and Abdrakhmatov, K.: *Rockslides and Rock Avalanches of Central Asia: Distribution, Morphology, and Internal  
Structure*, Elsevier, Amsterdam, 2018.
- 1390 Tavasiev, R. A., and Galushkin, I. V. Rock-ice collapse of Kazbek Mountain dated May 17, 2014. *Vestnik Vladikavkaz  
Scientific Center*, 14(2): 43-45, 2014.
- 1392 Thogersen, K., Gilbert, A., Schuler, T. V., and Malthe-Sorensen, A.: Rate-and-state friction explains glacier surge  
propagation, *Nat Commun*, 10, Artn 2823, <https://doi.org/10.1038/s41467-019-10506-4>, 2019.
- 1394 Tian, L. D., Yao, T. D., Gao, Y., Thompson, L., Mosley-Thompson, E., Muhammad, S., Zong, J. B., Wang, C., Jin, S. Q.,  
and Li, Z. G.: Two glaciers collapse in western Tibet, *J Glaciol*, 63, 194-197, <https://doi.org/10.1017/jog.2016.122>,  
2017.
- 1396 Tielidze, L. G., Kumladze, R. M., Wheate, R. D., and Gamkrelidze, M. The Devdoraki Glacier Catastrophes, *Georgian  
Caucasus. Hungarian Geographical Bulletin*, 68(1), 21-35, <https://doi.org/10.15201/hungeobull.68.1.2>, 2019.
- 1398 Toney et al., 2020. Reconstructing the dynamics of the highly-similar May 2016 and June 2019 Iliamna Volcano, Alaska  
ice–rock avalanches from seismoacoustic data. <https://doi.org/10.5194/esurf-2020-47>
- 1400 Tong, L. Q., Tu, J. N., Pei, L. X., Guo, Z. C., Zheng, X. W., Fan, J. H., Zhong, X., Liu, C. L., Wang, S. S., He, P., and Chen,  
H.: Preliminary discussion of the frequent debris flow events in Sedongpu Basin at Gyala Peri peak, Yarlung Zangbo  
River, *J. Eng.Geol.*, 26, 1552-1561, <https://doi.org/10.13544/j.cnki.jeg.2018-401>, 2018.
- 1402 Treichler, D., Kääh, A., Salzmann, N., and Xu, C. Y.: Recent glacier and lake changes in High Mountain Asia and their  
relation to precipitation changes, *Cryosphere*, 13, 2977-3005, <https://doi.org/10.5194/tc-13-2977-2019>, 2019.
- 1404 Truffer, M., Harrison, W. D., and Echelmeyer, K. A.: Glacier motion dominated by processes deep in underlying till, *J  
Glaciol*, 46, 213-221, <https://doi.org/Doi.10.3189/172756500781832909>, 2000.
- 1406 Truffer, M., Harrison, W. D., Osipova, G. B., Nosenko, G. A., Espizua, L., Kääh, A., Gilbert, A., Fischer, L., Huggel, C.,  
Craw Burns, P. A., and Lai, A. W.: *Glacier Surges*, in: *Snow and Ice-related Hazards, Risks, and Disasters*, 2nd  
edition, edited by: Haerberli, W., and Whitemann, C., Elsevier, Amsterdam, in press, 2021.
- 1408 Ugalde, F., Casassa, G., Marangunic, C., Mujica, R., and Peralta, C.: *El deslizamiento catastrófico del glaciar Aparejo: 35  
años después*, XIV Congreso Geológico Chileno, 2015,
- 1410 Ugalde, F., Marangunic, C., and Casassa, G.: Ice thickness changes at Aparejo Glacier in central Chile from interferometric  
satellite data, 76-79, 2017.
- 1412 Ugalde, F. I. P.: *Estimación de pelegro ante deslizamiento de glaciares en Chile Central: El caso del glaciar Aparejo.*  
Departamento de Geología, Facultad de Ciencias Físicas y Matemáticas, Universidad de Chile, Santiago de Chile.  
2016.
- 1414 van der Woerd, J., Owen, L. A., Tapponnier, P., Xu, X. W., Kervyn, F., Finkel, R. C., and Barnard, P. L.: Giant, similar to  
M8 earthquake-triggered ice avalanches in the eastern Kunlun Shan, northern Tibet: Characteristics, nature and  
dynam  *Geol Soc Am Bull*, 116, 394-406, <https://doi.org/10.1130/B25317.1>, 2004.
- 1420 Viskovatov, A. A. About periodic Kazbek blockage. *Zapiski Kavkazskago otdela Imperatorskago Russkago  
geograficheskago obshestva* 6: 186-219. Tiflis (in Russian), 1864.
- 1422 Wagner, S.: *Dreidimensionale Modellierung zweier Gletscher und Deformationsanalyse von eisreichem Permafrost.*  
*Mitteilungen der Versuchsanstalt für Wasserbau, Hydrologie und Glaziologie der ETH Zürich*, 146, 135pp, 1996.
- 1424 Wang, X., Liu, Q., Zhang, B., Zhang, R., and Liu, G.: Monitoring and analyzing collapse of KLSK-37 Glacier tongue in  
recent 40 years with multi-source remote sensing, *Geomatics and Information Science of Wuhan University*, 45,  
1687-1969, <https://doi.org/10.13203/j.whugis20200214>, (in Chinese with English abstract), 2020.
- 1426

- 1428 Wenyang, W.: Glaciers in the north-eastern part of the Ch'ing-hai-hsi-tsang (Qinghai-Xizang) Plateau (Tibet) and their  
variations, *J Glaciol*, 29, 383-391, 1983.
- 1430 Zaporozhchenko, E. V., and Chernomorets, S. S. History and studies of Kazbek blockages. *Vestnik Kavkazskogo gornogo  
obshestva* 5: 33-54 [https://istina.msu.ru/download/8871273/1k5k36:x\\_gHoGej2TQCeFRBrQCnhJLg7eU/](https://istina.msu.ru/download/8871273/1k5k36:x_gHoGej2TQCeFRBrQCnhJLg7eU/) (in  
Russian), 2004.
- 1432 Zemp, M., Huss, M., Thibert, E., Eckert, N., McNabb, R., Huber, J., Barandun, M., Machguth, H., Nussbaumer, S. U.,  
Gartner-Roer, I., Thomson, L., Paul, F., Maussion, F., Kutuzov, S., and Cogley, J. G.: Global glacier mass changes  
1434 and their contributions to sea-level rise from 1961 to 2016, *Nature*, 568, 382, [https://doi.org/10.1038/s41586-019-  
1071-0](https://doi.org/10.1038/s41586-019-1071-0), 2019.
- 1436 Zhang, W. J.: Identification of Glaciers with Surge Characteristics on the Tibetan Plateau, *Ann Glaciol*, 16, 168-172, 1992.

1438